# Fuel Cell Vehicle and Fuel Analysis:

## *A Comparison of energy use and emissions from Direct-Hydrogen, Indirect Methanol and Indirect Hydrocarbon Fuel Cell Vehicles and Fuel Production*


***Prepared by***
**Fuel Cell Vehicle Modeling Project (FCVMP)**
**http://fcv.ucdavis.edu**
**Institute of Transportation Studies**
**University of California, Davis**

**August 31, 2001**
**Davis, CA**

## ***Table of Contents***

## Contributors to the research and report

Dr. Robert Moore

Professor Myron Hoffman

Paravastu Badrinarayanan

J. Fernando Contadini

Joshua Cunningham

Dr. Claudia Villa Diniz

Anthony Eggert

David Friedman

Monterey Gardiner

Dr. Karl-Heinz Hauer

Dr. Sitaram Ramaswamy

Meena Sundaresan

Peter Vagadori

## Nomenclature and Conversions

***Nomenclature:***

| | |
|---|---|
| AS | Air Supply |
| ATM | Atmosphere |
| ATR | Auto Thermal Reformer |
| Aux nrg | Energy required for hotel loads |
| BP | Back pressure |
| $CH_4$ | Methane |
| CO | Carbon Monoxide |
| $CO_2$ | Carbon Dioxide |
| $CO_{2\text{-equiv.}}$ | $CO_2$ equivalent: global warming impact relative to The GWP of greenhouse gases |
| Comb | Combined |
| Comp | Compressor |
| Comp Elec nrg | Energy required for electric compressor |
| Cond | Condenser |
| Cyl | Cylinder |
| Deliv | Delivered fuel to vehicle tank |
| DH FCV | Direct Hydrogen Fuel Cell Vehicle |
| ECE | A standard European drive cycle |
| Eff | Efficiency |
| FC | Fuel Cell |
| FC System Loss | (Stack+aux) loss + FP loss (defined below) |
| FCV | Fuel Cell Vehicle |
| FP | Fuel processor |
| FP air nrg | Energy required for IHFCV FP air compressor |
| FP loss | Energy of lost hydrogen in FP due to burner vent and airbleed for CO oxidation |
| FT | Fisher-Tropsch |
| FTN | Fisher-Tropsch Naphtha |
| FUDs | Federal Urban Driving Schedule (US) |

| | |
|---|---|
| FUEEM | Fuel Upstream Energy and Emissions Model |
| $GJ_{deliv.}$ | Giga Joule of fuel delivered to the vehicle at the fuel station |
| $GJ_{req\text{-}upstream}$ | Giga Joule of all fuels required (consumed, lost and transformed) in the fuel upstream activities |
| GUI | Graphical users interface |
| GWP | Global Warming Potential |
| H/C | Humidification and cooling |
| HHV | High Heating Values |
| HIWAY | Federal Highway Cycle (US) |
| HTS | High Temperature Shift reactor |
| ICE | Internal Combustion Engines |
| IH FCV | Indirect Hydrocarbon Fuel Cell Vehicle |
| IM FCV | Indirect Methanol Fuel Cell Vehicle |
| J10-15 | A standard Japanese driving cycle |
| KPa | Kilo Pascal |
| LCA | Life Cycle Analysis |
| LCI | Life Cycle Inventory |
| LHV | Low Heating Values |
| LTS | Low Temperature Shift reactor |
| MeOH | Methanol |
| Motor loss | Motor energy loss |
| MPa | Mega Pascal |
| mtpd | metric tons per day |
| MY | Vehicle model year |
| NG | Natural Gas |
| NMOG | Non-Methane Organic Gas |
| NO | Nitric Oxide |
| $NO_x$ | Nitrogen Oxides |
| $N_2O$ | Nitrous Oxide |
| Nrg | Energy |

| | |
|---|---|
| O/C | Oxygen to carbon ratio |
| PEM | Proton Exchange Membrane |
| $PM_{10}$ | Particulate matters smaller than 10 μm |
| PNGV | Partnership for a New Generation Vehicle |
| POX | Partial Oxidation |
| PROX | Preferential oxidation |
| Propulsion | Energy required for vehicle propulsion |
| PSA | Pressure Swing Absorption |
| psi | pounds per square inch |
| Ptw | Fuel Pathway |
| Rad | Radiator |
| RH | Relative humidity |
| S/C | Steam to carbon ratio |
| SCAB | South Coast Air Basin (Los Angeles area, California) |
| Scn | Scenario |
| SCR | Selective Catalytic Reduction |
| SMR | Steam Methane Reformation |
| $SO_x$ | Sulfur Oxides |
| SR | Stoichiometric ratio |
| SS | Steady-state |
| Stack loss | Anode and cathode losses, membrane resistance |
| Stoic | Stoichiometric ratio |
| Tot fuel nrg | Energy of total fuel into vehicle |
| Trans loss | Drivetrain energy loss |
| Upst | Upstream |
| US06 | An addition US driving cycle |
| WTM | Water and thermal management |
| WTM Cond nrg | Energy required for condenser fan |
| WTM Rad nrg | Energy required for radiator fan |

| | |
|---|---|
| TTW | "Tank – to – Wheel" |
| WTT | "Well – to – Tank" |
| WTW | "Well – to – Wheels" |

***Conversions:***

1 Wh/mile = 0.0036 MJ/mile

1 Mile = 1.609 km

1 kJ/kg = 0.43 BTU/$lb_m$

1 Btu = 1.055 kJ = 0.293 Wh

1 $lb_m$ = 453.6 g

1 psi = 6.895 kPa = 68.95 mbar

$T(^oF) = 1.8\ T(^oC) + 32$

# 1 Introduction

The UC-Davis Fuel Cell Vehicle Modeling Program (FCVMP) began developing and analyzing fuel cell vehicle (FCV) simulation models in early 1998. Over the course of more than three years, the research group has completed three complete fuel cell system and vehicle models. Specifically, this includes the direct hydrogen (DH), indirect methanol (IM), and indirect hydrocarbon (IH) FCV models. In addition to the vehicle models, concurrent development has occurred on a fuel pathway model for each of the three fuels considered. This model is called the Fuel Upstream Energy and Emissions Model (FUEEM). This report is meant to provide a summary of the method of analysis and example results from this research.

The FCVMP research group operates in a university setting and receives funding from numerous industry and non-industry supporting donors. We believe the FCVMP research group is in the unique position to objectively highlight, analyze in a realistically balanced way, the specific issues and large uncertainties associated with both a well-to-tank (WTT) and tank-to-wheel (TTW) analysis for the three vehicle and fuel configurations modeled.

The purpose of this report is not to compete with other public well-to-wheel (WTW) analyses. Rather, the goal is to highlight the major issues associated with the three FCV and fuel configurations. Specifically, this report does not present combined well-to-wheel (WTW) results. Instead, the analysis presents the vehicle and fuel upstream results independently. This was done for two reasons. First, it was felt that given the uncertainties involved, we wanted to avoid presenting results perceived as "single point answers". Second, we wanted the emphasis placed on presenting a method of analysis rather than simple results.

We realize that the uncertainties involved both in vehicle design choices and in future fuel pathway developments are large and numerous, and that other choices could have been made. The examples presented in this report represent our current best estimate for vehicle configurations and fuels based on input from our supporting donors and other expert-networks. We are not attempting to state a specific simple answer for the very complex issue.

Given the magnitude of work that has been incorporated into the multi-year research that resulted in this report, it is impossible for us to summarize all aspects of the modeling, interactions, and results that we have investigated. This report represents what we consider the more important aspects of the modeling, as well as the key results generated from the project.

To review the sections that summarize the work from this analysis and research project, specifically refer to Sections 2.1, 2.2, and 4.1.3.

## 1.1 Scope and Limitations

There are many aspects to a vehicle and fuel pathway modeling that are required for a complete and realistic analysis. As with any analysis the ability to incorporate every factor is a function of available time and resources. The FCVMP attempted to analyze all the important aspects of the three vehicles and fuels, but we realize that there are still areas where improvements could be made by further refinements or extended scope of analysis.

The following is a brief description of our modeling scope and limitations. The list is not intended to be comprehensive, and only highlights the important aspects of what we have and have not covered. It is primarily intended to provide the reader with a context for interpreting our results. The statements apply to all three vehicle types and/or all three fuels unless stated otherwise.

### 1.1.1 Vehicle "Tank to Wheel" (TTW) Analysis

The complete fuel cell vehicle (FCV) model has four primary sub-models – 1) the driver, 2) the vehicle body/chassis, 3) the electric drivetrain, and 4) the fuel cell system. The following statements summarize areas we have modeled in detail:

1. The FCV model is a fully dynamic forward-looking model of a load-following vehicle without additional electrical energy storage and with associated control strategies for efficient operation and good dynamic response. Time traces of all system and component variables are available for each driving cycle, as well as aggregate metrics, through a graphical user interface (GUI). Transient effects are modeled and are key to an accurate simulation.
2. The vehicle model incorporates vehicle attributes including frontal area, associated aerodynamic drag, and rolling resistance. Conventional vehicle technology is assumed.
3. Individual vehicle weights were determined using component/system mass information from US DOE Guidelines along with specific drivetrain/vehicle characteristics.
4. The electric drive-train model incorporates a motor controller, electric motor, and transmission with associated energy losses.
5. The current/voltage interaction between the electric drive train and the fuel cell system is modeled dynamically including the voltage dependant motor characteristics.
6. The fuel cell stack model is based on a combination of first principles and laboratory cell data. The stack model enables accurate predictions of the variation in stack voltage and current with varying air and fuel input conditions such as varying pressures, flow rates and fuel concentrations.
7. The fuel cell system is modeled in terms of major sub-systems: a fuel delivery system (fuel processor and associated clean-up or pressurized hydrogen delivery system), fuel cell stack, air supply system, and the associated water and thermal management (WTM) system.

8. The fuel cell system incorporates an optimized air supply control scheme based on maximizing net fuel cell system output power. This optimized control incorporates power requirements for the air supply and water and thermal management systems and balances them with the power output of the fuel cell stack. The resultant steady-state control strategy is then placed in the vehicle model and incorporates specific air compressor pressure and flow schemes for any given stack output power. In the vehicle model, when a specific power is demanded of the stack, the vehicle controller attempts to operate on the optimized control scheme. However, additional required constraints and design criteria in the vehicle, such as rapid transient response, lead to system energy efficiency results less than that of the original steady-state optimization.
9. The water and thermal management of the system (not including fuel processor) is modeled as a parasitic load on the stack that maintains stack temperature and water self-sufficiency.
10. The air supply system is modeled as look-up tables from actual supplier performance data. Technology limitations on air mass flow and pressure capabilities are incorporated into the model, and a pressure drop is modeled across the fuel cell stack.
11. For the IM fuel processor, the reformer and burner are dynamically modeled taking into account reaction kinetics, mass transfer and heat transfer. In addition, the reformer and burner are modeled as a thermally integrated system, which was identified as the primary factor affecting the dynamic performance of the fuel processor.
12. For the IH fuel processor, the ATR is a thermodynamic model and the HTS and LTS are detailed dynamic models incorporating reaction kinetics, mass transfer and heat transfer. The water gas shift models also assume a decreasing temperature profile that helps ensure better CO cleanup.
13. The fuel assumed for reforming in the IH fuel processor is Iso-octane. This is slightly different from the fuel assumed for the upstream fuel calculations, that of Fisher-Tropsch Naphtha (FTN). All vehicle energy use and emissions will be based on Iso-octane.
14. NOTE: For all the vehicle / system energy calculations, the Lower Heating Value (LHV) of the respective fuel was used. This is different from the upstream fuel calculations where the Higher Heating Value (HHV) of the respective fuel was used. This disconnect occurs because conventional vehicle engineering studies use the LHV of the fuel, whereas readily available information for the upstream analysis was quoted in the HHV.

The following statements summarize areas where we have made simplifications:

1. The vehicles are assumed to be fully warmed-up (stack and fuel processor at operating temperature) for all the cycles analyzed.
2. We have not made an attempt to address cost and safety issues explicitly or quantitatively.

3. Although we have performed a rough analysis of system and vehicle volumes based on targets and currently available data to ensure our models are credible, the volume and packaging of these systems has not been fully investigated.
4. Validation of vehicle component models has been conducted wherever possible, or is based on experimental data (i.e. the air compressor). However, there has not been validation of the fuel processor components or of the system as a whole. Data are not available publicly for these validations.
5. Emissions during warm-up have not been evaluated.
6. As vehicle emissions are primarily from the fuel processor, for the IM fuel processor, nitric oxide (NO) kinetics were modeled for the burner and preliminary results indicate extremely low emissions; however, other burner emissions have not been investigated.
7. For the IHFCV, while the anode model does not explicitly include the extremely low levels of reformer CH4, it is assumed to be consumed in the anode exhaust burner. Burner emissions are not modeled.
8. Additionally, vehicle evaporative emissions have not been considered. In California, zero evaporative emission standards are assumed to be fully in force by 2010.
9. Hybrid vehicle/system configurations have not been considered in this analysis, given the resource availability of the project, and the scope of the modeling program in general. However, separate hybrid studies have been conducted by several members of the modeling team and are referenced.

### 1.1.2 Fuel "Well to Tank" (WTT) Analysis

The following statements summarize areas we have modeled in detail:

1. A panel of more than 25 experts (expert-network) from multiple international organizations was created and involved in the discussions of what input variables and selected pathways should be pursued (See Contadini et al., 2000d).
2. The uncertainties are represented in the calculation by using probabilistic curves (stochastic variables) and the uncertainties are carried out through the calculation using Monte Carlo Simulation. Curves with 90% confidence intervals are plotted.
3. Each major operational activity (e.g. fuel shipping via pipeline), for any given fuel pathway, is modeled and accounted for in component models. This allows for "calibration" of the curves with current "other resource" data and facilitates the investigation of some physical parameters.
4. FUEEM can easily be rearranged to perform regional-type analysis (as compared to a lumped national or global average). California's South Coast Air Basin (SCAB) was chosen for this analysis. See comments 7, 8, and 9 below.
5. The time-frame analyzed is 2010, when the fuel market for FCVs is expected to have characteristics of a well established market, avoiding situations that are only considered for the introductory phase of the vehicle. The chosen pathways for the analysis were carefully selected by the expert-network to represent the "most feasible" or the "most probable" cases when natural gas is the feedstock selected.

6. A combined scenario for each fuel type was created. This combined scenario allocates a specific fraction of the fuel production to each possible fuel pathway studied. This is in contrast to assuming that 100% of the fuel produced comes from one type of fuel pathway. This kind of scenario was created in order to try to simulate what happens in the real world. The results show that the allocation criterion is a very sensitive parameter.
7. FUEEM analyzes the total energy required in all fuel operational activities, from the "well to the vehicle tank", including secondary fuels such as coal used to produce electricity accounting for the "mining to the motor". FUEEM also presents its results in terms of fossil fuel and petroleum requirement.
8. The major concern for the analyzed region, the South Coast Air Basin (SCAB), is air quality. FUEEM provides the opportunity to analyze several criteria emissions, such as $NO_x$, NMOG, CO, $PM_{10}$, $PM_{2.5\text{-introductory}}$ and $SO_x$, in the respective area of occurrence. For the present example analysis $NO_x$, NMOG and CO emissions that occur inside of the basin (SCAB) were selected.
9. Additionally, FUEEM models the emissions of the major greenhouse gases ($CO_2$, $CH_4$ and $N_2O$) and also aggregates them in terms of $CO_{2\text{-equivalent}}$ using global warming potential factors (GWP). For the present analysis the results of $CO_2$ emissions only are presented.
10. For the indirect hydrocarbon example pathway, the final fuel composition (zero sulfur, no aromatics and high paraffin content) was the main reason to select NG over crude petroleum in the hydrocarbon (naphtha) case. Fisher-Tropsch Naphtha (FTN) was assumed. Future development of this project will include other feedstock options including crude oil, if resources are available.
11. NOTE: For all the upstream fuel calculations, the Higher Heating Value (HHV) of the respective fuel was used. This is different from the vehicle calculations where the Lower Heating Value (LHV) of the respective fuel was used.

The following statements summarize areas where we have made simplifications or have not reached a consensus among the experts:

1. The relative allocation of each pathway in the combined scenario is a very sensitive variable and we do not claim that the allocations used in these examples are forecasts of the future.
2. Not much data is available for criteria emissions in methanol and Fischer-Tropsch plants. For this SCAB analysis, criteria emissions for these plants occur overseas (outside of the region of SCAB) and are therefore not applicable. Other choices of regions may require consideration of these effects and more data will have to be obtained.
3. Fisher-Tropsch values (efficiency, selectivity and extra-steam) reflect an early stage of technology development and competitors withhold information as proprietary.
4. The "life cycle"[1] usage of coal, diesel and residual oil, which are used in secondary calculations, are extrapolations from the literature and are not modeled

[1] "Consecutive and interlinked stages of a product system, from raw material acquisition or generation of natural resources to the final disposal". (ISO 14040)

in the same level of detail as the other fuel pathways. Future development should apply the same methodology for these secondary fuels also.

5. The boundaries of the calculation do not include the commissioning and decommissioning phases for all facilities. Therefore the emissions generated to produce the materials used to construct the plants, for example, are not included.
6. The expert network has not made an attempt to address cost and safety issues explicitly and quantitatively.

## 1.2 Report Structure

This section gives the reader an idea of the structure of the report and the sequence of chapters in the complete report. To begin with, Section 2 provides an overview of vehicle and upstream results. This includes the calculated energy consumption of the three different types of fuel cell vehicles modeled, that of the Direct Hydrogen (DH), the Indirect Methanol (IM), and the Indirect Hydrocarbon (IH) vehicles. Specific energy loss characteristics are shown set in the context of the full energy potential of the fuel delivered from the vehicle tank. The upstream model results highlight the energy used and emissions produced upstream of the vehicle fuel tank to produce and deliver the fuel to the vehicle.

Section 3 highlights the major assumptions put into the modeling efforts. Additionally, the performance targets chosen for this particular study are highlighted.

Section 4 provides the detailed discussion of the modeled vehicles and upstream pathways. This includes details of the fuel cell system and all the related components, vehicle drivetrain characteristics, and a full discussion of the fuel pathway segments assumed. The fuel cell system discussion includes detailed analyses of the components and their contribution to the system performance, both in steady-state operation, and in relation to certain transient drive cycles.

Finally, the Appendix of the report includes additional information related to this study. This includes additional sensitivity characterizations of the fuel cell system.

# 2 Summary Results

## 2.1 Vehicle Results (TTW)

In this section, we shall compare and contrast the vehicle simulation results for the three different types of fuel cell vehicles considered here. The items of importance in the vehicle comparison include the dynamic performance criteria and energy consumption. First, results for the vehicle performance are presented and compared with the original goals for each of the vehicles. Second, the simulation results for the three types of fuel cell vehicles are compared from the viewpoint of energy consumption and efficiency, and to a minor extent, emissions. This section is limited to the summary of the results. Refer to Sections 4.1 and 5.1 for a more detailed presentation of the results. Much more information is available from the simulations conducted for this study, but are not summarized in this report.

As stated previously, the following two notes apply to the vehicle / system calculations, and are important when attempting to compare the vehicle and upstream results:

- The fuel assumed for reforming in the IH fuel processor is Iso-octane. This is slightly different from the fuel assumed for the upstream fuel calculations, that of Fisher-Tropsch Naphtha (FTN). All vehicle energy use and emissions will be based on Iso-octane.
- For all the vehicle / system energy calculations, the Lower Heating Value (LHV) of the respective fuel was used. This is different from the upstream fuel calculations where the Higher Heating Value (HHV) of the respective fuel was used. This disconnect occurs because conventional vehicle engineering studies use the LHV of the fuel, whereas readily available information for the upstream analysis was quoted in the HHV. We have not attempted to resolve this disconnect for this study.

### 2.1.1 Vehicle Acceleration and Range

#### Dynamic Requirement

Table 1: Vehicle Acceleration and Maximum Speed

| | Target Values | DH | IM | IH |
|---|---|---|---|---|
| 0-60mph (sec) | 12 | 12.2 | 12.2 | 11.7 |
| Max. Speed, min (mph) | 85 | 94 | 94 | 94 |
| 0-30mph (sec) | NOT A TARGET | 5.0 | 5.0 | 5.1 |

The vehicle acceleration and top speed constituted the dominant performance criteria used for sizing the system components in the vehicles. It is therefore not

surprising that the output results for the three types of fuel cell vehicles are similar. The proposed performance targets were achieved with the three fuel cell vehicle design simulations.

### Range

The vehicle range depends on the tank size and the specific energy consumption of each vehicle. The tank has been sized to satisfy the range requirement of 380 miles for the IH and IM vehicle. For the DH vehicle, using roughly similar total 'fuel and fuel cell system' volumes compared to the IM and IH platforms, the resulting range is only 300 miles. The reason is that a compressed hydrogen tank for 5.3 kg of hydrogen (enough for 380 miles range) would have a volume (without wall and structure) of 230 L (assuming a maximum storage pressure of 5,000psi). Because of packaging constraints, a maximum realistic tank volume of approximately 180 L was assumed. This assumption is somewhat arbitrary and depends of course on the vehicle configuration details. In addition to the pure tank volume the cylindrical shape may cause package constraints. Range, fuel mass carried, tank volume and tank weight are stated in Table 2. All vehicle ranges have been calculated using the US Combined Cycle vehicle fuel economy simulation results. In this context, the combined cycle is the EPA certification test that takes the FUDs (without the warm-up period) and the HIWAY driving cycles into account.

Table 2: Tank Characteristics

| | DH | IM | IH |
|---|---|---|---|
| Range (miles) | 300 | 380 | 380 |
| Fuel mass carried (kg) | 4.13 | 46.6 | 25.8 |
| Volume (L) | 180 | 59 | 37.6 |
| Tank weight, empty (kg) | 64.7 | 10 | 10 |
| Tank weight, full (kg) | 68.8 | 56.6 | 35.8 |

* NOTE: IH fuel used is Iso-octane.

## 2.1.2 Vehicle Drive Cycle Results

### Energy Results

Vehicle drive cycle results are presented in Figure 1 for seven drive cycles. All three systems are characterized in terms of Wh/mile for each drive cycle. For every drive cycle, the DH vehicle showed the lowest energy consumption, whereas the IH vehicle results were the highest. However, the relative differences among the results for the three vehicles did not remain the same for every drive cycle.

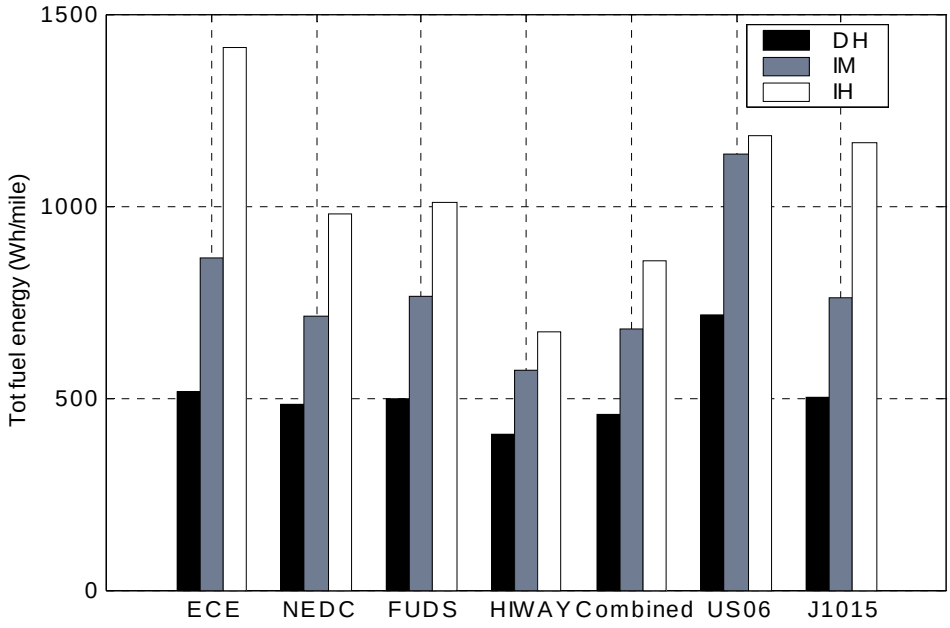


Figure 1: Vehicle energy consumption for several driving cycles

* NOTE: The results in Figure 1 assume the vehicles are fully warmed up over the entire drive cycle

* REFERENCE: A fully warmed up vehicle achieving a fuel economy of 25mpg (9.41L/100km) would equate to 1350 Wh/mile, and a fuel economy of 35mpg (6.72L/100km) would equate to 960 Wh/mile using conventional gasoline.

With higher average power drive cycles, such as the US06, the differences in energy consumption between the IM and IH vehicles were smaller. This is largely a result of a higher fuel cell system efficiency for the IH platform (which reflects the effects of characteristics of the subsystems and associated control systems). Typically at higher (but less dynamic) power demands, the IH fuel processor efficiency increases and approaches that of the IM fuel processor, thus affecting the system efficiency overall. Refer to Section 4.1.3 for additional details.

Not surprisingly, the HIWAY cycle resulted in lower energy consumption than the FUDS cycle for all three vehicles simulated. The FUDS cycle has a larger number of acceleration (and more importantly, deceleration) demands as well as sustained idle operation, which is inherently inefficient. This combination leads to higher energy requirements.

Overall, the energy consumption for the DH, IM and the IH vehicle vary significantly for different drive cycles. Specifically, on the FUDs cycle, the Wh/mile for the IM and IH were higher than the DH by approximately 45% and 100% respectively. On the US06 cycle, the percentage differences were approximately 60% and 65% respectively. The reasons for these variations are discussed further in the Fuel Cell System (and the fuel processor sub-system) sections in the full report.

Figure 2 displays the same vehicle performance information as shown in Figure 1, but in terms of the overall vehicle efficiency instead. The trends shown in Figure 2 are inverted compared to those in Figure 1. Vehicle efficiency is defined as:

$$\textbf{Vehicle Efficiency} = \frac{(Energy\ At\ The\ Wheel)}{(Fuel\ Energy\ Consumed)} * 100$$

where

**(energy at the wheel)** = (braking friction energy) + (climbing energy) + (energy needed to overcome aerodynamic drag) + (energy needed to overcome tire rolling resistance)

**(fuel energy consumed)** = fuel LHV energy content

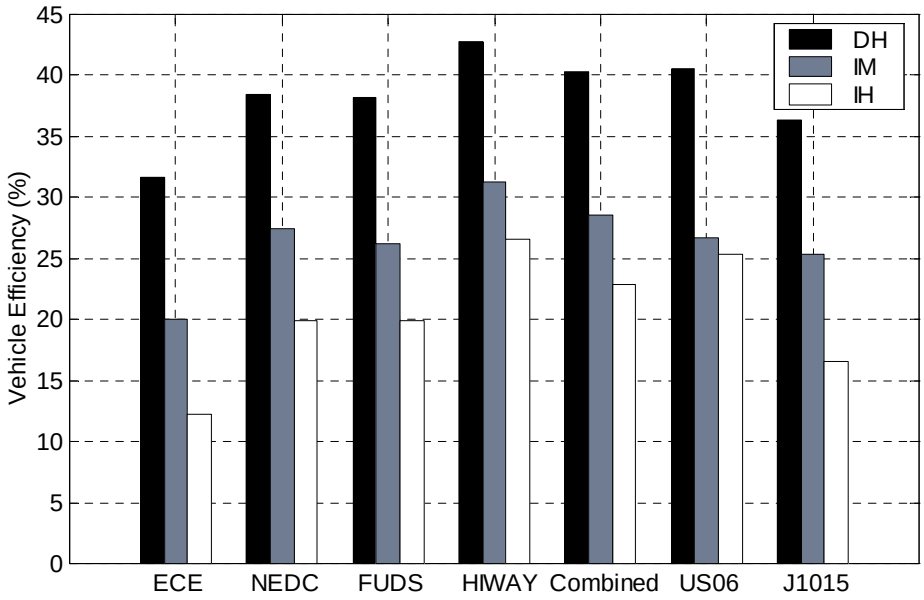


Figure 2: Vehicle energy efficiency for several drive cycles

Table 3 shows specific vehicle efficiencies for the three vehicle types in three drive cycles, FUDS, HIWAY, and the US06.

Table 3: Vehicle Efficiency, %

| | DH | IM | IH |
|---|---|---|---|
| FUDS | 38.2 | 26.2 | 19.8 |
| HIWAY | 42.9 | 31.3 | 26.7 |
| US06 | 40.6 | 26.7 | 25.3 |

The IM and IH vehicle efficiency values are similar for the US06 drive cycle, in contrast to the more apparent differences seen in all other drive cycles. The DH energy use is less variable with drive cycles than the IM and IH systems.

Figure 3 (A, B, C, D and E) shows the relative breakdown of the vehicle side energy consumptions. The main point that leaps out from these figures is that on the vehicle side, there is very little difference from the viewpoint of the propulsion, transmission, motor or auxiliary system losses. For all of the cycles, the primary difference in energy losses between the three vehicle types is from the fuel cell system.

This issue is discussed further in the Vehicle Section 4.1.3. Specifically, the energy spent for propulsion is approximately 200Wh/mile for the FUDs cycle and 300Wh/mile for the US06.

One should note that plots C, D and E in Figure 3 are drawn to different scales to better illustrate the vehicle side losses. Plots A and B in Figure 3 illustrate the varying requirements from the viewpoint of the energy consumption associated with these three vehicle types for the FUDS and US06 cycles respectively.

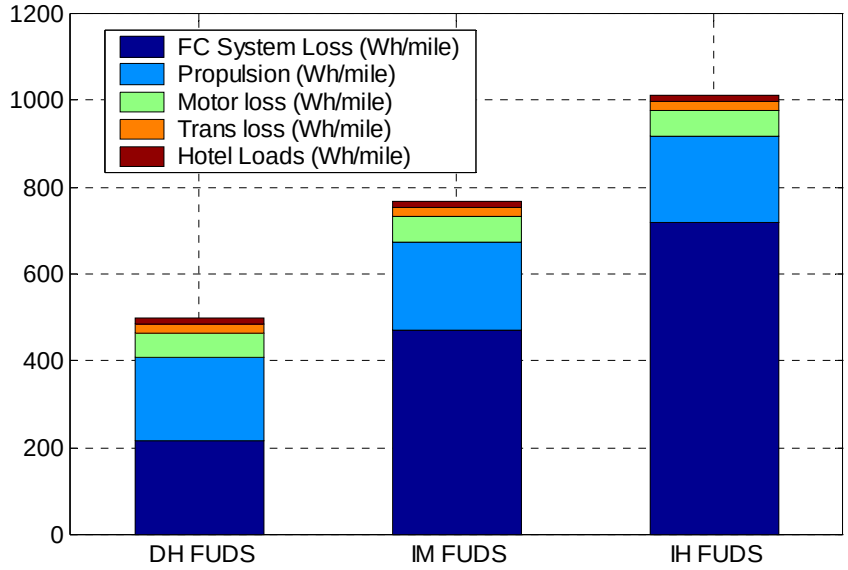


**(A) FUDS**

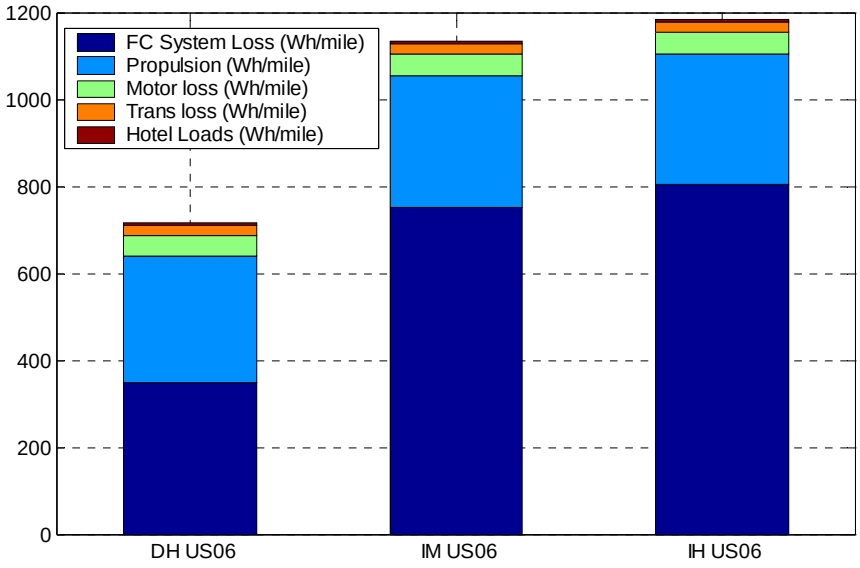


**(B) US06**

* Note, (A)/(B): The order of the items in the key are reversed relative to the figure

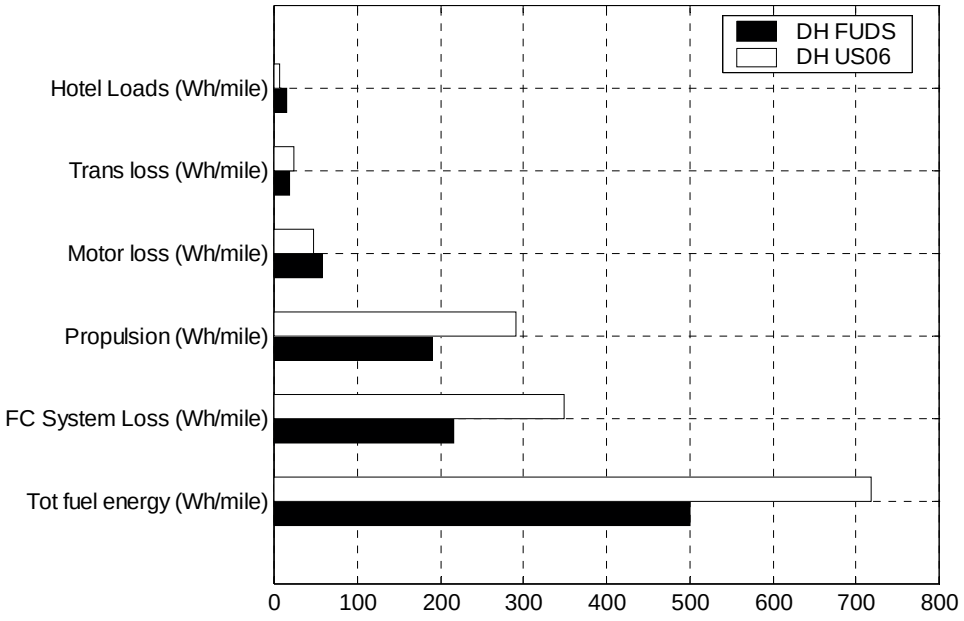


**(C) Direct Hydrogen**

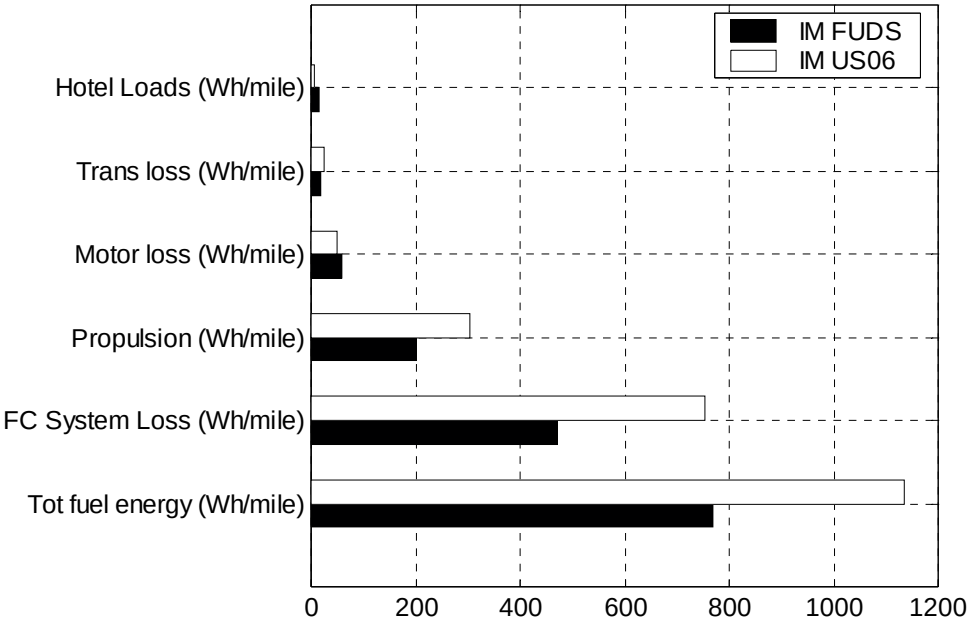


**(D) Indirect Methanol**

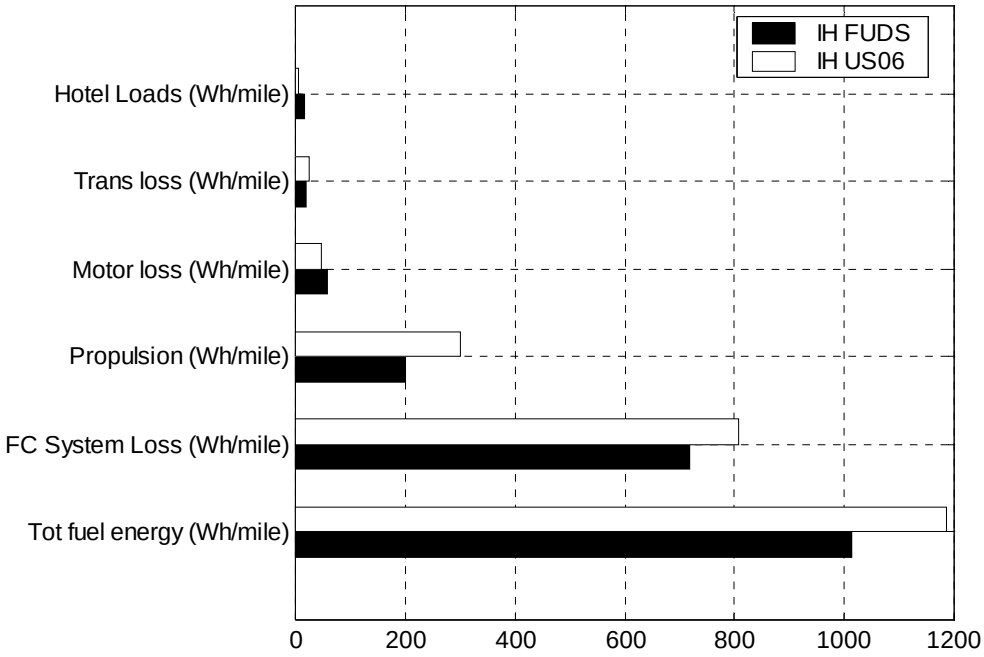


**(E) Indirect Hydrocarbon**

Figure 3: Fuel Cell Vehicle energy characteristics

* NOTE 1: Refer to Figure 29 in Section 4.1.3 for the corresponding Fuel Cell System energy diagrams.
* NOTE 2: Notice that the scales for the Wh/mile in parts C, D, and E are different.
* NOTE 3: The Tot fuel energy is the total fuel energy required for the vehicle operation over the entire drive cycle.

## Vehicle CO2 Emissions Results

The levels of CO2 emissions are shown below for different drive cycles and simply reflect the trends seen in the fuel consumption values shown for the drive cycles. For Direct Hydrogen there are no vehicle CO2 emissions. CO2 vehicle emissions for the IH are higher than for the IM in every drive cycle.

Table 4: CO2 emissions/mile in the different cycles (grams/mile)

CO2 emissions (moles/mile) * CO2 MW (44 grams/mol)

| | ECE | NEDC | FUDS | HIWAY | Combined | US06 | J-1015 |
|---|---|---|---|---|---|---|---|
| **DH** | 0 | 0 | 0 | 0 | 0 | 0 | 0 |
| **IM** | 216 | 176 | 189 | 141 | 167 | 282 | 189 |
| **IH** | 352 | 242 | 251 | 167 | 216 | 295 | 290 |

Table 5: CO2 emissions in the different cycles (moles)

(IM== total CH3OH ; IH== 8*total iso-octane)

| | ECE | NEDC | FUDS | HIWAY | Combined | US06 | J-1015 |
|---|---|---|---|---|---|---|---|
| **DH** | 0 | 0 | 0 | 0 | 0 | 0 | 0 |
| **IM** | 3.0 | 27 | 32 | 33 | 32 | 51 | 11 |
| **IH** | 5.0 | 38 | 42 | 39 | 41 | 53 | 17 |

Table 6: CO2 emissions/mile in the different cycles (moles/mile)

| | ECE | NEDC | FUDS | HIWAY | Combined | US06 | J-1015 |
|---|---|---|---|---|---|---|---|
| **DH** | 0 | 0 | 0 | 0 | 0 | 0 | 0 |
| **IM** | 4.9 | 4.0 | 4.3 | 3.2 | 3.8 | 6.4 | 4.3 |
| **IH** | 8.0 | 5.5 | 5.7 | 3.8 | 4.9 | 6.7 | 6.6 |

### 2.1.3 Major Observations: Tank-To-Wheel (TTW) Analysis

The following are the major overview observations from the analysis. Each of the observations is described in greater detail later in the complete report. Sub-system or component specific performance is not discussed here. Refer to Section 4.1.4 for these details.

Reference Figure 1 and Figure 3 (a) and (b) for the following comments:

1. The difference in vehicle mass for the three vehicle types analyzed is small (<7%), and the aerodynamic characteristics were kept the same. This results in minor differences in energy requirements at the wheel (propulsion energy) for a given drive cycle. The energy spent for propulsion is nearly the same for all three vehicles, approximately 200Wh/mile for the FUDs cycle and 300Wh/mile for the US06. Therefore, the primary reason for the differences in energy consumption for the three vehicle types is their fuel cell system efficiencies over the drive cycles analyzed. Note: Refer to Section 3.2.1 for a simple vehicle weight sensitivity study.
2. Generally, the energy consumption for the Direct Hydrogen (DH) vehicle is lowest for all simulated drive cycles. Additionally, the energy consumption for the Indirect Methanol (IM) vehicle is intermediate between that of the DH vehicle and the energy consumption of the Indirect Hydrocarbon (IH) vehicle for all the drive cycles. The difference in energy consumption among the vehicle types is significant. Refer to Section 4.1.3 for details regarding the fuel cell system efficiency differences.
3. Specifically, on the FUDs cycle, the Wh/mile for the IM and IH were higher than the DH by approximately 45% and 100% respectively. On the US06 cycle, the percentage differences were approximately 60% and 65% respectively.

Reference Figure 2 for the following comments:

4. The vehicle efficiencies for the DH, the IM, and the IH vehicle platforms on the FUDs cycle were approximately 38%, 26%, and 20% respectively. On the HIWAY cycle, the approximate efficiencies were 43%, 31%, and 27%. Additionally, on the US06 cycle, the approximate vehicle efficiencies were 41%, 27%, and 26%.
5. The IM and IH vehicle efficiency values are similar for the US06 drive cycle, in contrast to the more apparent differences seen in all other drive cycles. Refer to Section 4.1.3 for additional details.
6. The DH energy use is less variable with drive cycles than the IM and IH systems.

## 2.2 Upstream Energy Use and Emission Results (WTT)

Here it is important to remember that all the discussion, probabilistic curves and results are based on a 90% confidence range. Also all the upstream energy parameters use the higher heating value (HHV) of the respective fuel. Also note, as stated previously: For the indirect hydrocarbon example pathway, the final fuel composition (zero sulfur, no aromatics and high paraffin content) was the main reason to select NG over crude petroleum in the hydrocarbon (naphtha) case. Fisher-Tropsch Naphtha (FTN) was assumed.

### 2.2.1 Efficiency or Energy requirement:

The results change if the analysis considers different pathways or different combinations of pathways. For a single pathway analysis one can see that the best efficiency value for Fisher-Tropsch Naphtha (FTN) is in the range of 66 to 68% or 1.46 to 1.52 $GJ_{req\text{-}upstream}/GJ_{fuel\text{-}deliv.}$, assuming plants with cobalt catalyst, low temperature reactors and extra-steam exportation. In contrast, one will see a FTN pathway with efficiency around 48 to 51% if air is considered instead of oxygen in the syngas production and no extra-steam exportation is considered.

Similar efficiency variation can be observed for the hydrogen pathways, ranging from 63 to 67% (1.50 to 1.58 $GJ_{req\text{-}upstream}/GJ_{fuel\text{-}deliv.}$), for the centralized plant pathway. However 46 to 49% (2.04 to 2.16 $GJ_{req\text{-}upstream}/GJ_{fuel\text{-}deliv.}$) is observed for the decentralized hydrogen production pathway.

The methanol pathways have more concentrated results with the efficiency around 65 to 66% (1.51 to 1.53 $GJ_{req\text{-}upstream}/GJ_{fuel\text{-}deliv.}$) for the most efficient pathway (mega size plants, combined SMR and POX, extra-steam exportation) and 59 to 63% (1.60 to 1.69 $GJ_{req\text{-}upstream}/GJ_{fuel\text{-}deliv.}$) for the less efficient scenarios (typical size, SMR, no extra-steam exportation). See Section 4.2.5 for the details.

The combined scenarios analyzed in this study reflect a smaller variation in the parameters for each methanol pathway (i.e. the horizontal axes in Figure 83). Additionally, a smaller probability is associated with the hydrogen fuel pathway with the lowest energy efficiency, that of the decentralized plants (i.e. the horizontal axes in Figure 80). Reflecting this, the data in Figure 4 and Figure 5 show that the methanol efficiency ranges from 63 to 65% (1.55 to 1.59 $GJ_{req\text{-}upstream}/GJ_{fuel\text{-}deliv.}$), the hydrogen efficiency ranges from 54 to 60% (1.66 to 1.84 $GJ_{req\text{-}upstream}/GJ_{fuel\text{-}deliv.}$) and the FTN efficiency ranges from 56 to 58% (1.72 to 1.79 $GJ_{req\text{-}upstream}/GJ_{fuel\text{-}deliv.}$). See Section 4.2.4 for more details. See Table 7 below for a summary of this combined scenario.

Table 7: Upstream energy use, combined pathway scenario

| | Hydrogen | Methanol | FTN | |
|---|---|---|---|---|
| Upstream energy factor (mean), MJ/MJ or Wh/Wh | 1.66 | 1.55 | 1.72 | low = 5th percentile |
| | 1.75 | 1.57 | 1.75 | mid = mean |
| | 1.84 | 1.60 | 1.79 | high = 95th percentile |
| | *SD = 0.06* | *SD = 0.01* | *SD = 0.02* | |
| Upstream energy efficiency, % | 60.2 | 64.6 | 58.1 | |
| | 57.1 | 63.7 | 57.1 | |
| | 54.2 | 62.6 | 56.1 | |

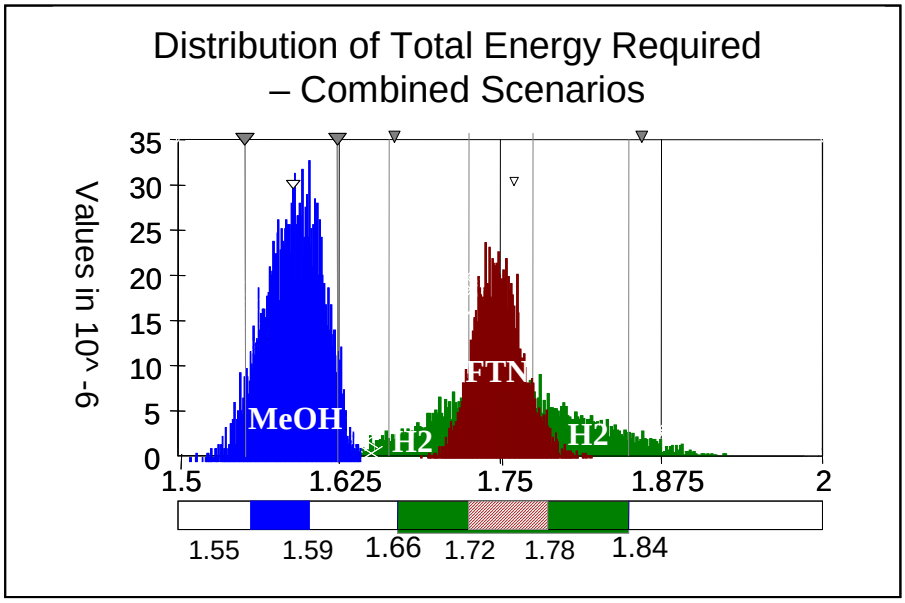


Figure 4 : Distributions for the total energy required upstream in the combined scenario ($GJ_{req\text{-}upstream}/GJ_{fuel\text{-}deliv.}$) – HHV

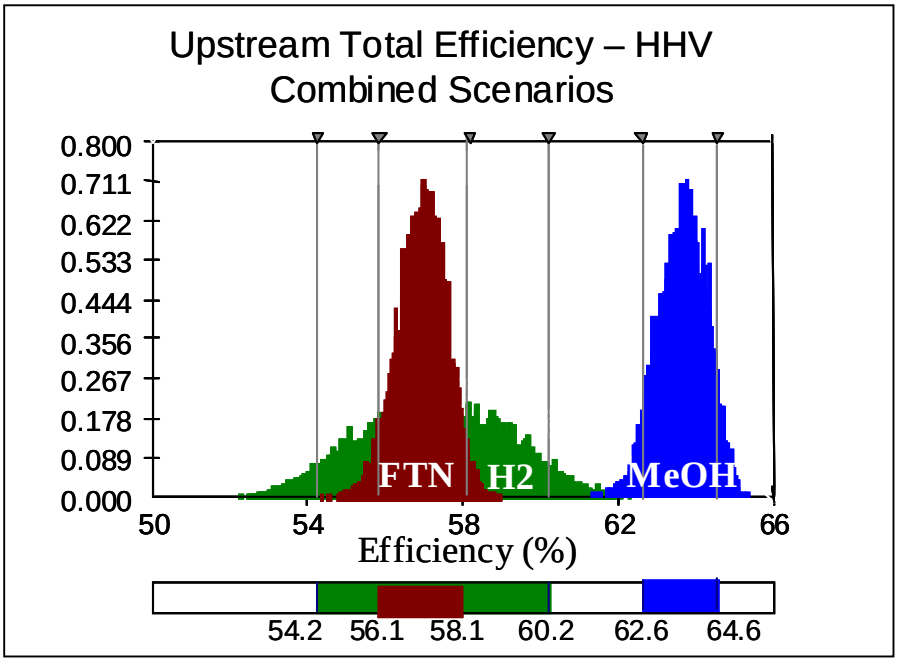


Figure 5 : Distribution for the total efficiency upstream in the combined scenario

### 2.2.2 $CO_2$ Emissions

In the same way as for efficiency, $CO_2$ emissions at the upstream level should be analyzed only as a reference per unit energy of fuel produced. The resulting upstream $CO_2$ is a function of the fuel pathway energy efficiency, the amount of energy consumed upstream needed to deliver the unit fuel to the vehicle fuel tank. The $CO_2$ emissions are also a function of the carbon content of the fuel (methanol contains 1 carbon atom per molecule and FTN approximately 8 carbon atoms per molecule). For the hydrogen fuel pathway, and only for this fuel, all of the feedstock fuel (NG) carbon content is released during the upstream processes. The fuel delivered, that of neat hydrogen, is carbon free.

Figure 6 shows the distribution of the upstream $CO_2$ emissions for the combined scenario. Within any given fuel pathway, the differences in $CO_2$ emissions are directly proportional to the energy efficiency of the particular process in the pathway. See Figure 83 in Section 4.2.6 for the upstream energy requirement for methanol and FTN fuels, the parameter affecting upstream $CO_2$ emissions.

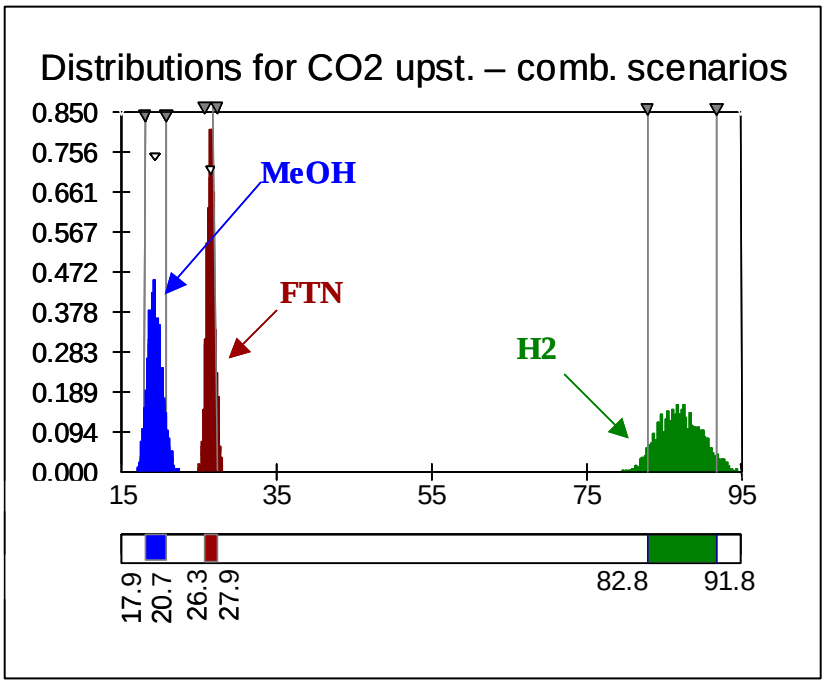


Figure 6 : Distributions for upstream $CO_2$ emissions of the combined scenario ($kg/GJ_{fuel\text{-}deliv.}$) - HHV

### 2.2.3 Criteria Emissions (In-Basin only)

The major concern for criteria emissions is when they are emitted in high-populated areas, because of the possibility of human exposure. FUEEM calculates the emissions disaggregated for each area. For the present analysis only the criteria emissions emitted inside the South Coast Air basin (SCAB) and the rest of California are presented.

Since the gas-to-liquids fuels (methanol and FTN) are produced overseas, the only SCAB criteria emissions come from the tanker activities in the port area through to the refueling process at the fuel stations. In contrast, hydrogen is assumed to be produced inside the basin and the emission calculations account for all the fuel pathway processes - from natural gas distribution to hydrogen production and through to the refueling process at the fuel stations.

### $NO_x$ Emissions

The hydrogen $NO_x$ emissions range from 5.53 to 8.06 grams per gigajoule of fuel delivered with a mean value of 6.70 $g/GJ_{deliv.}$, for the combined pathway scenario analyzed. For the variation in the different pathways see Section 4.2.5.

Methanol and FTN assume the same distribution and marketing activities for all pathways per unit volume of fuel. The $NO_x$ emissions for methanol range from 0.40 to 0.49 $g/GJ_{deliv.}$, with a mean of 0.45 $g/GJ_{deliv.}$. The lowest emissions occur for the FTN, ranging from 0.20 to 0.24 $g/GJ_{deliv.}$, with a mean value of 0.22 $g/GJ_{deliv.}$

The majority of these emissions come from internal combustion engines (ICE) used in the port activities (tug boat, pumps, etc.) and in the diesel trucks for distribution of the liquid fuels (methanol and FTN). The difference between the $NO_x$ emissions of methanol and FTN is related with the heating values and the fuel density differences. In the hydrogen case, $NO_x$ emissions from the natural gas reformers and from the electricity production determine the overall emission levels.

### CO Emissions

CO emissions follow the same rationale but with smaller differences between hydrogen and the liquid fuels (methanol and FTN). The hydrogen combined scenario CO emissions are from 2.08 to 4.53 $g/GJ_{deliv.}$, with a mean value of 3.29 $g/GJ_{deliv.}$. The methanol CO emissions go from 0.91 to 1.18 $g/GJ_{deliv.}$, with a mean value of 1.04 $g/GJ_{deliv.}$. The FTN CO emissions go from 0.43 to 0.56 $g/GJ_{deliv.}$, with a mean value of 0.49 $g/GJ_{deliv.}$.

### NMOG Emissions

Fugitive emissions are generally the predominant source of NMOG emissions generated in the fuel upstream activities. The evaporative and fugitive emissions of liquid fuels are larger than those for the hydrogen fuel. In the hydrogen case, the fugitive emissions are more associated with the natural gas fugitive emissions, which has NMOG components in its composition. The differences between the liquid fuels (methanol and FTN) NMOG emissions are due to the differences in vapor pressure, density and heating values of the fuels.

For the combined scenarios, methanol emits from 7.25 to 25.04 $g/GJ_{deliv.}$, with a mean value of 12.91 $g/GJ_{deliv.}$. FTN emits from 6.22 to 14.89 $g/GJ_{deliv.}$, with a mean value of 9.20 $g/GJ_{deliv.}$. Finally hydrogen emits from 1.21 to 4.97 $g/GJ_{deliv.}$, with a mean value of 2.96 $g/GJ_{deliv.}$.

### 2.2.4 Major Observations: Wheel-to-Tank (WTT) Analysis

The results presented in this summary section are the results of the example combined scenario fuel pathway only. Refer to Section 4.2.3 for a description of the combined scenario process. The example combination of pathways is still under discussion and does not represent a consensus selection from the expert-network. Considering the pathway choice is a very sensitive parameter for the energy requirement and $CO_2$ analysis, one should keep this in mind and refer to the other sections of the report for different pathway scenario results (Sections 4.2.5). Also remember that energy requirement analysis and $CO_2$ analysis only make sense on the entire life cycle (including the fuel being consumed in the vehicle), therefore the results here are only for reference. All the upstream energy values are based upon higher heating values (HHV).

Reference Figure 4, Figure 5, and Table 7:

1. Efficiency: Methanol has the best energy efficiency for the upstream activities (63.7% - mean). Fischer-Tropsch naphtha (FTN) and hydrogen have equal mean values (57.1 %). As shown in Figure 5, however, 33% of the hydrogen cases have better efficiency than FTN (58 up to 60 %) and, in the same manor, 29 % of the hydrogen cases have worse efficiency than FTN (56 down to 54 %). Refer to the variability of the efficiency in Figure 5. This shows the effect of the allocation of pathways for the fuels presented.
2. Total fuel $CO_2$ emissions: Methanol has the lowest mean upstream emissions (19.3 $Kg/GJ_{deliv.}$) followed by FTN (27.1 $Kg/GJ_{deliv.}$) and then hydrogen (87.1 $Kg/GJ_{deliv.}$). Note that this does not include vehicle $CO_2$ emissions from the three types of FCVs.

The significant differences in the levels of $NO_x$ and CO released inside of the urban air basin (SCAB) for the three fuels are due to the assumption (for this study) that hydrogen production is inside of the Basin and the gas-to-liquid fuels (methanol and FTN) are produced overseas (outside of the Basin). For NMOG, evaporative emissions of liquid fuels (methanol and FTN) are the major contributor, and the combination between the fuel density and the fuel vapor pressure define the major differences between the liquid fuels.

Reference Figure 73, Figure 74, Figure 77, and the tables in Appendix 5.3:

1. $NO_x$ emissions inside the basin (SCAB): FTN has the lowest emissions (0.22 $g/GJ_{deliv.}$ – mean), followed by methanol (0.45 $g/GJ_{deliv.}$ – mean) and hydrogen with a factor of more than ten compared to the methanol (6.70 $g/GJ_{deliv.}$ – mean).
2. CO emissions inside the basin (SCAB): FTN has the lowest emissions (0.49 $g/GJ_{deliv.}$ – mean), followed by methanol (1.04 $g/GJ_{deliv.}$ – mean) and hydrogen (3.29 $g/GJ_{deliv.}$ – mean).
3. NMOG emissions inside the basin (SCAB): Hydrogen has the lowest emissions (2.96 $g/GJ_{deliv.}$ – mean), followed by 38.3 % of the FTN cases (from 6.22 up to 7.25 $g/GJ_{deliv.}$). The rest of the FTN cases are tied with methanol (from 7.25 up to 14.89 $g/GJ_{deliv.}$) and 29.9 % of the methanol cases have the worse emissions (from 14.89 up to 25.04 $g/GJ_{deliv.}$).

# 3 Simulation Inputs and Assumptions

## 3.1 Simulation Performance Targets

The Partnership for a New Generation of Vehicles[2] (PNGV) defined for the 3X[3] car a set of vehicle targets. In this analysis a subset of these parameters are incorporated within the fuel cell vehicle design criteria. This subset is shown in Table 8.

Table 8: PNGV requirements for 3X car[i]

| PNGV Requirements | Target |
|---|---|
| 0..60 mph time | 12.0 sec |
| Maximum speed | 85 mph |

These targets primarily relate to the performance of the vehicle though there are many other attributes, e.g. noise, comfort, safety, package reliability etc., that are not addressed explicitly but are considered as much as possible in this discussion.

## 3.2 Simulation Inputs

### 3.2.1 Vehicle Model Inputs

All three vehicles (direct hydrogen, indirect methanol and indirect hydrocarbon) are configured as load following vehicles without additional energy storage and without the provision of regenerative braking. Figure 7 shows the energy flow and arrangement of the main vehicle components.

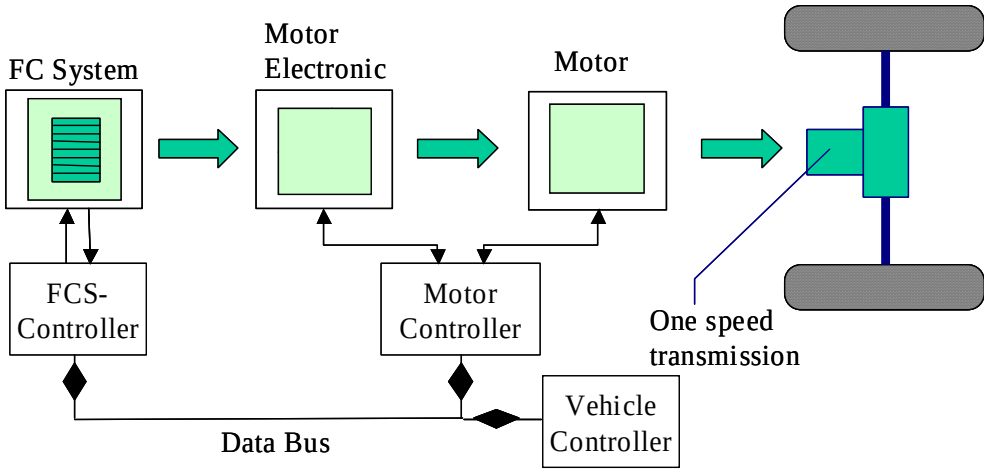


Figure 7: Configuration of the load following vehicle

[2] The Partnership for a New Generation of Vehicles (PNGV) is an public/private partnership between the U.S. government (7 agencies and 20 federal laboratories) and Chrysler, Ford, and General Motors that aims to strengthen the United States' competitiveness by developing technologies for a new generation of vehicles.

[3] PNGV's long term goal, dubbed the "Supercar" goal , is to develop an environmentally friendly car with up to triple the fuel efficiency of today's midsize cars-- without sacrificing affordability, performance, or safety.

The electric energy provided by the fuel cell system is fed into the drive-train. The motor electronic converts the dc power at the fuel cell stack terminals into ac power fed to the terminals of the AC induction motor. The motor provides the mechanical shaft energy via a one-stage reduction gear and a differential to the wheels. A fuel cell controller, a motor controller and an overall vehicle controller guarantee the optimum component interaction for all vehicle and component states.

## Methodology

The vehicle properties, such as aerodynamic drag coefficient, frontal area, tire diameter, and tire friction are kept unchanged for all three vehicles. However, the overall vehicle mass varies from concept to concept. Specifically, the IM vehicle is approximately 7% more massive than the DH vehicle.

The vehicles are designed on an equal performance basis. For all three vehicle types the electric drive-train including the transmission has been assumed to be the same. The justification for this is that the vehicles could meet within tolerances the minimum requirements stated in Table 8.

The main differences among the three vehicles are in the fuel cell system and the fuel used. These differences result in different fuel economy values and emissions. From the stack terminals to the wheels the performance differences between the vehicles are small and can almost be neglected. They are not zero due to different current voltage characteristics of the fuel cell stack and the differences in dynamic behavior of the three systems. Both effects force the electric side of the drive train to operate at slightly different operating points in each vehicle design even if the required drive cycle is the same.

In modeling the vehicles analyzed here, it is necessary to specify values for a number of vehicle parameters. These are essentially the input values that describe either the vehicle or, in certain cases, component properties. The parameters are either single-valued (i.e. the aerodynamic drag coefficient), tables (i.e. battery resistance as a function of the state of charge), or two-dimensional efficiency maps (i.e. motor and transmission efficiency). It is important to understand that the values of these parameters, or the technologies used (with their inherent parameters), are chosen so that the complete vehicle is able to meet the vehicle requirements as stated in Table 8. Therefore, the process of "designing" the vehicle is inherently iterative, and the parameter values in Table 9 are partially the result of this iteration process.

In addition, several parameters are determined at the beginning of the process, such as the aerodynamic drag and the frontal-area represent PNGV requirements. Several other component parameters are fixed, such as the shape and the values of the motor efficiency map and the transmission efficiency map. In contrast, other parameters such as the gear ratio and the fuel cell system net output power are the direct result of the iteration process.

In this section, the parameters in Table 9 will be reviewed and explanations will follow detailing their origination and assumptions. Additionally, the impact of variations in the parameters shall be discussed qualitatively.

Table 9: Vehicle Parameters

| Vehicle Type | Direct Hydrogen Vehicle | Indirect Methanol Vehicle | Indirect Hydrocarbon Veh | Comments |
|---|---|---|---|---|
| Vehicle | | | | Comparable to mid size passenger vehicle |
| Drag Coefficient | 0.3 | 0.3 | 0.3 | Comparable to mid size passenger vehicle |
| Frontal area | 2.20 $m^2$ | 2.20 $m^2$ | 2.20 $m^2$ | Comparable to mid size passenger vehicle |
| Wheels<br>Wheel radius<br>Total wheel inertia<br>Rolling friction coefficient | <br>0.3556 m<br>4 kg*m*m<br>0.01 | <br>0.3556 m<br>4 kg*m*m<br>0.01 | <br>0.3556 m<br>4 kg*m*m<br>0.01 | 14 ‘ wheel radius |
| Vehicle hotel load | 0.3 kW | 0.3 kW | 0.3 kW | |
| Maximum mechanical brake force | 10.000 N | 10.000 N | 10.000 N | |
| Test weight | See end of table | See end of table | See end of table | |
| Fuel cell system | | | | |
| Net Power<br>Power density<br>Static efficiency map | 66.5 kW<br>0.35 kW/kg<br>Figure 21 | 75 kW<br>0.25 kW/kg<br>Figure 21 | 70.5 kW<br>0.25 kW/kg<br>Figure 21 | |
| Fuel cell stack technology<br>Number of cells<br>Cell area<br>Membrane Resistance<br>Open circuit voltage<br>Polarity plot | PEM<br>450<br>360 $cm^2$<br>0.07 Ohm $cm^2$<br>0.9 V/cell<br>Figure 36 | PEM<br>450<br>470 $cm^2$<br>0.07 Ohm $cm^2$<br>0.9 V/cell<br>Figure 36 | PEM<br>450<br>650 $cm^2$<br>0.07 Ohm $cm^2$<br>0.9 V/cell<br>Figure 36 | |
| Fuel processor and gas clean up | - | Methanol steam reformer with | Gasoline (Iso Octane) | |

| | | | | |
|---|---|---|---|---|
| | | water gas shift reactor and preferential oxidation stage | Autothermal reformer with water gas shift reactor and preferential oxidation stage | |
| Burner | - | Catalytic - for anode exhaust and additional Methanol | Catalytic - for anode exhaust | |
| Reformate buffer<br>Volume<br>Maximum pressure<br>Minimum pressure | - | NOT USED IN THIS ANALYSIS<br>60 l<br>3 atm absolute<br>1.2 atm absolute | NOT USED IN THIS ANALYSIS<br>60 l<br>3 atm absolute<br>1.2 atm absolute | |
| Compressor | Vairex Twinscrew without expander | Vairex Twinscrew without expander | Vairex Twinscrew without expander | |
| Water and thermal management system | Water sustainable $80^{O}$C stack temperature | Water sustainable $80^{O}$C stack temperature | Water sustainable $80^{O}$C stack temperature | |
| Transmission | | | | |
| Number of gears | 1 | 1 | 1 | |
| Total gear ratio incl. differential | 8.9 | 8.9 | 8.9 | |
| Transmission efficiency map | Figure 8 | Figure 8 | Figure 8 | Transmission designed for EV |
| Electric Motor | | | | |
| Technology: | 75 kW Induction Motor | 75 kW Induction Motor | 75 kW Induction Motor | |
| Maximum Torque | 260 Nm | 260 Nm | 260 Nm | |
| Maximum Speed | 10.000 rpm | 10.000 rpm | 10.000 rpm | |
| | | | | |

| | | | | |
|---|---|---|---|---|
| Characteristic speed | 2750 rpm @ nominal voltage | 2750 rpm @ nominal voltage | 2750 rpm @ nominal voltage | |
| Nominal voltage | 312 V | 312 V | 312 V | |
| Motor efficiency map | Figure 10 | Figure 10 | Figure 10 | |
| Torque as a function of voltage | Figure 9 | Figure 9 | Figure 9 | |
| Motor inertia | 0.1 $kgm^2$ | 0.1 $kgm^2$ | 0.1 $kgm^2$ | |
| Scale factor (for torque only) | 1.0 | 1.0 | 1.0 | |
| Mass balance | | | | |
| Shell mass | 1000 kg | 1000 kg | 1000 kg | |
| Payload<br>Driver<br>Luggage | <br>75 kg<br>60 kg | <br>75 kg<br>60 kg | <br>75 kg<br>60 kg | From PNGV 300 lb payload |
| Fuel cell system mass[4] | 190 kg | 300 kg | 282 kg | |
| Motor mass (including power electronic and transmission) | 112.5 kg | 112.5 kg | 112.5 kg | Based on Ford Ecostar 68 kW, scaled |
| Fuel (full tank assumed) | 4.13 kg hydrogen equivalent to 68.8 kg full tank mass for 300 miles[5] | 59 l for 380 miles equivalent to 46.6 kg +10 kg (Tank) | 37.6 l for 380 miles equivalent to 25.8 kg +10 kg (Tank) | Compressed hydrogen storage capacity: 6 % weight @ 5000 psi<br>Methanol density: 0.79 kg/l<br>Iso-Octane density: 0.69 kg/l |
| "Test" weight incl. driver | 1506 kg | 1604 kg | 1565 kg | |

[4] Includes water and thermal management system. Excludes fuel tank, fuel and dc-dc converter.
[5] Combined cycle.

### Aerodynamic Drag Coefficient

The aerodynamic drag coefficient (0.3) and the frontal-area (2.20 $m^2$) represent values for a mid size passenger vehicle. In comparison, the Ford Taurus has an aerodynamic drag coefficient of 0.3. Decreasing the aerodynamic drag coefficient from 0.3 to 0.27 leads to a decrease in overall energy consumption of 1.1% for the FUDS cycle and of 4.0% for the US06 cycle. Even if the vehicles would have slightly different drag coefficients because of different cooling loads the overall influence seems to be minor in the relative comparisons of the three vehicles.

### Wheels

The wheels are described by the parameters *wheel diameter*, *wheel inertia* and *rolling resistance*. The wheel diameter together with the gear ratio relates the motor shaft speed to the vehicle velocity. This parameter therefore influences the vehicle acceleration and maximum speed significantly. However, this influence can be corrected by choosing an appropriate gear ratio. For this reason, the wheel diameter of a typical mid-size sedan (tire size 185/70 R 14) was chosen and remained constant.

The assumed wheel inertia is a good approximation for the inertia of an average steel wheel. This property mainly influences the acceleration time considering the rotational inertia of the wheels effectively increases the inertia of the vehicle (nominally given by the vehicle mass) during the acceleration phase.

The third wheel parameter is the rolling resistance. For the purposes of this first analysis, the rolling resistance is kept constant (independent from the vehicle velocity), though the model allows the optional use of a velocity dependent rolling resistance. The assumed value for the rolling resistance corresponds to tires with very low rolling friction and can be increased if comfort and safety issues are paramount. Again, the influence of this parameter on the overall energy consumption has been determined. A decrease of the tire friction coefficient from 0.01 to 0.009 reduces the energy consumption by 1.8% in the FUDS cycle and 1.7% in the US06 cycle.

### Fuel Cell System

See Section 4.1.2.

### Transmission

For the transmission model, the single speed transmission has been assumed. This transmission has been specially designed for electric drive train applications. As the transmission ratio (first gear reduction and differential) a value of 8.9 has been assumed. The overall transmission ratio largely influences the vehicle acceleration and top speed. A higher transmission ration increases the acceleration but decreases the top speed of the vehicle. To avoid compromising between the acceleration and top speed, a two-speed transmission could be used in the model. However, since the vehicle can meet the current performance requirements (acceleration from 0-60 miles in 12 sec and a maximum speed of 85 mph) a single-speed transmission was used. Besides the overall gear ratio, the other main input parameter into the model is a two-dimensional efficiency map.

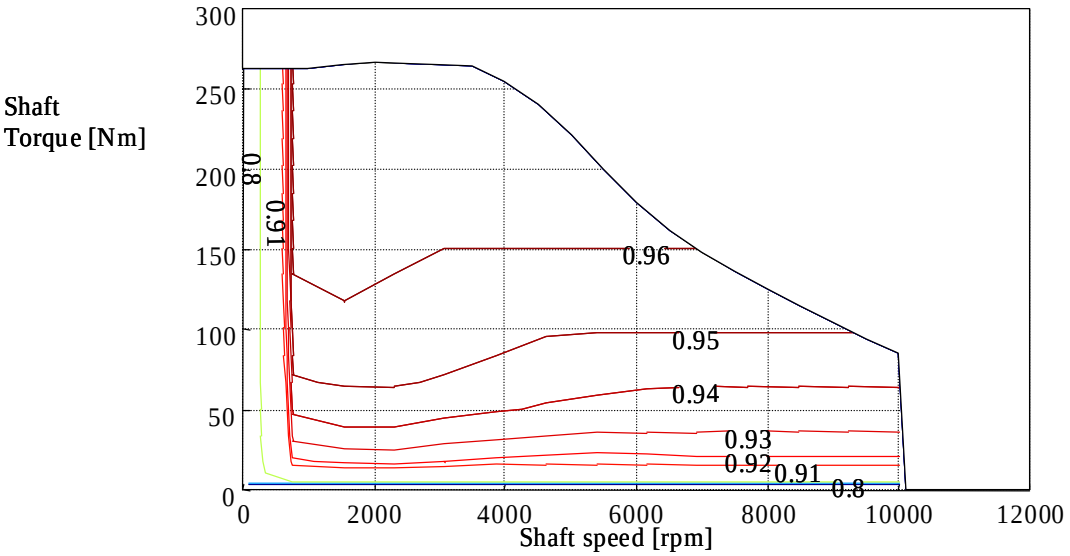


Figure 8: Transmission efficiency map (1-speed transmission including differential)

## Electric Motor

The basis for the electric motor model is a 75 kW 3-phase induction motor. The applied motor model specifies a line of maximum torque as a function of the motor speed (rpm) and supply voltage (Figure 9), a two-dimensional lookup table, providing the efficiency as a function of torque and motor speed (Figure 10), the motor inertia, the maximum speed and finally the motor mass[6].

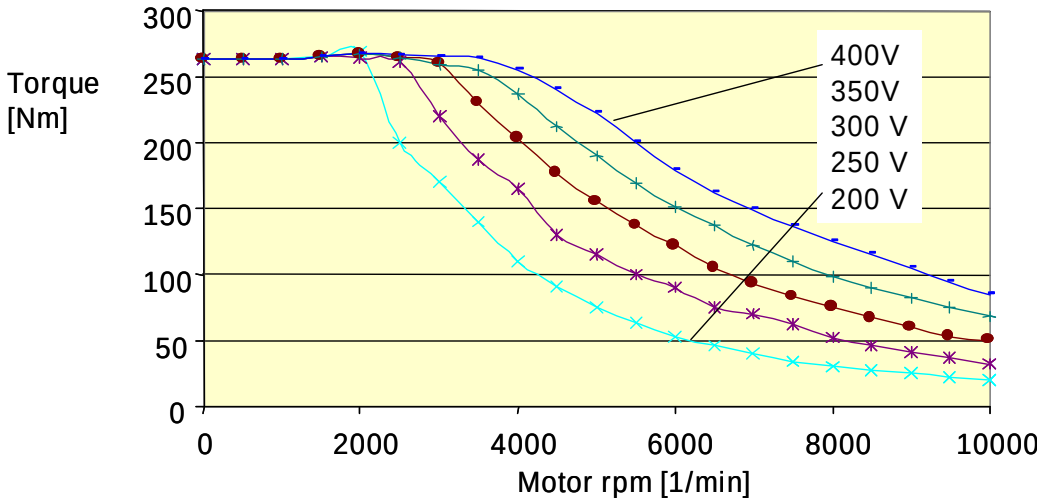


Figure 9: Motor torque speed characteristic (75 kW induction motor)

[6] The motor mass has been estimated based on the weight of a 68 kW transaxle motor (Ford Ecostar 2001). The motor weight entered in the model includes the weight of the motor, the power electronics and the transaxle transmission. It has been scaled linearly with the peak power (the peak power increase from 68 kW to 75 kW results in a weight increase from 102 kg to 112.5 kg).

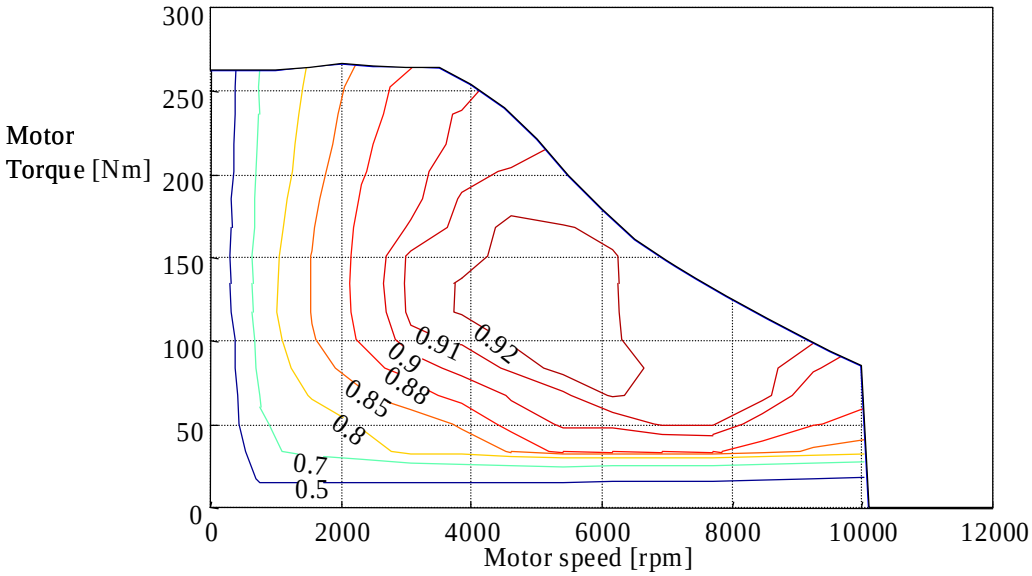


Figure 10: Motor efficiency map (75 kW induction motor)

### Vehicle Hotel Load

The vehicle hotel load represent the drive cycle average power consumption of electric accessories such as lights, indicators, power steering, power locks, windshield wipers, control systems, electronics, stereo and others. The total load is set to 0.3 kW. Not included is the air conditioning system, which would intermittently require an additional 3-5 kW. Also, a possible electric heating system is assumed to be turned off.

The hotel load of 300W is small which benefits the overall fuel economy of the vehicles. However, considering all vehicles are modeled in the same manner, the above assumption should not impact the relative vehicle comparisons. The accessory loads associated with the fuel cell system (the major effects are from the compressor and fans) are modeled, and taken into account in the Fuel Cell System Model (see Section 4.1.2)

### Mass

The vehicle mass is the sum of shell mass, payload including driver, fuel cell system mass, hydrogen storage mass, and motor and transmission mass and fuel mass. In the model, the vehicle shell mass also includes the mass of the cooling system A shell mass of 1000 kg is assumed which is derived from the weights of current passenger vehicles by subtracting 33% of the weight for the engine, exhaust etc. The vehicle shell is then loaded with the fuel cell system, the electric drive system, fuel (for the DH, the weight of the hydrogen storage system) and pay load (75 kg driver and 60 kg luggage). The final overall vehicle weight is stated in Table 9 and varies between vehicle concepts.

A simple sensitivity study was conducted on the effect of total vehicle mass on the resulting vehicle energy usage (fuel consumption energy). Specifically, for the DH platform on the FUDs driving cycle, if the vehicle mass is increased by 10% from 1500 kg to 1650 kg, the energy consumption increased by 7%. Alternately, for the same vehicle platform on the US06 cycle, the same 10% mass increase resulted in an 8%

increase in fuel consumption. This points out that although the energy consumption does not proportionally increase with vehicle mass, it is dependent on the driving cycle used.

Table 10: Example vehicle weights of mid size passenger vehicles, MY 2001

| Vehicle | Class | Engine Size | Weight [lb] |
|---|---|---|---|
| Honda Accord | Midsize | 3.0L, 6cyl | 3329 |
| Toyota Camary | Midsize | 3.0L, 6cyl | 3241 |
| Ford Taurus | Large | 3.0L, 6cyl | 3392 |
| Chevrolet Malibu | Midsize | 3.1L, 6cyl | 3077 |
| Chevrolet Lumina | Midsize | 3.1L, 6cyl | 3327 |
| Dodge Stratus | Midsize | 2.7L, 6cyl | |
| Dodge Intrepid | Large | 2.7L, 6cyl | 3489 |
| Volkswagen Passat | Midsize | 2.8L, 6cyl | |
| **Average** | | | **3309 (1500 kg)** |

* Source: EPA certification data

### 3.2.2 Inputs into Upstream Energy and Emissions Model

See Section 4.2 for this information.

# 4 Vehicle and Fuels Analysis - Details

## 4.1 Fuel Cell Vehicle Analysis (TTW)

### 4.1.1 Vehicle Characteristics

#### Physical Vehicle Model

In this section the model for the vehicle and it's main components and component arrangements will be explained. The main vehicle control model contains the four sub blocks "Drive Train", "Vehicle Curb", "Power Source" and "Vehicle Controls" (Figure 11).

The inputs of this block are the brake pedal position and the acceleration pedal position. Both are derived in the previous chapter. The model output is the actual vehicle velocity. The acceleration pedal position feeds into the block "Drive Train" and determines the fraction of the maximum motor torque available supplied to the vehicle wheels. The brake pedal position feeds into the block "Vehicle Controls". This block separates regenerative braking (in hybrid vehicles only) and mechanical braking. The request for regenerative braking is fed to the block "Electric Motor" and the request for mechanical braking is fed directly to the block "Vehicle Curb".

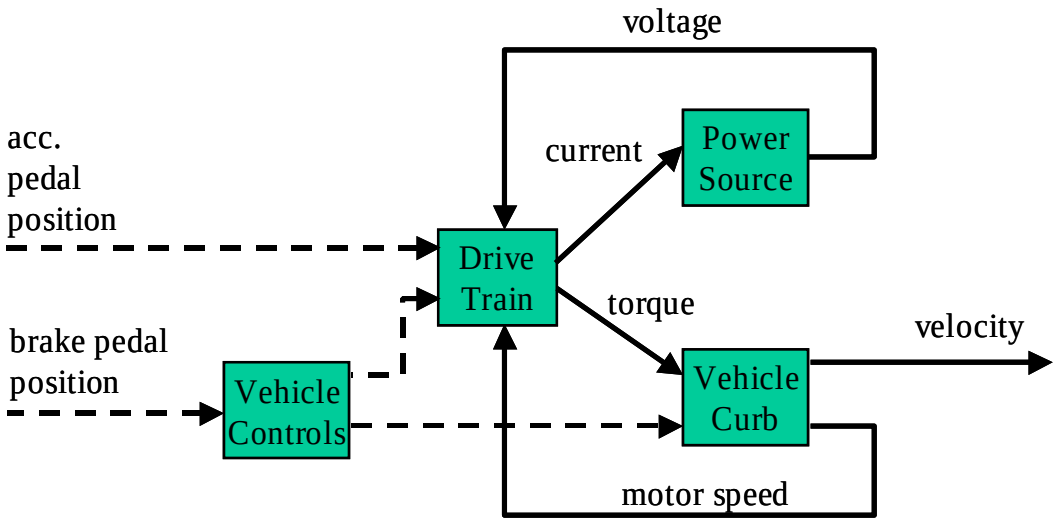


Figure 11: Contents of the vehicle control model

The block "Drive Train" includes models for the power electronics for the electric motor, the electric motor, controls for the electric motor and the transmission. Depending on the driver request, expressed by the acceleration pedal position and brake pedal position, the block "Drive Train" provides torque to the wheels and draws current from the power source (battery, ultra capacitor or fuel cell stack).

The block "Vehicle Curb" models the mechanical properties of the vehicle curb such as aerodynamic drag, rolling resistance, mass etc. The inputs into this block are the applied wheel torque and the signal for the mechanical brake fraction. The outputs are

the vehicle velocity and the motor speed. In designs not considering tire slip and a one-speed transmission both values are directly correlated with one another.

The block "Power Source" could include models for a fuel cell system, a battery system, an ultra capacitor system or a combination of all three systems. The input of this block is the electric current drawn by the motor. The output is the voltage seen by the dc terminals of the power electronics for the electric motor. For the case of a non-hybrid fuel cell vehicle this is the same voltage as the fuel cell stack voltage. In hybrid designs this voltage could be the battery voltage or any other voltage depending on the exact design.

The overall design of the vehicle model incorporates two major feedback loops motivated by the dependence of the maximum motor torque of the electric drive train on the voltage supply and the motor speed. As soon as the driver signals a torque request the electric drive train starts providing torque to the wheels. Because of this torque supply the vehicle accelerates and the motor speed increases. This increase in motor speed feeds back to the block "Drive Train" because of the sensitivity of the motor torque to fluctuations of motor speed. This feedback loop represents the feedback on the mechanical side of the vehicle.

As soon as the motor starts spinning it provides mechanical power to the wheels. It can only do this by drawing electrical power from the block "Power Source". As the result the motor draws an electric current from the power source. Due to the internal resistance[7] of the power source the voltage at the motor terminals drops depending on the load current drawn. Because of the sensitivity of the maximum motor torque on the supply voltage the drop in voltage feeds back to the electric drive train. This feedback loop represents the feedback effects on the electrical side. Mechanical and electrical feedback together determine the overall characteristics of the combined system drive train, power source and vehicle curb, which form the overall vehicle model.

This setup of the vehicle is close to the setup of a physical vehicle. The only interface[8] between the drive train and the source of electric power is the electric connection between both components. This interface can be fully described by change of voltage and current over time. On the mechanical side the interface variables between the drive train and the vehicle curb are the wheel torque and the wheel speed. Similar to the electric side the interface can be fully described by providing both values in time.

### Properties of the vehicle and the vehicle environment

The overall vehicle is modeled according to the force balance stated in Equation 1. This equation accounts for the aerodynamic drag force, friction force due to the rolling resistance of the tires, the vehicle inertia including rotational inertia of tires, motor and transmission, and the climbing force necessary to climb a hill. The sum of all these forces is the required force to operate the vehicle ("motor" force and friction brake force).

$$F_{motor} + F_{brake} = F_{friction} + F_{drag} + F_{inertia} + F_{climb} \quad (1)$$

The sum of all forces impacting the vehicle determines, together with the vehicle mass, the vehicle acceleration. The integration of the vehicle acceleration results in the

[7] The internal resistance could vary over time
[8] Except information flow

vehicle velocity. The required starting value at t=0 sec represents the vehicle velocity at t=0 sec. This initial velocity is set to 0 km/h.

### Vehicle energy analysis

In the following section the energy flows in the vehicle (starting at the dc terminals of the power electronics and ending at the wheel including the different loss mechanism) will be analyzed. The objective is to investigate the impact of the variations in energy flows from vehicle type to vehicle type and its potential impact on the variations of fuel economy.

Figure 1 shows the overall energy consumption of the three different vehicles for a total of seven different drive cycles. The drives cycles are three US drive cycles (Federal Urban Drive Schedule, Federal Highway Cycle and US06 cycle), the US combined cycle, two European drive cycles, and one Japanese drive cycle. The following conclusions can be drawn about the DH, IM, and IH vehicle energy consumption:

- The energy consumption for the direct hydrogen vehicle is lowest for all simulated drive cycles.
- The energy consumption for the Indirect Methanol vehicle is in all drive cycles higher than the energy consumption of the direct hydrogen vehicle but lower than the energy consumption of the indirect hydrocarbon vehicle.
- The energy consumption of the indirect hydrocarbon vehicle is highest for all drive cycles.
- The difference in energy consumption of the vehicles is significant. For example the energy consumption of the direct hydrogen vehicle is roughly half the energy consumption of the indirect hydrocarbon vehicle in the FUDS cycle.
- For the US06 cycle the difference in energy consumption between indirect methanol and indirect hydrocarbon is small.

In the following discussion the reasons for the differences in fuel economy are investigated. The investigation starts at the vehicle side with the comparison of the energy losses at the wheel and the drive train. After this, the energy flows and losses in the different fuel cell systems will be discussed. For better readability only three of the in total five drive cycles will be considered in this investigation. These are the FUDs cycle the Highway cycle and the US06 cycle.

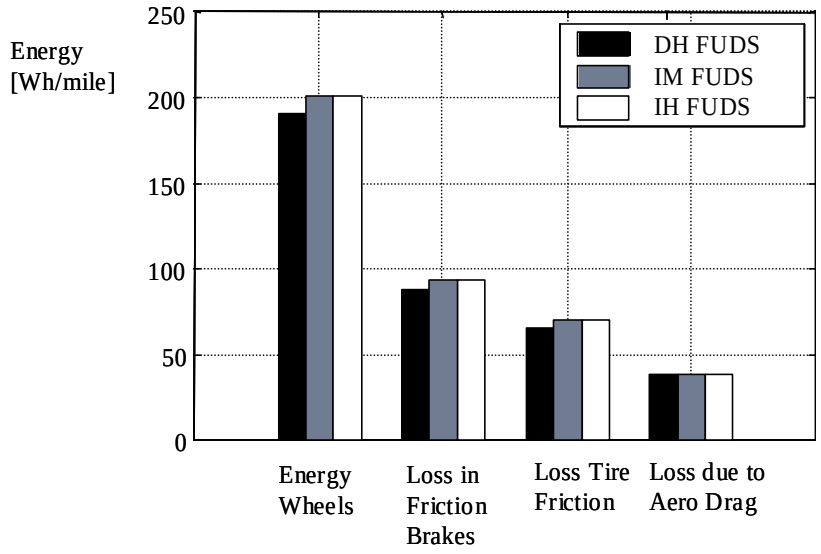


Figure 12: Energy at the wheel for the different vehicle concepts in the FUDs cycle.

Figure 12 displays the energy flows at the wheel for the FUDs cycle. It should be noted that the Aerodynamic drag losses are equal for all three vehicles. This is a direct result of the assumption of the same drag coefficient and frontal area for the vehicles or in other words of the same vehicle body shape. The tire friction losses of the indirect methanol and indirect hydrocarbon vehicle are also identical while the tire friction loss of the direct hydrogen vehicle is slightly lower. The reason for the identical tire friction loss of the vehicles with on board reformer is the assumption of an identical test weight for these vehicles. In contrast the direct hydrogen vehicle has slightly lower weight resulting in less tire deformation and friction losses. The weight differences are also responsible for differences in brake friction losses. For the same cycle (FUDs) the heavier vehicles require higher braking forces resulting in higher brake frictional losses. The wheel energy required to move the vehicle over the cycle is the sum of the aerodynamic drag losses, the brake friction losses and the tire friction losses. Consequently the wheel energy supplied to the wheel varies only little (less than 5%) among the different vehicle types. It could be concluded that this difference is not responsible for much larger differences in vehicle fuel economy.

The discussion above was done for the FUDs cycle. It could be repeated with the Highway and US06 cycle. However the energies displayed in Figure 13 for the Highway cycle and Figure 14 for the US06 cycle show a very similar pattern for these cycles.

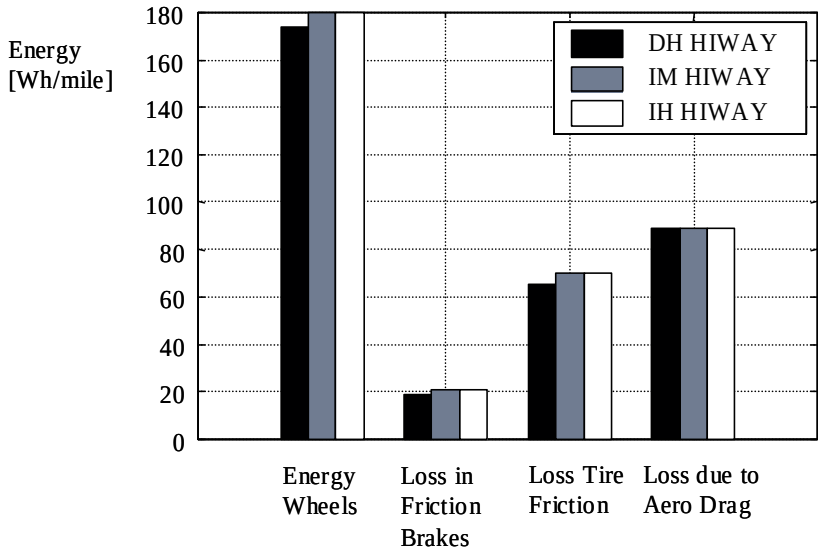


Figure 13: Energy at the wheel for the different vehicle concepts in the Highway cycle.

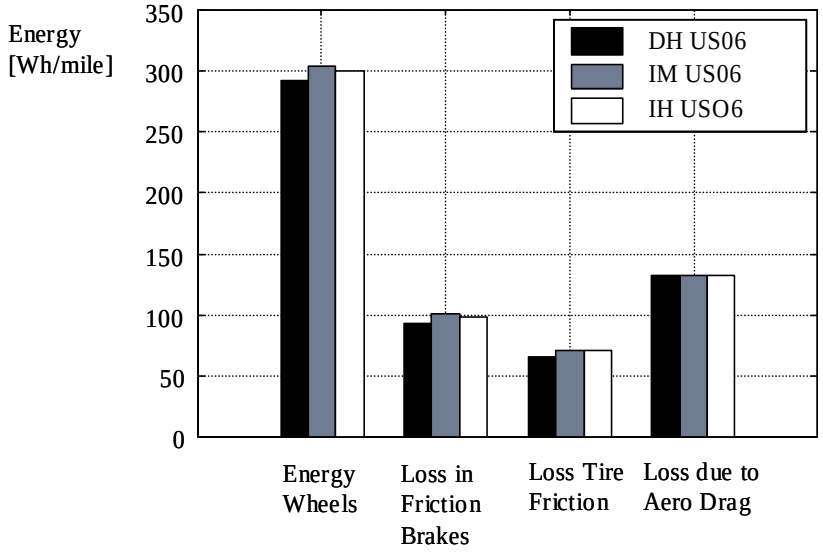


Figure 14: Energy at the wheel for the different vehicle concepts in the US06 cycle.

The main reason for showing Figure 13 and Figure 14 is that they allow a consistency check, which increases the level of confidence in the modeling work. Comparing Figure 12 with Figure 13 it could be seen:

- In the Highway cycle the aerodynamic drag losses are significantly higher than in the FUDs cycle.
- In the Highway cycle the brake friction losses are lower than in the FUDs cycle.
- The tire friction losses are equal in the Highway and in the FUDs cycle (This is a consequence of the assumption of an velocity independent tire friction coefficient).

Comparing Figure 12 with Figure 14 it could be seen:

- The braking losses in the significantly more dynamic US06 cycle are higher than in the FUDs cycle and also higher than in the Highway cycle.
- The aerodynamic drag losses in the US06 cycle are higher than in the two other cycles (result of the in average higher vehicle velocity of the US06 cycle)
- The tire friction losses in the US06 cycle stay unchanged compared with the other cycles.

*Summary wheel Energy:*
It could be concluded that:

- The differences of the energy supplied to the wheel could explain why the vehicles show different energy consumption values in different drive cycles.
- The differences in wheel energy are small and do not explain why the energy consumption vary significantly from vehicle type to vehicle type, e.g. between the direct hydrogen and indirect hydrocarbon fuel cell vehicle.

In the next step the effects of the drive train losses will be investigated. Figure 15, Figure 16, and Figure 17 show the electric energy flowing into the terminals of the motor power electronic, the mechanical energy at the motor shaft and the mechanical energy supplied by the transmission[9] to the wheels.

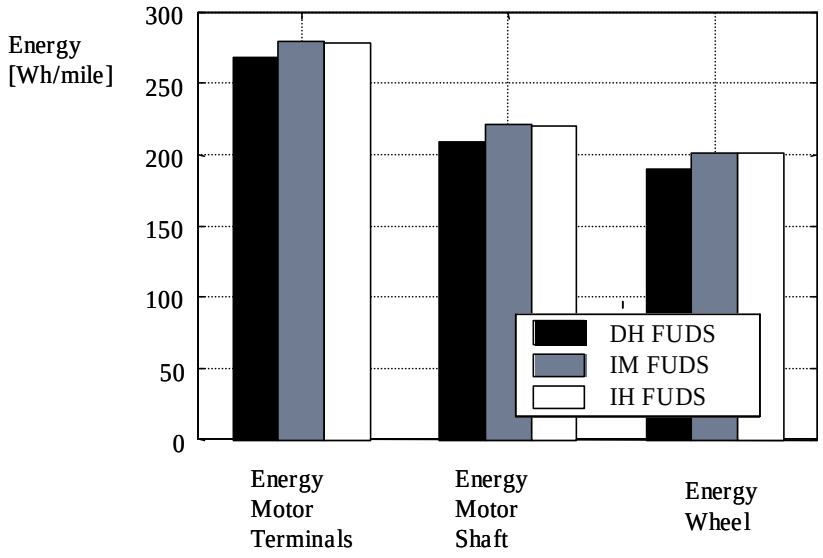


Figure 15: Energy flow from the motor terminals to the wheel for the FUDs cycle

Figure 15 shows the energy flow (per mile) for the FUDs cycle. It could be seen that the electric energy supplied to the motor is almost identical for the indirect methanol fuel cell vehicle and the indirect hydrocarbon fuel cell vehicle. The existing small differences are due to the different voltage characteristics of the fuel cell systems

[9] In this analysis the transmission and differential losses are lumped together.

supplying the energy to the electric motor. This differences in supply voltage force the drive train to operate at slightly different operating points, which results in different motor and transmission efficiencies. Compared to the two vehicle concepts with on board reformer the vehicle with direct hydrogen storage draws less power at the motor terminals (ca. 5%). This lower energy consumption is a direct result of the lower vehicle mass. The same trends observed at the electrical side of the motor could be seen at the mechanical side (motor shaft) and at the wheels. The differences are that the energy flow at the motor shaft is reduced because of the motor losses (including the losses in the power electronic) and the energy flow into the wheels is reduced by the transmission losses (including differential).

The average efficiency of the motor in the FUDs cycle is ca. 79% for all three-vehicle types. The average efficiency of the transmission (including differential) in the FUDs cycle is ca. 91%.

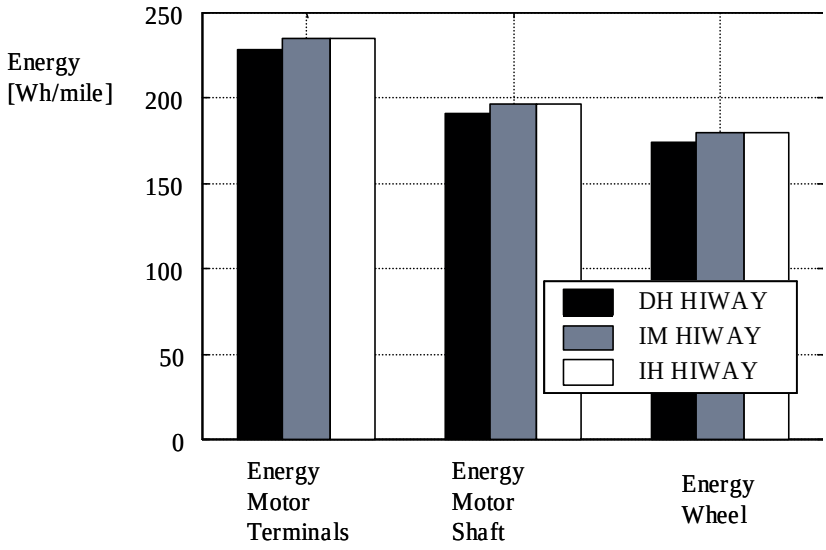


Figure 16: Energy flow from the motor terminals to the wheel for the Highway cycle

The same trends as in the FUDs cycle could be observed for all other investigated cycles. For the federal Highway cycle the average motor efficiency is 84% the average transmission efficiency is 91%. Figure 16 shows the energy flows for all three vehicle types for the federal highway cycle.

Figure 17 shows the energy flows in the drive train for the US06 cycle. The average motor efficiency in this cycle is 87% and the average transmission efficiency is 93%.

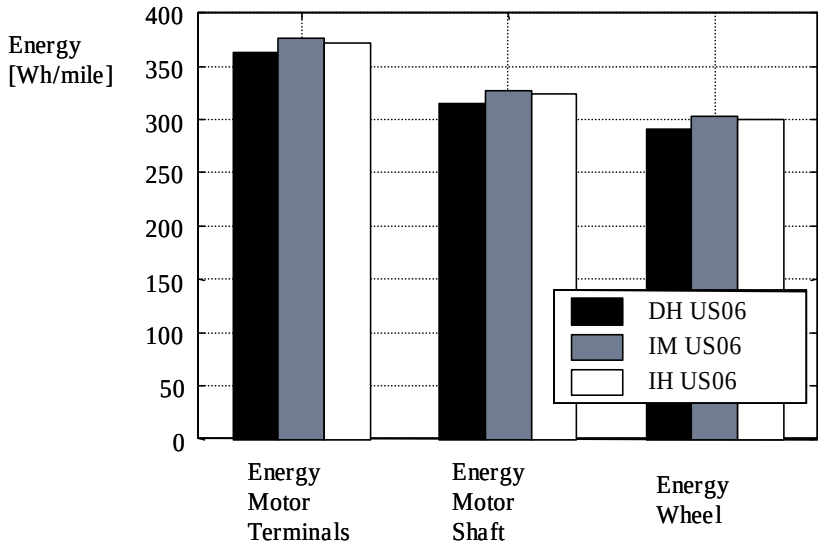


Figure 17: Energy flow from the motor terminals to the wheel for the US06 cycle

Summary: The differences in Fuel economy shown in Figure 1 for the different vehicle types cannot be explained with the different energy requirements at the wheel nor with the different energy requirements at the dc-dc terminals of the motor power electronics. Because the vehicle auxiliaries (headlights, indicators and fans) are assumed as a constant load of 300 W and are not different from vehicle type to vehicle type it could be concluded that the bulk part of the differences in vehicle fuel economy of the different vehicles is due to differences in the processes within the fuel cell system. Only a fraction of the higher fuel economy of the direct hydrogen vehicle could be explained with the lower mass of this vehicle. The lower weight of the direct hydrogen vehicle would result in a ca. 5% higher fuel economy compared to the indirect methanol or indirect hydrocarbon fuel cell vehicles.

### 4.1.2 Fuel Cell System (Overview)

As mentioned in the sections above, three distinct fuel cell systems were considered for this study: a) the direct hydrogen system, b) the indirect methanol fuel processor based system and c) the indirect hydrocarbon based fuel cell system.

Within each of the systems the dominant components were identified and care was taken to understand the level of model complexity needed to adequately capture their impact on the overall system. The final selection of the baseline systems were made after a careful review of the different possible fuel cell configurations from the viewpoint of enhancing performance and minimizing system complexity. The configurations are **not** to be considered definitive “designs” but simply baseline models and the results presented in this study may change with alterations in the system design. The model per se is flexible enough to handle a variety of different system configurations.

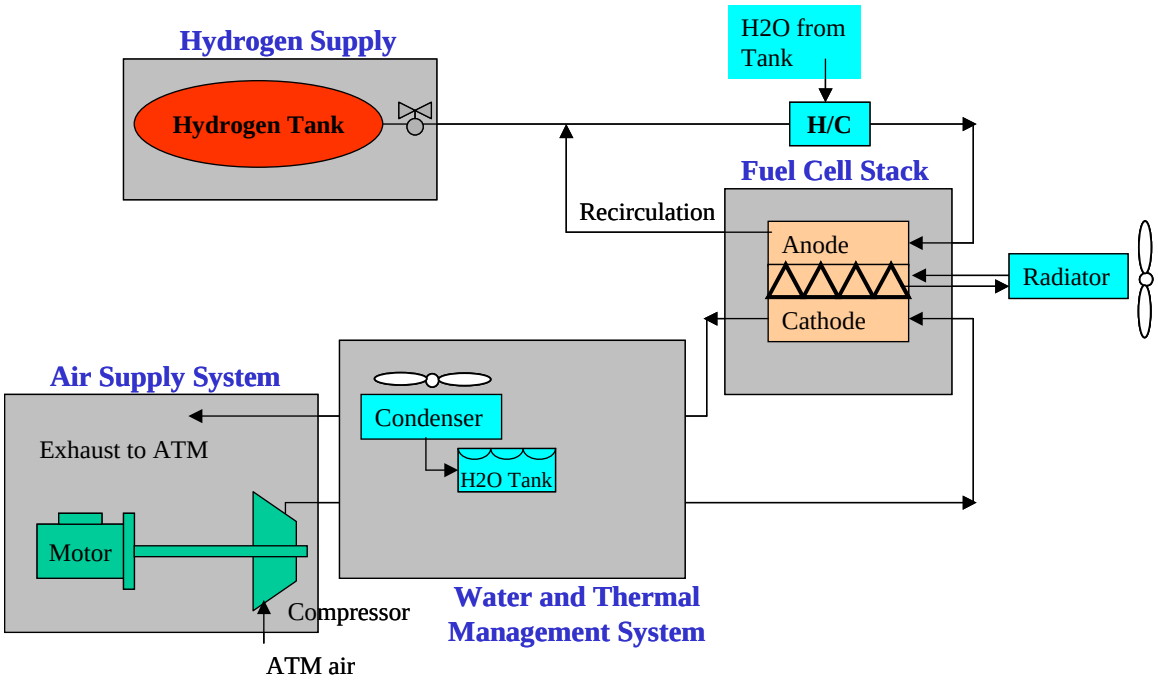


Figure 18: DHFC System

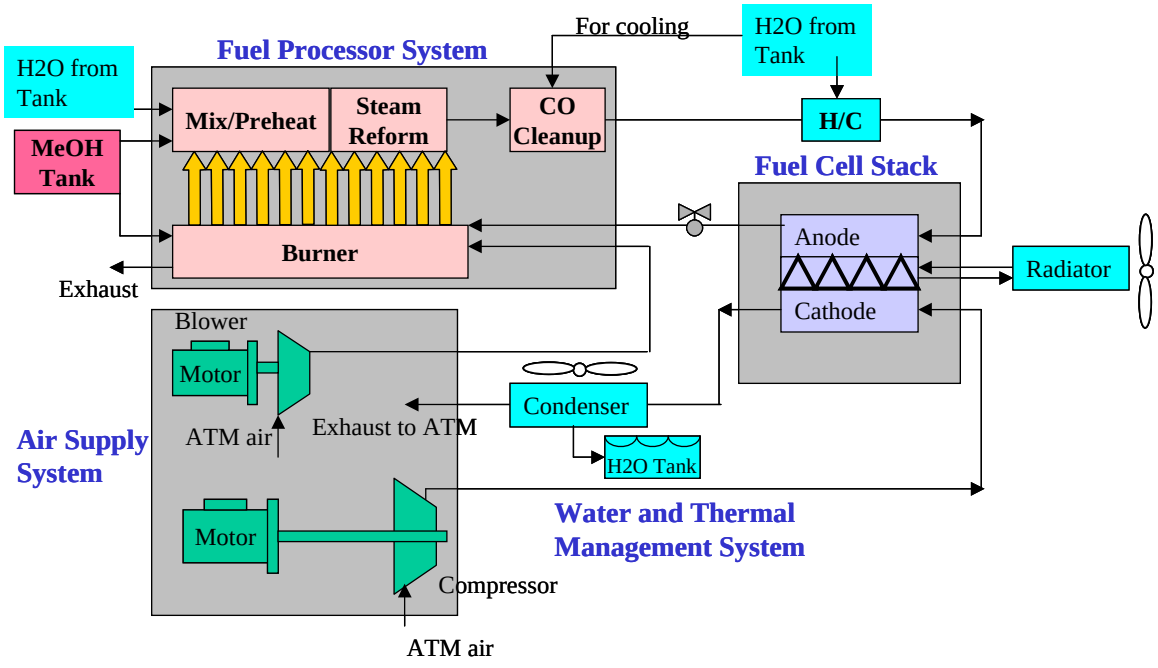


Figure 19: IMFC System

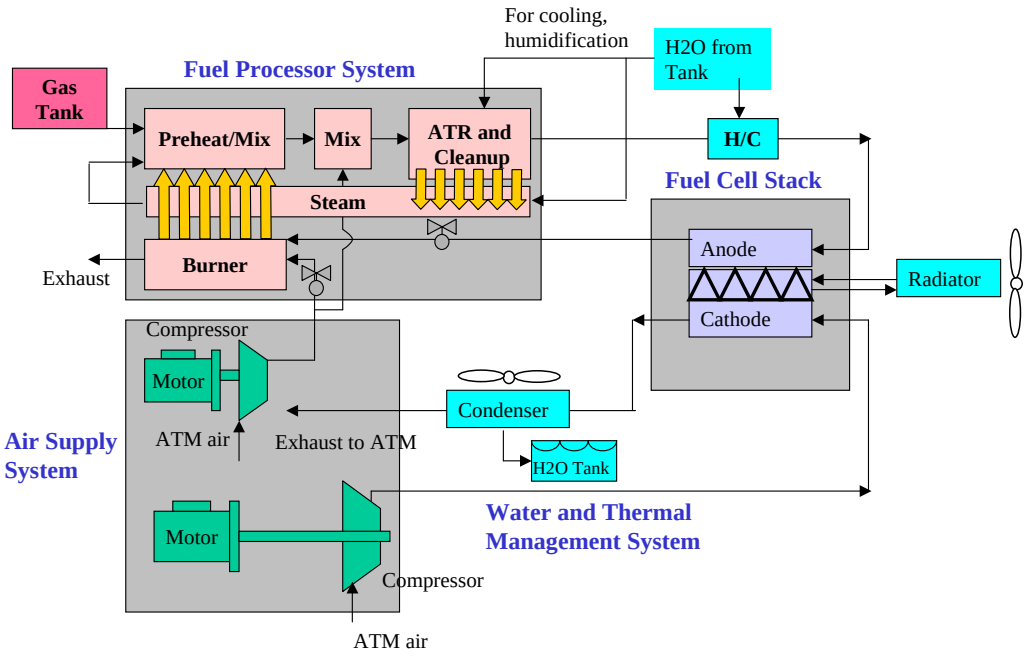


Figure 20: IHFC System

In all the systems above, a fuel cell stack, primary air supply sub-system, and a water-thermal management sub-system are included (the radiator is part of this sub-system). The obvious difference in the DH system is the lack of a fuel processor. Here, a high pressure (5000psi) storage tank and delivery mechanism are included. The fuel processors for the IM and IH system differ. Specifically, the IM platform uses a steam reformation process and the IH uses an autothermal-type processor. Detailed descriptions of these components can be found in Section 4.1.4.

### 4.1.3 Fuel Cell System Energy and Efficiency Comparison

#### Steady State Analysis

A steady-state analysis was conducted for each system to generate an ideal cathode-side operation. Specifically, a pressure and air flow control scheme are determined for the range system net power, and is specific for the components and stack size chosen.

As stated previously, the system sizes were determined such that each vehicle could achieve the acceleration requirements. The result is that all three vehicles have approximately the same (SS system peak net power) / (vehicle weight) ratio. The IM vehicle is heavier than that of the IH due to the larger mass of the fuel stored on board, leading to a higher required net system power to maintain the acceleration requirements. Refer to Table 9 for vehicle mass details. Not suprisingly, the DH system peak net power is the lowest given that the vehicle mass is lower for the DH platform.

A mass compounding effect can be seen with this system mass parameter. Considering the net power capability is slightly higher for the IM FCV, the system mass is also slightly larger given the power density parameters found in Table 9.

The following plots show the SS system efficiencies for all three configurations. Each plot shows details of where in the system the efficiency is reduced. Net system efficiency ("Net, all" in the figure below) is defined as:

$$\textbf{Net Efficiency} = \frac{(Net\ Electric\ Power\ to\ Vehicle\ Controller)}{(LHV_{fuel}) * (Mass\ Flow\ Rate\ of\ Fuel)}$$

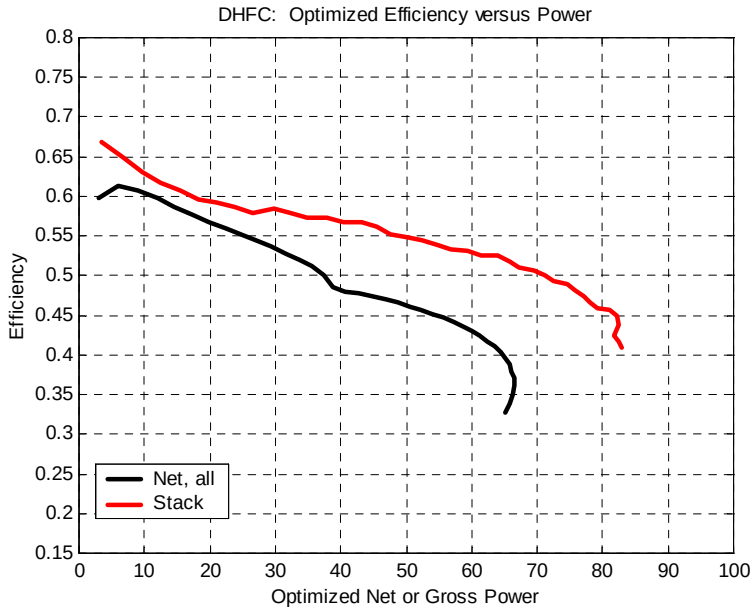


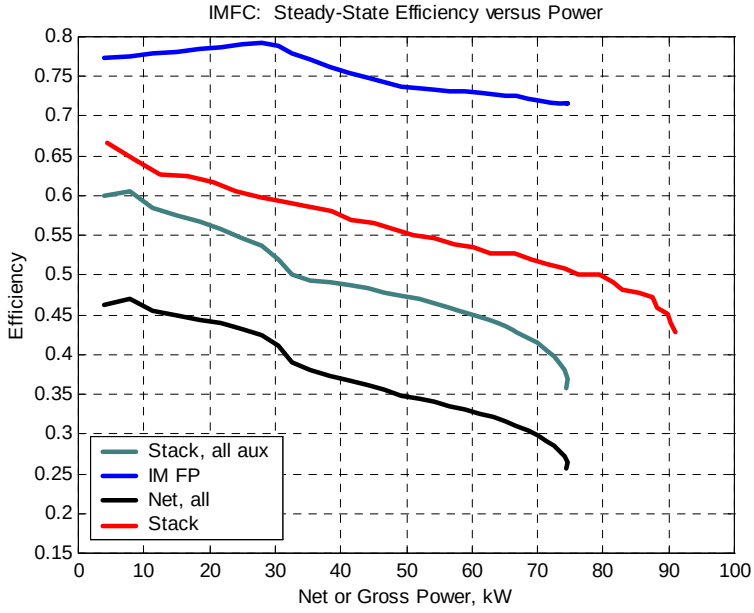

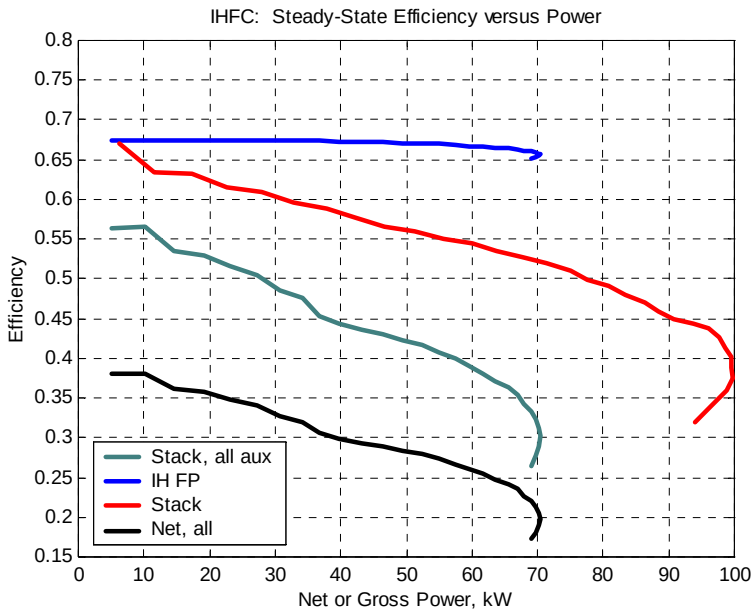


Figure 21: Steady-state efficiency for the fuel cell systems

Figure 22 below directly compares the "Net, all" system efficiency lines from the three plots in Figure 21. Note that the difference in peak Net system power can be seen in Figure 22, but is also highlighted in
Table 11.

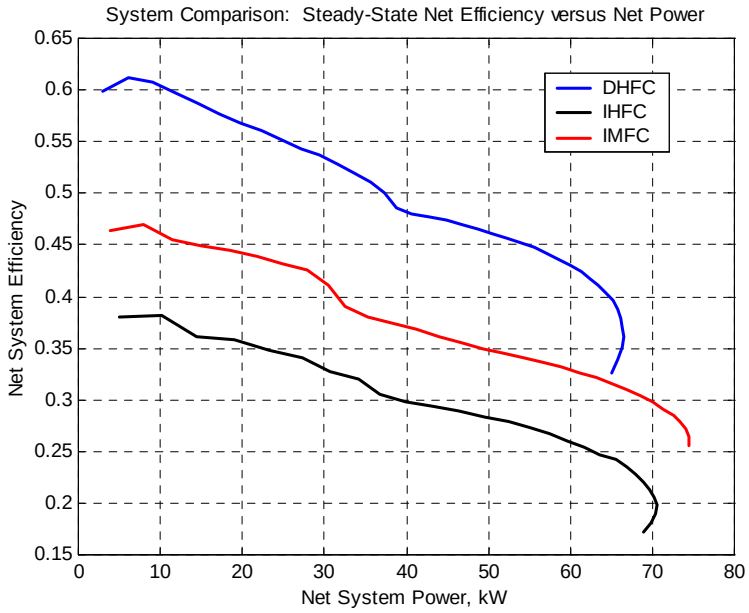


Figure 22: Comparison of the steady-state Net System efficiency

Table 11: Comparison of peak system net power – Steady State (SS)

| Fuel Cell System | System Peak Net Power |
|---|---|
| Direct Hydrogen (DH) | 66.5 kW |
| Indirect Methanol (IM) | 74.5 kW |
| Indirect Hydrocarbon (IH) | 70.5 kW |

Several observations can be made from Figure 21 and Figure 22. Over the entire power load, the IH system showed the lowest steady-state efficiency characteristic. This is partly due to the lower fuel processor efficiency (especially at the low power region) compared to that of the IM fuel processor. However, a larger aspect of the efficiency difference is due to the additional auxiliary load inherent in the IH system, that of the second air compressor for the IH fuel processor. This is especially apparent in Figure 21 when looking at the difference between the "stack" and the "stack, all aux" lines on the plots for the IH versus the other systems.

In contrast, the DH Net system steady-state efficiency was the highest over the entire power region. As stated in the previous paragraph, the DH system has one less parasitic load compared to that of the IM and IH, that of the second air blower or compressor respectively, necessary for the fuel processing. However, in the DH system, the parasitic loads of the components that are common to the IM and IH systems also differ. For example, considering the fuel cell stack is smaller for the DH system, the air compressor requirements are less at the peak net system power. Additionally, because there is no fuel processor in the DH system, the water condensation requirements are reduced, resulting in smaller condenser fan parasitic loads. Finally, there is a slight advantage in the DH system due to increased stack operating efficiency when using neat hydrogen, compared to that of a reformate on the anode performance.

An additional observation can be made from Figure 21. The horizontal axis shows power in kW. All of the lines, except for the "stack", reference the same power value, that of the Net system power. The "stack" line references the gross fuel cell stack power. At peak load, a simple comparison of peak stack and net power capability is possible. Table 17 also has reference peak load net system and stack gross power values.

## System Control

Fuel cell system control methodology can have an appreciable effect on the performance and characteristics of the vehicle. In reference to Figure 11, the fuel cell system corresponds to the "Power Source" block in the control diagram. The following three sections are a brief description of the system control algorithms used for each of the three systems.

### *DHFC*

The direct hydrogen system is perhaps the easiest of the three systems to control. There is virtually no transient delay of hydrogen to the stack (assumed to be instantaneous) and anode re-circulation alleviates the concern of hydrogen loss from the system. The control of the system, as shown in Figure 23, works basically as follows:

The motor current as derived from the motor controller is added to the auxiliary currents of the air supply and water and thermal management subsystems. This becomes

the overall 'stack current' that acts as a control signal to the air supply determining the air flow into the stack, as well as the hydrogen flow into the anode. The stack current also acts as a disturbance to the stack with the resulting stack voltage calculated as a function of these parameters. Because the hydrogen flow is assumed to be immediate, there is no lag between the current request and the supply of hydrogen. The amount of hydrogen into the stack is determined by the following equation:

$$\dot{m}_{H_2}^{req\_current} = \frac{I_{Stack}}{4 \cdot F \cdot u} \cdot n_{cell}$$

*where*:

$\dot{m}_{H_2}^{req\_current}$ = requested hydrogen due to the stack current [moles · sec$^{-1}$]

$I_{Stack}$ = Fuel cell stack current [A]

$F$ = Faraday constant [A · sec · mole$^{-1}$]

$u$ = utilization rate [1]

$n_{cell}$ = number of cells in stack [1]

**(2)**

The air supply has a small time lag between the current request and the output as determined by the 'optimized' pressure and airflow control lines.

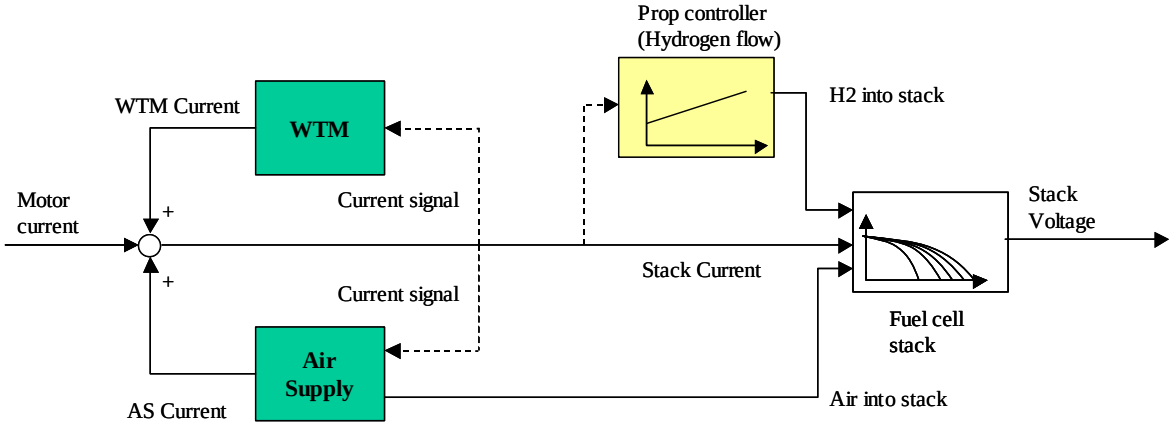


Figure 23: DHFC System Control Diagram

***IMFC***

The indirect methanol system is a substantially more complicated system to control and all the aspects of the control are not discussed here. For more information, the reader is encouraged to read the following reports: Ramaswamy (Section 5.4, fuel processor, SAE 2001-01-3111), and Hauer (Section 5.4, vehicle modeling, SAE 2000-01-0370).

The basic input into the "Power Source" blocks are slightly different in the case of the indirect methanol. In addition to the motor current, the power source also receives the control variables of the 'accelerator pedal position' and the 'stack voltage'. The system level control is shown in Figure 24 and is very similar to the direct hydrogen case with the exception of the fuel processor. The fuel processor and the fuel cell stack interactions greatly influence the need for a more complicated control scheme than the one for the direct-hydrogen fuel cell vehicle.

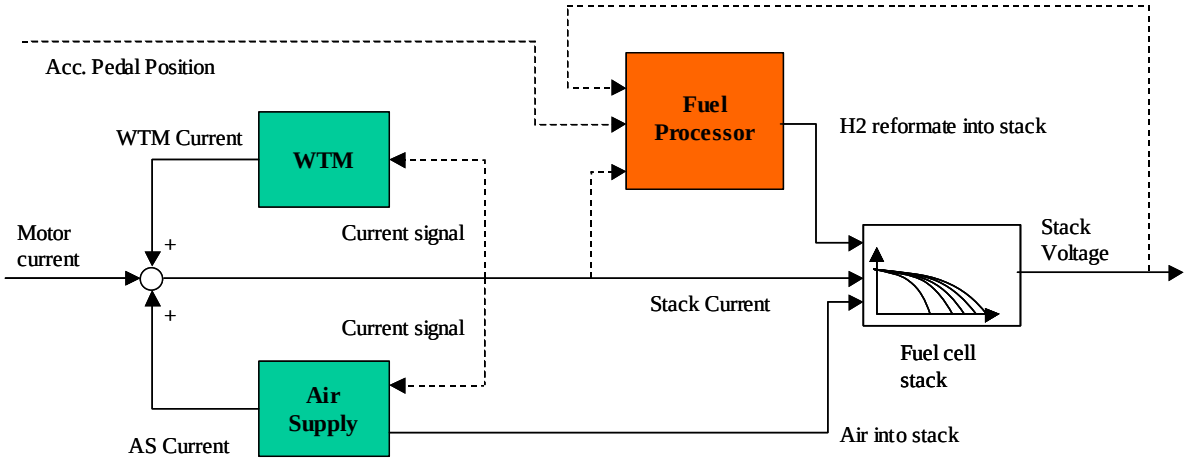


Figure 24: Indirect Methanol System Control

***Fuel processor controller***

The primary aim of the fuel processor controller is to ensure adequate supply of hydrogen to the fuel cell stack with the aim of ensuring that there is no possibility of stack hydrogen starvation (which can lead to stack failure and extremely low voltages). In order to ensure this the fuel processor fuel flow controller has three inputs. The motivation for choosing these three control variables for the fuel processor is to ensure good vehicle acceleration and reasonable fuel consumption at the same time under all operating conditions. However it should be noted that this controller only partially succeeds in meeting our goals. In practice another controller discussed in the fuel processor section 4.1.4.2 is also needed to meet the sometimes rapidly varying stack hydrogen requirements while ensuring reasonably high utilizations ***and*** overall efficiencies. Briefly, that control algorithm assumes that the stack utilization can be measured without any lag and that fuel processor backpressure can also be controlled without any lag. The full details can be found in the fuel processor section 4.1.4.2.

This system level fuel processor controller details along with the significance of the three inputs associated with this controller are discussed below. As shown in Figure 25, the three inputs to the controller are:

- *The stack current*
- *The derivative of the acceleration pedal position*
- *The stack voltage*

The stack current is the dominant control variable during steady state or nearly steady state vehicle operation e.g. cruising on the highway with constant speed. The actual stack current is taken and converted into a molar hydrogen request (Equation 2).

On the other hand, the derivative of the acceleration pedal position dominates the operation of the fuel processor during positive transients e.g. acceleration. In this mode, a large amount of hydrogen is requested by the reformer to guarantee high stack voltages

leading to high maximum motor torque and therefore good vehicle acceleration. This request is zero during periods of low vehicle dynamics (Equation 3)

$$T_1 \cdot \frac{d\dot{m}_{H_2}^{req\_pedal}}{dt} + \dot{m}_{H_2}^{req\_pedal} = K_1 \cdot T_2 \cdot \frac{dp}{dt}$$

*where*:

$K_1$ = controller time constant [moles/sec]

$T1, T2$ = controller time constants [sec]

$\dot{m}_{H_2}^{req\_pedal}$ = requested hydrogen due to the derivative of the acceleration pedal position [$moles \cdot sec^{-1}$]

$p$ = normalized acceleration pedal position

**(3)**

The third input variable is the stack voltage. The stack voltage is compared with a minimum stack voltage and depending on this comparison, additional hydrogen is requested from the fuel processor (Equation 4). This helps ensure that even if the current and acceleration requirements are met at any instant, the stack voltage minimum limit is never violated.

$$T_3 \cdot \frac{d\dot{m}_{H_2}^{req\_voltage}}{dt} = K_3 \cdot T_3 \cdot \frac{d(V_{stack} - V_{\min})}{dt} + K_3(V_{stack} - V_{\min})$$

*where*:

$T_3$ = controller time constant

$\dot{m}_{H_2}^{req\_voltage}$ = requested hydrogen flow due to the fuel cell stack voltage [$moles \cdot sec^{-1}$]

$K_3$ = contoller constant [$moles/sec \cdot V^{-1}$]

$V_{stack}$ = fuel cell stack voltage [V]

$V_{\min}$ = minimum fuel cell stack voltage [V]

**(4)**

The aggregated hydrogen request is then used to derive the methanol injected into the reformer. For this, the hydrogen request is compared with the actual hydrogen flow at the reformer outlet (downstream towards the fuel cell stack). The derivation of the methanol flow is accomplished with a Proportional Integral (PI) control algorithm (Equation 5)

$$T_4 \cdot \frac{d\dot{n}_{CH3OH}}{dt} = \frac{1}{cv} \cdot \frac{d}{dt}\left(\max\left(\dot{n}_{H_2}^{req\_current}, \dot{n}_{H_2}^{req\_pedal}\right) + \dot{n}_{H_2}^{req\_voltage} - \dot{n}_{H_2}^{actual}\right) +$$

$$\frac{1}{cv} \cdot \left(\max\left(\dot{n}_{H_2}^{req\_current}, \dot{n}_{H_2}^{req\_pedal}\right) + \dot{n}_{H_2}^{req\_voltage} - \dot{n}_{H_2}^{actual}\right)$$

*where*:

$T_4$ = time constant for reformer controller [sec]

$cv$ = conversion rate [moles of $H_2$ / mole of $CH_3OH$]

$\dot{n}_{CH3OH}$ = methanol flow into reformer [moles $\cdot$ sec$^{-1}$]

$\dot{n}_{H_2}^{actual}$ = actual hydrogen flow at the reformer exit [moles/sec]

**(5)**

The complete control algorithm is shown visually in Figure 25. Equation 2 – 5 represent the full set of equations allied to derive the hydrogen flow request from the reformer depending on the above-mentioned measures.

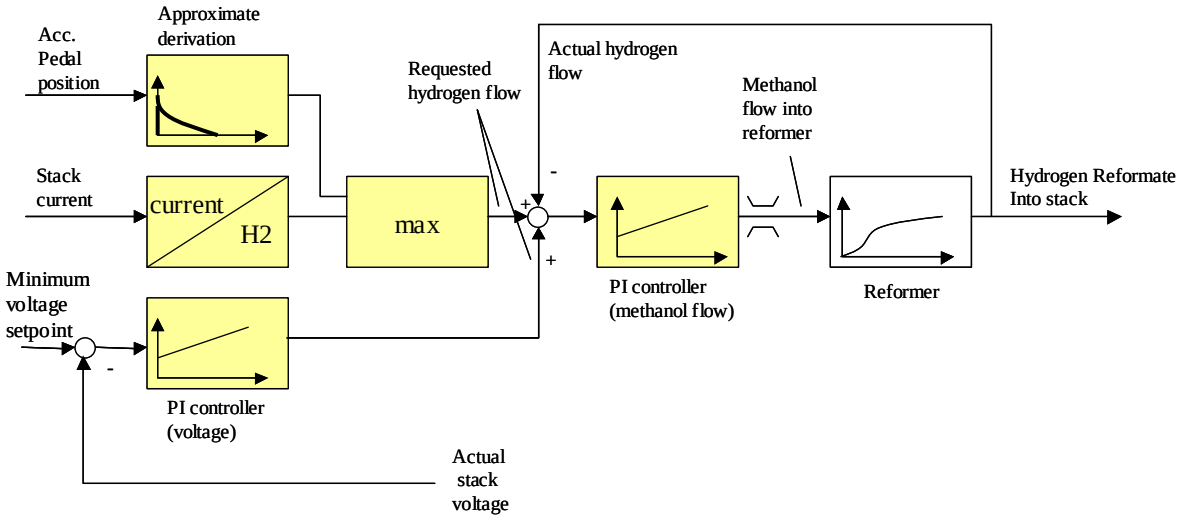


Figure 25: IM Fuel Processor System controller

In addition to the system fuel processor controller, there are additional controls within the fuel processor itself to help maintain high fuel utilization and efficiency, as well as to ensure good gas cleanup. These are discussed in further detail in the fuel processor section.

***IHFC***

The system level controller for the IH fuel processor as shown in Figure 27 is very similar to the controller for the IM fuel processor. The primary difference is that

instead of the ‘motor current’ as an input variable, an ‘adjusted motor current’ is used, as shown in Figure 26.

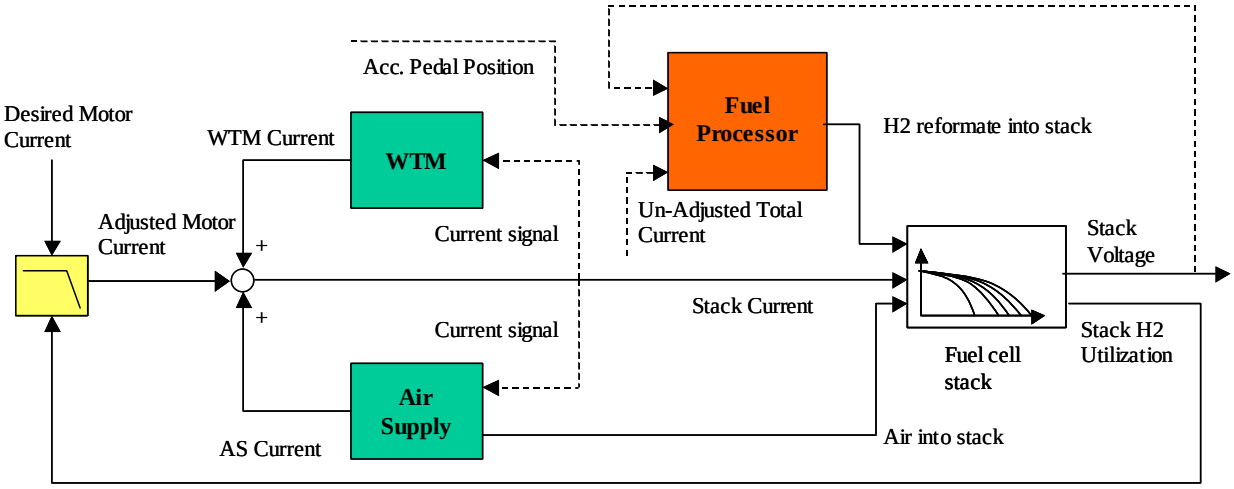


Figure 26: Indirect Hydrocarbon System Control

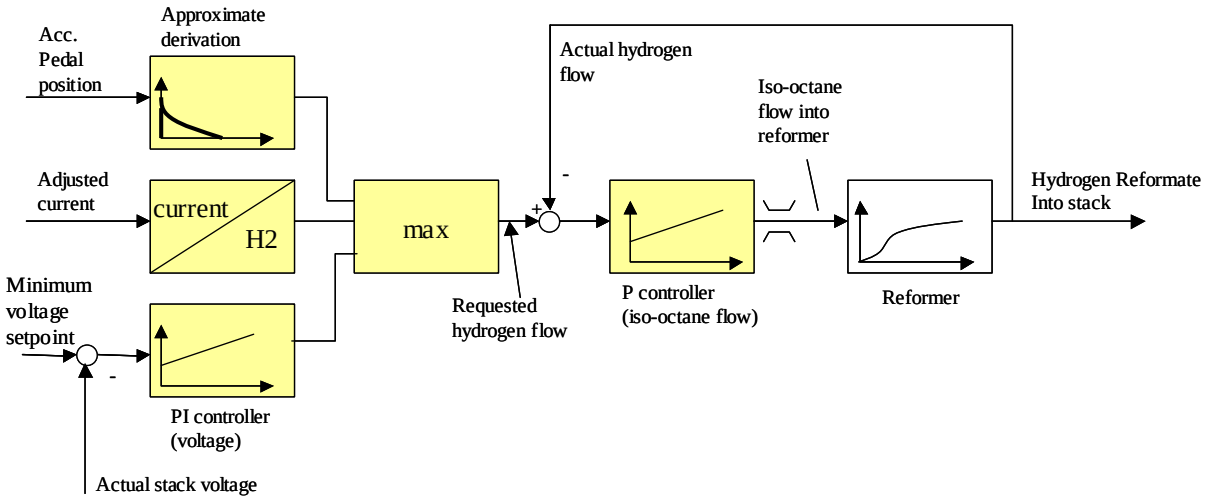


Figure 27: IH Fuel Processor System Controller

***Adjusted Motor Current***

Under steady state conditions, the system controller will attempt to supply excess hydrogen to the system such that the average stack utilization is around 85%. Under transient conditions, it is not always possible for the fuel processor to supply enough hydrogen to maintain this level of utilization. To avoid starvation of the stack, the control algorithm 'senses' the hydrogen utilization within the stack and reduces the motor current draw when the utilization increases above 90%. The motor current draw on the system is reduced by the magnitude of the 'motor current multiplier' shown in Figure 28. It should be noted that determination of the exact nature of the motor current multiplier is

somewhat arbitrary. The location of the bend in the curve can significantly influence the fuel cell system efficiencies. If the location of the bend in Figure 28 is moved towards the left (i.e. lower utilizations), the efficiency of the fuel cell system will be adversely affected due to the possibility of increased amounts of wasted hydrogen. If it is moved towards the right (i.e. higher utilizations), the efficiencies may increase but the chances for stack hydrogen starvation (and consequently stack failure) will increase. Because the motor current is part of the total current, and the total current is one of primary control variables that dictates fuel flow into the fuel processor, the un-adjusted (non-reduced) total current is still used as the primary control variable.

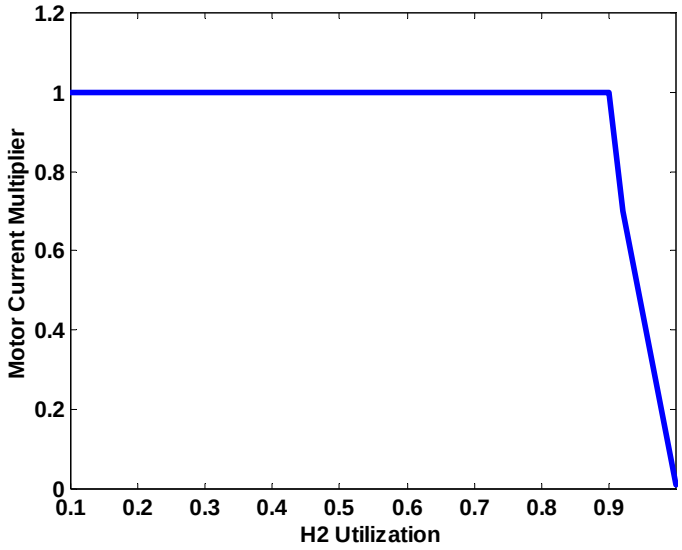


Figure 28: Motor Current Multiplier

## Transient Analysis

The following Figure 29 shows the resulting energy consumption for the fuel cell system in the context of the vehicle model and a dynamic driving cycle demand. The largest bar, that of the "FC System Loss" is the exact same value shown in the vehicle overview section, Figure 3.

The energy values quoted can be considered accumulated energy losses over the entire cycle. Specifically, for auxiliary components such as the air compressor and the fans, the lost energy is that which is directly consumed by the electric motors of the components. For the fuel cell stack and the fuel processor, the lost energy is that which is not converted to either stack electrical power or reformate stream potential energy, respectively.

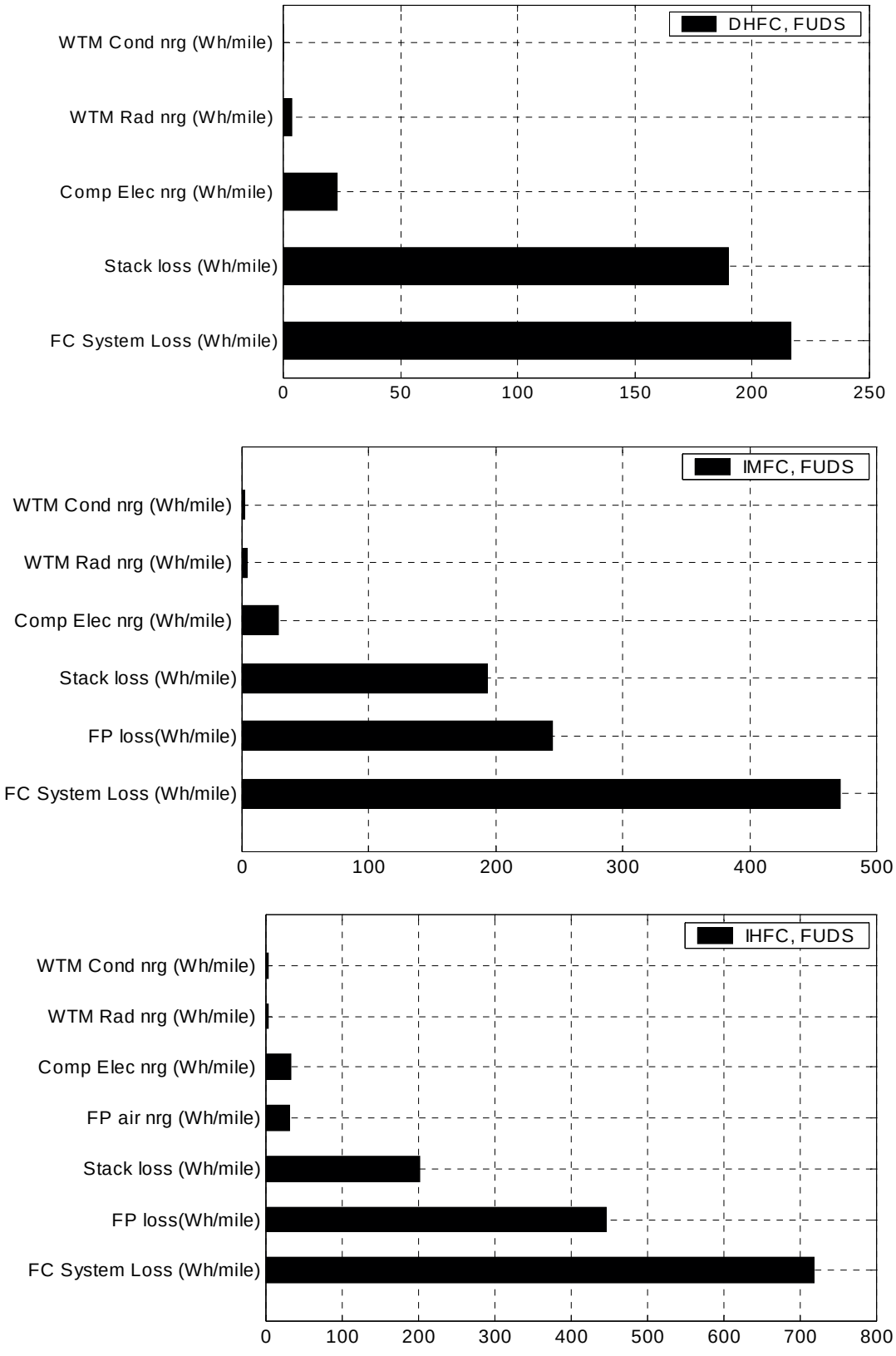


Figure 29: System/Vehicle total energy usage, per drive cycle

As shown in the figure above, the DH "FC System Loss" was the lowest for the three system types, approximately 215 Wh/mile. This is largely due to the lack of a fuel processor as well as a fuel cell stack operating on neat hydrogen. The system with the largest "FC System Loss" was that of the IH system, with a total system loss of approximately 720 Wh/mile.

Also apparent in Figure 29, by observing the number of bars presented per system, is the use of additional system components for the IM and IH platforms. Specifically, in addition to the use of fuel processors not found in the DH platform, the IH platform uses a second air compressor for the fuel processing system. This auxiliary load is relatively large considering the IH fuel processor operates at a fixed gas pressure of approximately 3 atms.

The ratio of peak stack gross power to system net power can have an impact on the system efficiency across systems for the same drive cycle. Specifically, the IH system has a higher gross stack power to account for the additional aux load (FP AS), which makes the power ratio (gross/net) higher. The simplest way to understand how this affects the system efficiency is to examine the general characteristics of a fuel cell stack and air supply's net efficiency relative to the net power capability. Efficiency rises and reaches a maximum in the lower net power region and then gradually decreases with increasing net power. Because the IH stack size is larger than the other systems, for the same net power values, the IH stack will be operating at lower gross power levels relative to its maximum capability and thus the stack operating efficiency may be positively affected. However, this is only one variable in analyzing and comparing stack performance in different systems (i.e. anode stream gas content, etc).

The following figure compares the fuel cell system efficiency derived from the dynamic operation of the system/vehicle on multiple drive cycles. The system efficiency is defined as:

$$\textbf{FC System Efficiency} = \frac{(\textit{System Electrical Energy})}{(\textit{Fuel Energy Consumed})} * 100$$

where

**(system electrical energy)** = net electrical energy delivered to the vehicle controller from the fuel cell system, also represented as [(current delivered to the vehicle drive motor) * (fuel cell stack voltage)]

**(fuel energy consumed)** = fuel LHV energy content

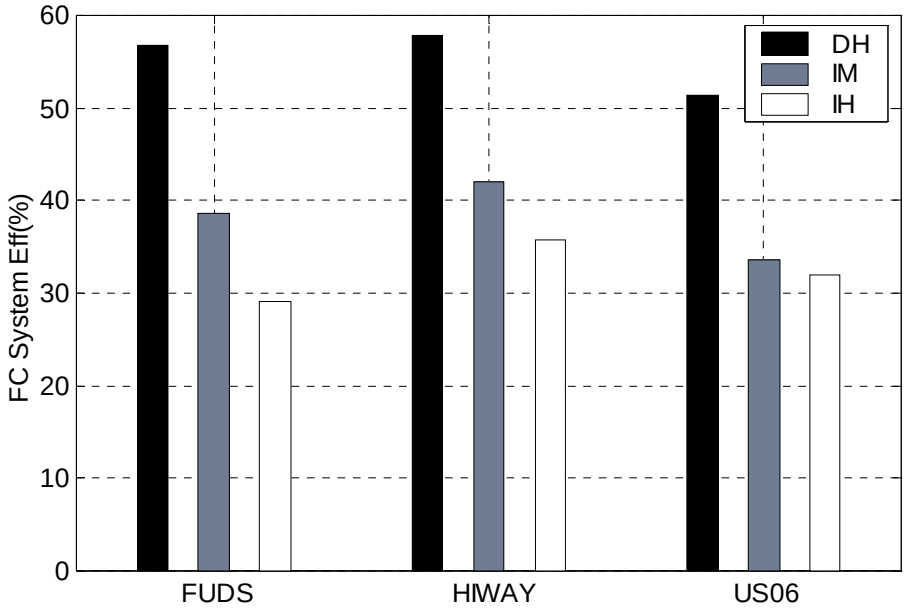


Figure 30: Dynamic Fuel Cell System Efficiency, per drive cycle

The efficiency values shown in the above figure are derived from the actual energy in a dynamic drive cycle. This is in comparison to the steady-state Net System efficiency values shown in Figure 21. The values in a dynamic setting will typically be lower than that of a steady-state operating environment.

As discussed in Section 2.1.2, the actual operating efficiency of the IM and IH platforms are more similar on the US06 drive cycle than any other cycle simulated in this study. The bulk of this difference occurs in system operation, as compared to the vehicle drivetrain. Furthermore, this difference can be largely isolated to the fuel processor. The fundamental control schemes for the two system types are different. The IM platform uses a "back-pressure" control mechanism that essentially allows the internal fuel processor volume space to be used as a reformate buffer. This characteristic improves the system dynamic response to reformate demand. The IH system, on the other hand, uses a "stack utilization" control scheme, which is inherently less efficient in a dynamic setting.

However, the US06 drive cycle is less dynamic (fewer demanded changes in the vehicle velocity) compared to that of the FUDs cycle, yet has higher average power demands. Given this reduced "dynamic" operation, and the IM fuel processor steady-state efficiency degrades at higher system power levels, the two fuel processors have similar operating efficiency values on this cycle. Refer to Table 13 and Table 14 for additional fuel processor details.

### 4.1.4 Component Discussions

#### 4.1.4.1 Fuel Cell Stack

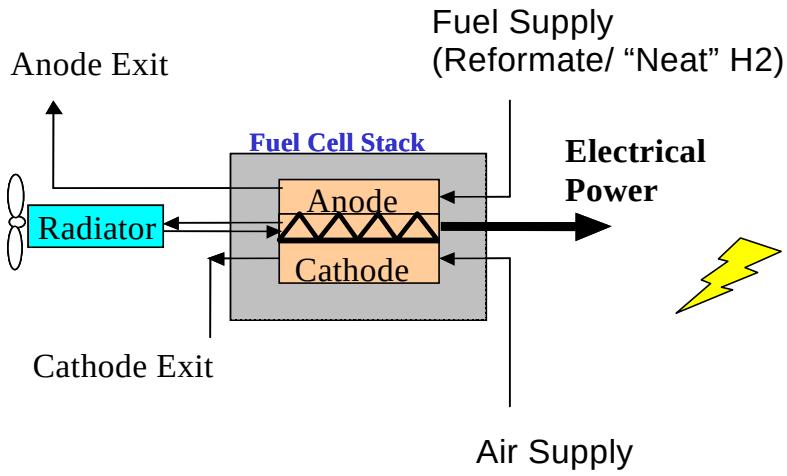


Figure 31: Fuel Cell Stack

**Description**

The fuel cell stack is the primary energy producer in the load following fuel cell vehicle. A simple illustration of a fuel cell is given in Figure 31. The anode side of the fuel cell stack is supplied with pure hydrogen or hydrogen containing reformate depending on the type of fuel cell system. The cathode side is supplied with oxygen from the ambient air by an air supply system (typically a compressor or a blower). The stack performance is strongly dependant on the anode and cathode conditions, namely the pressure, the stoichiometry and the humidity. The variation in performance with a variation in these parameters will be shown in the following sections.

***Stack Sizing***

We can expect the stack performance and characteristics to be different for the three different systems i.e. the DH, IM and IH systems. As mentioned in the earlier sections, the fuel cell vehicle that is modeled here is based on the PNGV specifications. The stack sizing was performed for the three different load following vehicles in an attempt to meet the PNGV goals. This resulted in different stack sizes for the three systems. *Typically, the "size" of the fuel cell stack is defined by the total number of cells AND the active area of each cell.* The size of the stack is dependant on

1. The stack characteristics of the three systems. The anode overpotential, or simply the anode losses, associated with the three systems are different because of the distinctive characteristics of their fuel stream, i.e. "neat" hydrogen for the DH and reformate for the IM and IH.
2. Vehicle weights: The vehicle weights are different for the three systems considering the components involved. The stack power and hence the stack size needs to be attuned to vehicle weight to meet the same performance criteria.

3. The air supply system: Generally, for a given fuel cell system, the stack size will be larger for blower-operated system when compared to a compressor-operated system for same peak power requirements. The presence of an expander in the air supply system can also change the sizing requirements. **However, in this analysis, for ease of comparison, a single air supply system comprising a twin-screw compressor and no expander is used for the three systems.**

In order to have some degree of "commonality" for the three different stacks, the cell number was kept a constant and the cell area was varied. The stack sizes that are used in this analysis are given in Table 12 below: (All fuel cell systems used a twin-screw compressor)

Table 12: Stack sizes for the three systems

| System Type | Number of Cells | Cell Area |
|---|---|---|
| DHFCV | 450 | 360 |
| IMFCV | 450 | 470 |
| IHFCV | 450 | 650 |

**** Note: The reader is asked to bear the stack sizes in mind while viewing the results in this analysis.***

## Methodology:

The fuel cell stack analysis is performed using a fuel cell model similar to the model developed by Springer and co- workers at Los Alamos National Labs. (Springer, 1993). Based on this initial cell model, an extensive stack model was developed allowing the prediction of the stack voltage for varying stack current, anode and cathode conditions (pressure and air mass flow). The following major effects are taken into account in the stack study:

- Anode overpotential losses: Reaction and transport losses in the anode catalyst layer.
- Diffusion losses in the anode backing layer
- Cathode overpotential losses: Reaction and transport losses in the cathode catalyst layer.
- Diffusion losses in the cathode backing layer
- Ionic membrane resistance
- Water management in the membrane
- Electronic resistance of the catalyst, backing layer and bipolar plates
- Anode air bleed to mitigate effect of CO poisoning
- Hydrogen dilution effects if reformate gas is supplied to the stack instead of hydrogen.

For an explanation of the detailed model the reader is encouraged to study the listed references (Springer 1993 and Friedman 1998)

In our analysis of the stack, in principle, three different loss mechanisms are considered. These are the anode losses due to the mass transport limitations and reaction losses on the anode, ohmic membrane losses, and the cathode losses due to mass

transport and reaction losses on the cathode[10]. In the vehicle, the overall stack potential available at the stack terminals can be calculated by Equation 6.

$$V_{stack} = n_{cell} \cdot \left(V_0 - \eta_{anaode}(p_{H_2}, I) - R_{cell} \cdot I - \eta_{cathode}(p_{ox}, I)\right)$$

*where* :

$V_{stack}$ = Stack voltage [V]

$n_{cell}$ = Cell number [1]

$V_0$ = Reference cell voltage [V]

$\eta_{anaode}$ = Anode overpotential [V]

$p_{H_2}$ = Partial pressure of hydrogen [Pa] (6)

$I$ = Stack current [A]

$R_{cell}$ = Cell resistance [Ω]

$\eta_{cathode}$ = Cathode overpotential [V]

$p_{ox}$ = Partial pressure of oxygen [Pa]

On the anode side the impact of the fuel supply is accounted for as a voltage loss that is a function of hydrogen (reformate) mass flow rate, pressure, composition (in the case of IM and IH systems), and current. Each particular flow rate and current results in a different partial pressure of hydrogen and in a different anode voltage loss.

On the cathode side the impact of air supply is accounted for in the stack in the form of a voltage loss that is a function of the partial pressure of oxygen at the catalyst layer-gas diffusion layer interface and the stack current. Similar to the anode side the maximum cell current for a particular constant supply of oxygen is indicated by an increase in cathode voltage losses. However this increase in cathode voltage losses is more gradual than on the anode side.

The third loss mechanism considered on the vehicle level is the ohmic voltage loss due to the ionic resistance of the membrane plus the electronic resistance in the catalyst layer, the backing layer and the bipolar plates. This loss is proportional to the applied stack current.

### Steady State Analysis

Figure 32 shows the results of this model for the variation in cell voltage due to air flow rate. It can be seen that the voltage variation is small at lower current densities. However, as the current demand increases, the lower flow rate curves begin to drop off. Ultimately the drop off becomes quite sharp. From a stack standpoint the higher the flow rate, the higher the voltage. This implies that the stack will be more efficient and will be able to produce higher power for higher air flows.

[10] The net output power of the combined system of stack and air has been maximized adopting an "optimal control strategy" for varying pressure and stoichiometric ratios of the cathode air supply.

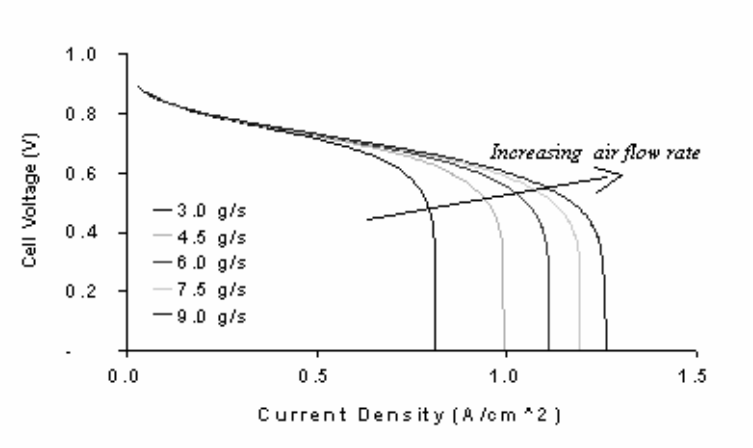


Figure 32: Variation In PEM fuel cell Voltages due to variation in air-flow rates

Figure 33 shows the cell characteristics when the air pressure is varied. In this case, the voltage variation exists across all current densities. Again, from the standpoint of the stack, higher pressure leads to higher voltage and therefore higher efficiency and peak power.

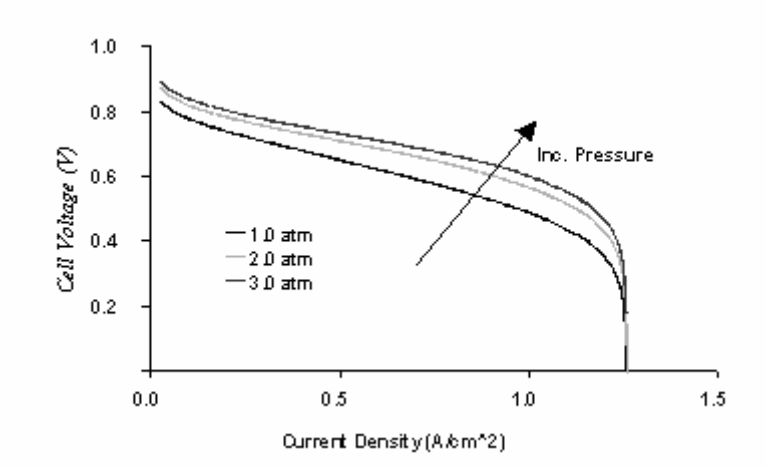


Figure 33: Variation in PEM Fuel Cell Voltages due to variations in air pressures

Figure 34 depicts the effect of variation in cell performance with variation in hydrogen concentration in the reformate stream.

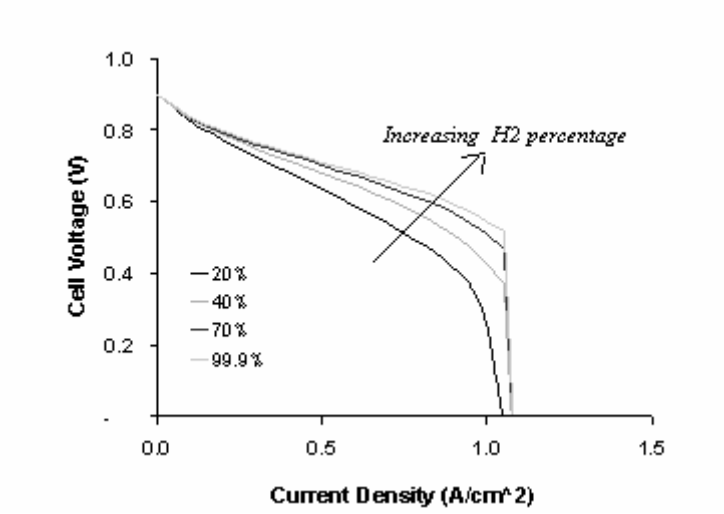


Figure 34: Variations in cell voltage due to variations in dry hydrogen concentration.

The impact of hydrogen flow rate variations are quite different for reformate than any of the variations seen to this point. In all other cases there was either no impact in the region of operation, or the impact was relatively gradual, producing a clear voltage signal showing the variation. Figure 35 shows that, until a specific point, the impact of varying hydrogen flow rates seems nil or at least small enough to ignore. Once that specific point is reached, however, the voltage of the cell drops like a rock.

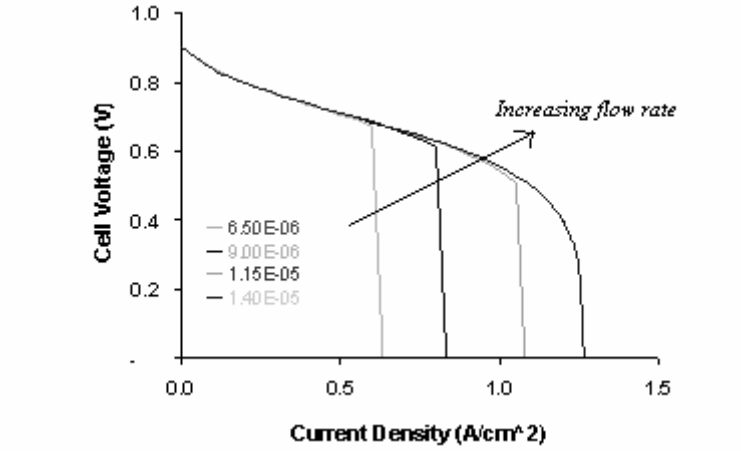


Figure 35:Variation in cell voltage due to variations in reformate (hydrogen) flow rate (in moles/sec).

It is important to understand that the shape of the polarity plot has significant impact on the vehicle acceleration due to the dependence of the motor torque on the supply voltage at the terminals of the power electronics.

Figure 36 illustrates a set of "optimized" cell polarization curves for the DH, IM and IH cases. The cathode conditions that have been employed while generating these curves are the result of an optimization process that takes into account the stack, air

supply and the water and thermal management requirements. The anode conditions have been kept constant and the particulars are mentioned inside the plot. These curves will change depending on the air supply system and the nature of the water and thermal management components. These curves that are shown here are viewed as purely illustrative.

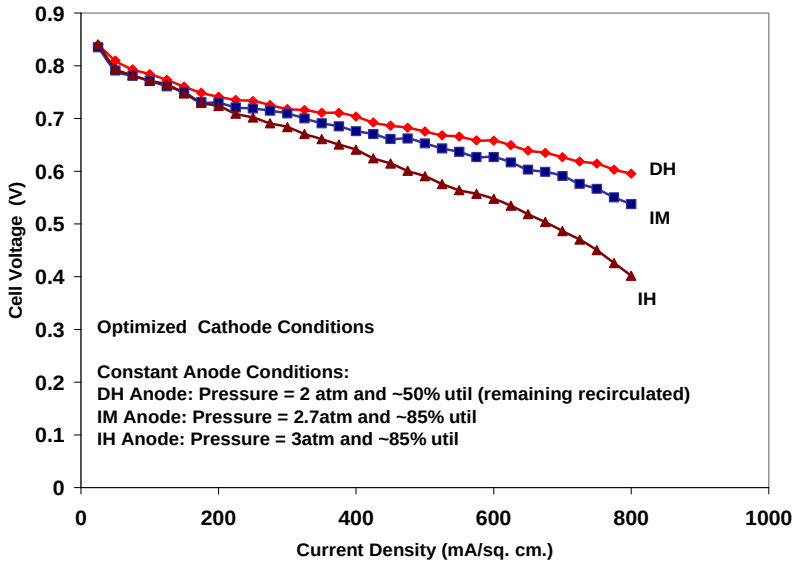


Figure 36: "Optimized" Polarization curves for the DH, IM and IH Fuel Cells.

The graph in Figure 37 shows the optimized net power vs. stack current density for the three systems. One important item to note is that for a given net power level, the three systems have different current densities with the IH the lowest and the DH the highest. This will have an impact on the stack efficiency comparisons between the three vehicles for similar power requirements (cycles). The lower current density (for a given net power) for the IH system will partially offset some of the effect of increased anode over-potential (due to the lower hydrogen partial pressure at the anode catalyst) making the stack efficiencies appear similar. Given our requirement of a similarly performing vehicle (0-60, etc.), and a reasonable voltage range requirement (400-250V), this was a necessary disparity.

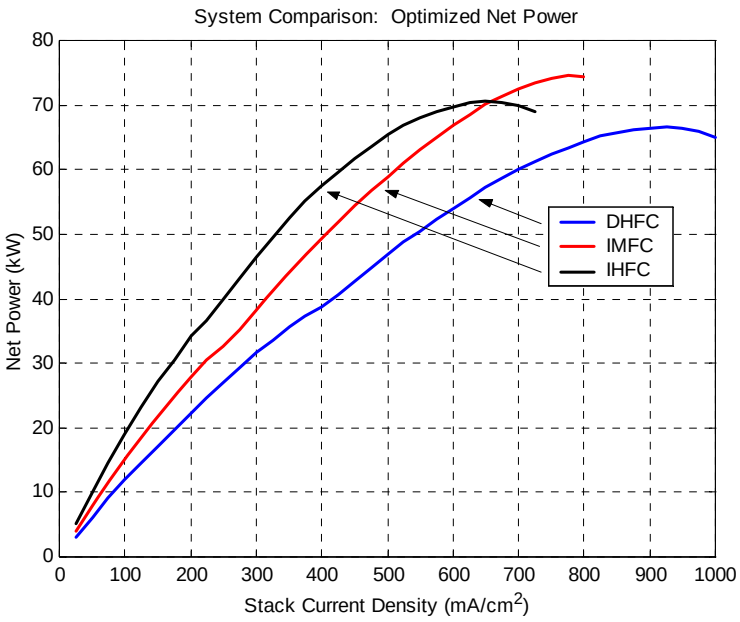


Figure 37: Steady state net power for the three fuel cell systems

**Transient Analysis:**

In this section, the fuel cell stack characteristics will be analyzed over the drive cycles.

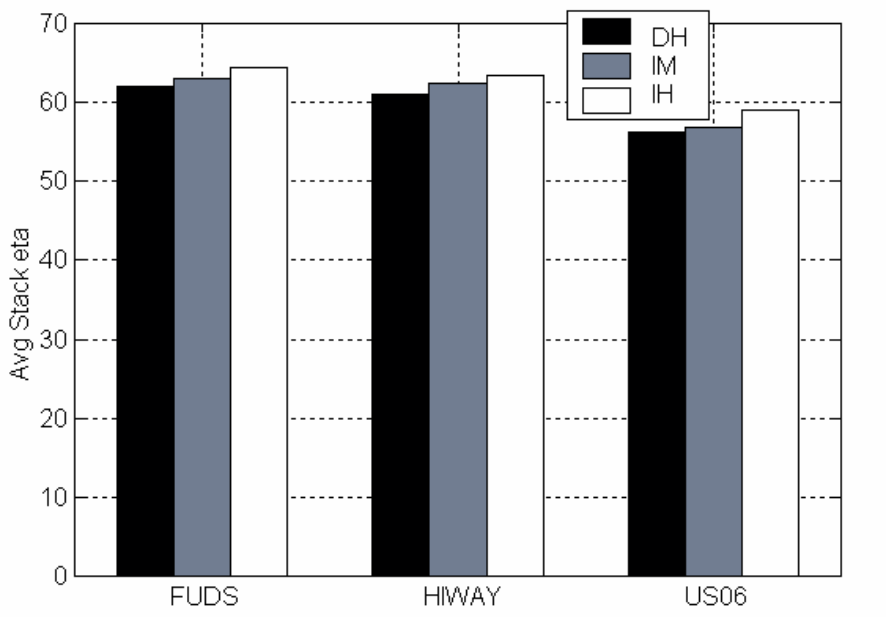


Figure 38: Fuel Cell Stack Efficiencies over the Drive Cycles for the three systems

Figure 38 compares the stack efficiencies of the three different systems over the complete FUDS, HIWAY and the US06 cycles. The stack efficiency is defined as follows:

$$\textbf{Stack efficiency} = \frac{(Electrical\ Energy\ From\ Stack\ During\ Drive\ Cycle)}{(Maximum\ Theoretical\ Energy)} * 100$$

where maximum theoretical energy (MTE) is defined as

**MTE** = *(Lower Heating Value of H2 (kJ/mol))*( moles of H2 utilized during the drive cycle)*

For all the three cycles, it can be seen that the stack efficiencies are the highest for the IH and the least for the DH. This might seem counter-intuitive at first as the IH fuel cell has a significant anode loss when compared to the other two. This trend can possibly be explained by the different stack sizes used for the three systems. As mentioned in the previous section, the stack size for the IH is the largest. Hence over a drive cycle, on average, the stack in the case of the IHFCV is probably operating at lower *normalized* power when compared to the IM and the IH (Although the stacks might be operating at similar power levels). The stack efficiency, in general, drops with an increase in power outputted. So, the stack efficiency of the IH is greater than that of IM and DH.

Also, it can be seen that the stack efficiencies for the US06 for all the systems are lower than the efficiency for the FUDS and HIWAY. A similar reasoning can be done for this. The US06 is a high power cycle when compared to the other two. So, the stacks, on an average, tend to operate at a higher normalized power leading to a less efficient operation.

Figure 39 illustrates the average stack power over the FUDS, HIWAY and the US06 cycles for the three systems. It can be seen that the average power is the highest for the US06 and least for the FUDS cycle.

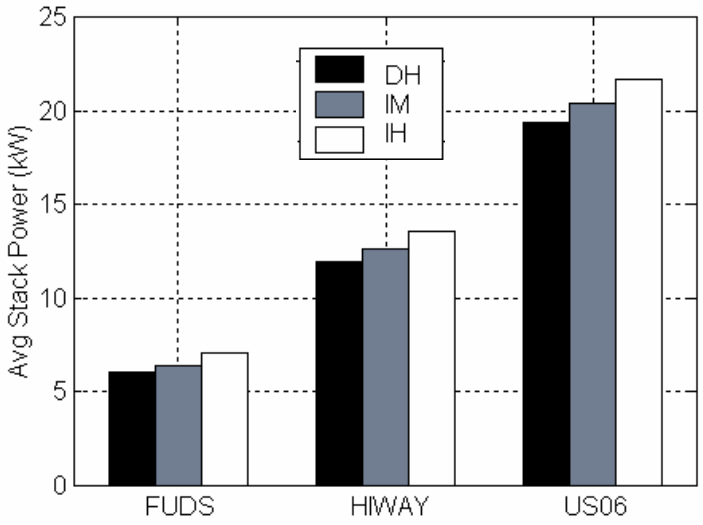


Figure 39: Average Stack Power Over FUDS, HIWAY, US06 cycles, three systems

Figure 40 illustrates the total energy loss (due to inefficiency) at the stack over the FUDS, HIWAY and US06 drive cycles. It can be seen that in general the stack losses in Wh/mile are the highest for the US06 cycle and the least for the HIWAY cycle. This

might seem counter-intuitive after seeing the average stack power in Figure 39. Also, it can be noticed that, for the case of the US06 cycle, the losses seem highest for the IM, then for the DH and the least for the IH. However, the trend is different for the HIWAY and FUDS. The latter can be possibly be explained by the fact that the stack sizes employed are different for the three systems. The air supply characteristics might also be playing a role in this. To understand the former, it is important to understand Figure 41 that shows the stack total gross power over the drive cycle.

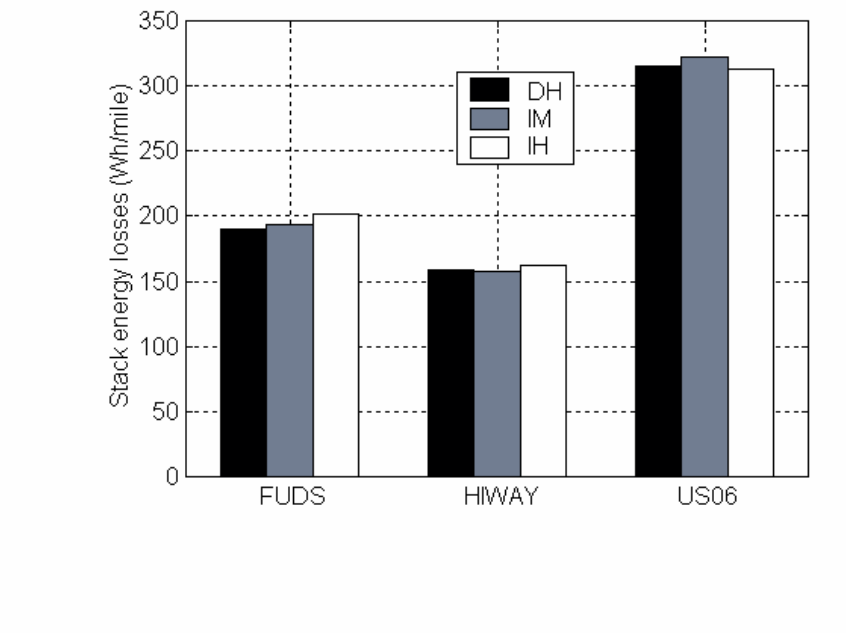


Figure 40:Energy Loss at the stack over the FUDS, HIWAY and US06 drive cycles

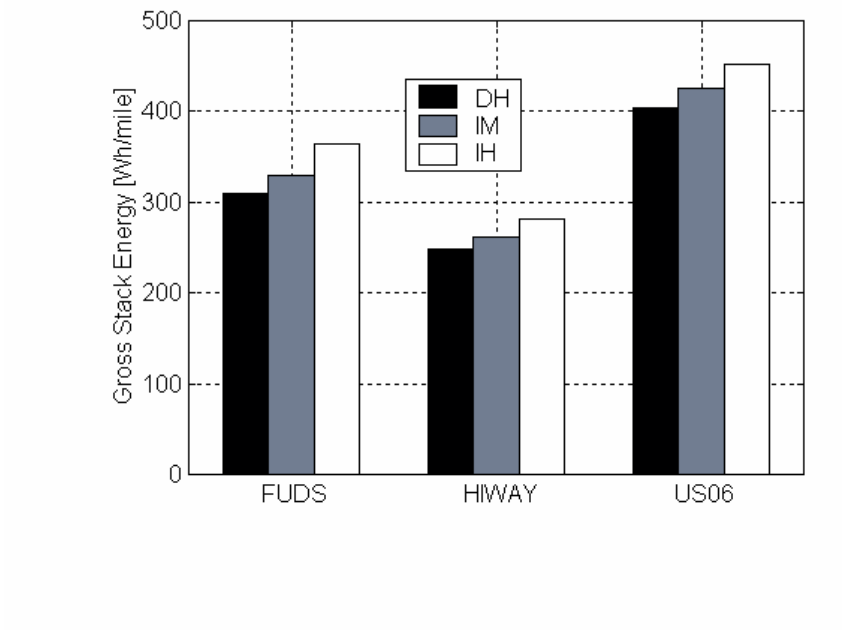


Figure 41: Gross Stack Energy over the FUDS, HIWAY and US06 drive cycles

It can be seen that the gross stack energies in Wh/mile are the highest for the US06 cycle and the least for the HIWAY cycle, the same trend as seen in Figure 40. The reason for this type of trend is the metric of comparison, i.e. Wh/mile. Although the HIWAY cycle is a higher average power cycle compared to the FUDS cycle (Figure 39), a lower amount of energy PER mile is required for the cycle. This can be attributed to the fact that the FUDS cycle has a relatively higher idling time when compared to the HIWAY cycle.

#### 4.1.4.2 Fuel Processor (IH and IM only)

### Introduction

This section provides a description of IM and IH Fuel Processor components and their functions and a detailed summary of steady state and dynamic results for both systems. Specifically, the focus will be on parameters such as energy efficiency and transient response, both of which are influenced by various factors discussed in this section. Finally, a comparison will be made between the two systems to distinguish optimization and control strategies.

### Indirect Methanol Fuel Processor - Description of the Components

Figure 42 shows the IM fuel processor's main subsystems, which include a fuel/water pre-heater/mixer, steam reformer, CO cleanup unit (shift and PROX), and burner. In addition, a controller is used to determine the methanol supply to the reformer and burner.

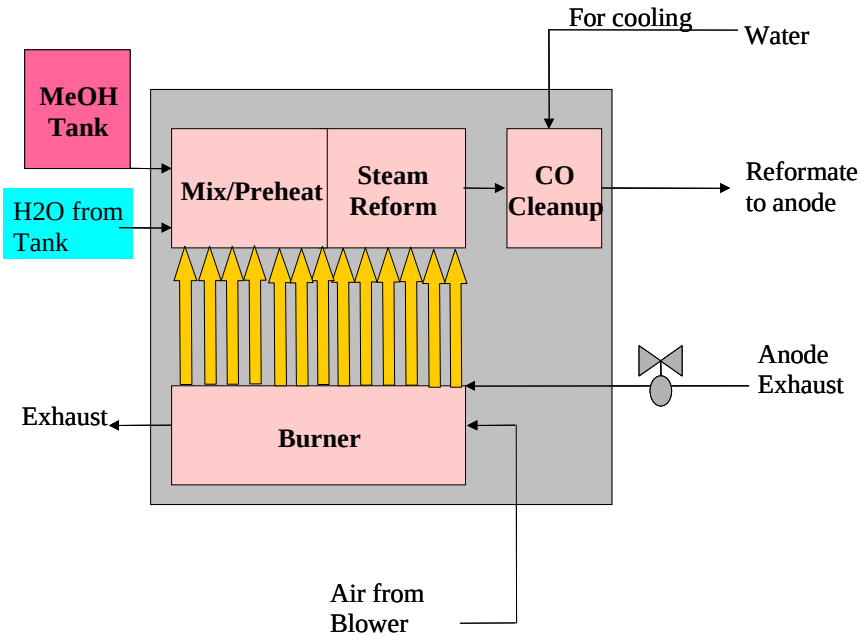


Figure 42: Details of IM Fuel Processor

***Fuel pre-heater***

The fuel pre-heater unit accepts liquid fuel streams from the water and methanol tanks and is responsible for preheating and superheating the streams prior to entry into the reformer. The burner and an optional additional heater supply the heat required for this process. The pre-heater is a simple thermodynamic lumped parameter model.

***Reformer***

The reformation process used in the IM fuel processor is steam reformation, for which the full reaction can be expressed as:

$$CH_3OH + H_2O \rightarrow CO_2 + 3H_2 \qquad \Delta H = +50kJ/mol \text{ Gaseous reactants}$$
$$\Delta H = +131kJ/mol \text{ Liquid reactants}$$

The steam reformation of methanol is an endothermic process that needs a heat source for providing the necessary energy for the process. Adequate heat transfer is imperative for good reformer transient response and some form of thermal integration with a heat source is required. The reformer is dynamically modeled taking into account kinetics based on Amphlett (1994), mass transfer and heat transfer related processes taking place inside the reformer.

***Burner***

A burner is used to oxidize the fuel cell anode exhaust gas that contains combustibles such as hydrogen. In addition, as needed, some primary fuel can also be added to the anode exhaust in order to supply the heat of evaporation and heat of reaction for the steam reformer. Emissions from the fuel processor are primarily associated with the burner, as nitric oxide (NO) is produced during the burning process. With a catalytic burner (which is thermally integrated with the reformer), NO levels are kept extremely low. The burner is dynamically modeled taking into account kinetics based on Ito (1990), mass transfer and heat transfer related processes taking place inside the burner. NO kinetics are based on Wark and Warner (1981).

***CO cleanup***

There are several methods for removing CO from the reformate, as it is detrimental to the fuel cell catalyst performance. Low temperature water-gas shift reactors are typically used as the first step of CO cleanup in IM fuel processors.
The shift chemical reaction can be expressed as:

$$CO + H_2O \Leftrightarrow CO_2 + H_2, \qquad \Delta H = -40.6kJ/mol \tag{7}$$

As the CO content is high in the reformate, the shift reaction generates additional hydrogen when CO is converted to $CO_2$. Traditional shift reactors are large because the reaction rate is relatively low; therefore, more water needs to be evaporated and injected into the shift reactor to drive the equilibrium to lower CO levels.

The Preferential Oxidation (PROX) unit is the last operation in the process stream and is employed as a step to further reduce CO to levels acceptable to the fuel cell stack

(10-100 ppm). The PROX reactions are exothermic with the oxidation of CO and, to a lesser extent, $H_2$.

$$CO + \frac{1}{2}O_2 \Rightarrow CO_2, \quad \Delta H = -283 kJ / mol$$

$$H_2 + \frac{1}{2}O_2 \Rightarrow H_2O, \quad \Delta H = -242 kJ / mol \tag{8}$$

The PROX selectively catalyzes the oxidation of CO while consuming a minimum amount of $H_2$. Temperature control is important to catalyst selectivity, and based on relative heats of adsorption of CO and $H_2$ on Pt, CO selectivity is likely to be reduced at higher temperatures. While higher temperatures produce higher reaction rates that require lower catalyst loading, selectivity is adversely impacted by higher temperatures and can have a corresponding efficiency impact due to $H_2$ consumption.

Based on the initial evaluation of the fuel processor performance, the final representation of the CO cleanup units in our vehicle system was as a lumped parameter model with 40% overall selectivity (based on Kahlich, et al, 1997).

***Airbleed***

Air bleed is used to meet the requirements of CO tolerance in the stack. The airflow is considered as 3% of the dry reformate flow exiting the CO clean-up unit based on an estimated concentration of 100 ppm of CO in the H2 exit flow.

***Controller***

The controller associated with the fuel processor accepts the hydrogen (or Methanol) request from the system (see section 4.1.2) and decides both the amount of methanol to be supplied to the reformer and to the burner (and preheater). Proper choice of controller parameters and algorithms is very essential from the viewpoint of increasing the transient response and overall efficiency. In general, the methanol feed to the burner will depend directly on the methanol feed to the reformer. Too high a burner methanol flow will result in higher reformer temperatures and hence higher CO production and lower efficiencies. Too little methanol will mean that there is insufficient energy available for the endothermic steam reformation reaction and this will lead to lower conversions of methanol to hydrogen in the reformer.

In addition, the anode exhaust flow-stream from the stack contains hydrogen, carbon dioxide and some water and is also an input stream flowing into the burner. The catalytic hydrogen combustion provides part of the thermal energy needed by the reformer and has to be taken into account when deciding the methanol flow into the burner. Since the amount of hydrogen in the anode exhaust depends on the utilization inside the stack, which is influenced by the fuel cell and vehicle operating strategies, this is another point at which the fuel processor is closely coupled to the rest of the system.

In the Indirect Methanol case, in order to maintain the utilization around 85% (stack specifications typically specify this value), and the corresponding hydrogen supply to the stack under dynamic load conditions, it was found essential to have a “back-pressure” control strategy as opposed to a simple feed-forward control strategy (as noted in section 4.1.2). This method takes advantage of the presence of hydrogen rich mixture inside the volume of the fuel processor (intrinsic hydrogen “buffer”) at the cost of

permitting the pressure inside the fuel processor to vary around 1-5%. This ensured fairly rapid hydrogen supply response to the dynamic load demand from the stack (of course, the hydrogen thus lost from the intrinsic fuel processor "buffer" would have to eventually be replenished).

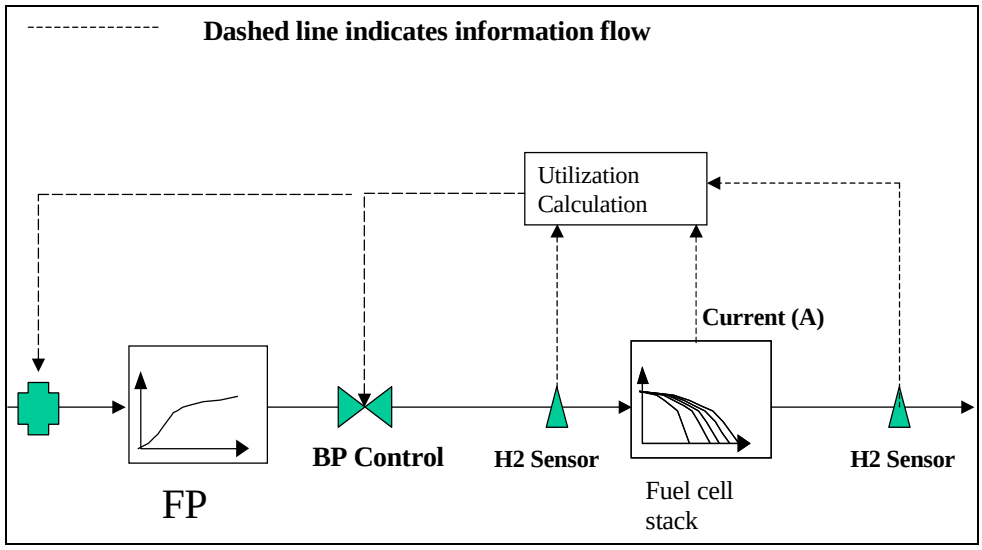


Figure 43 – Flow Control System

This algorithm however assumes that there is zero lag in both the utilization sensor and the backpressure value actuator – assumptions that may need to be validated in practice.

### Indirect Hydrocarbon Fuel Processor - Description of the Components

Figure 44 shows the IH fuel processor's main subsystems, which include a fuel, steam and air pre-heater/mixer, autothermal reformer, CO cleanup unit (high and low temperature shift reactors and PROX), steam generator and burner.

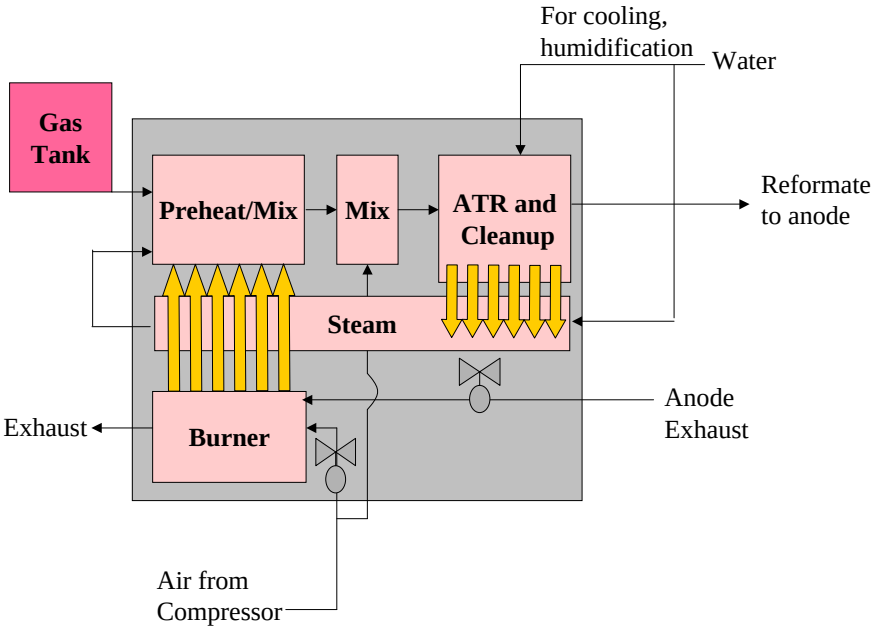


Figure 44: Details of IH Fuel Processor

***Fuel, steam and air pre-heater/mixer***

The fuel pre-heater unit accepts liquid fuel streams from the gasoline tank and mixes with steam provided by the steam generator. The mixture combines with air before being sent to the ATR, and the burner supplies the heat required for this process.

***Autothermal Reformer***

The autothermal reaction can be expressed as

$$C_nH_mO_p + x(O_2+3.76N_2) + (2n-2x-p)H_2O = nCO_2 + (2n-2x-p+m/2)H_2 + 3.76xN_2 \quad (9)$$

where $x$ is the oxygen-to-fuel molar ratio. The autothermal reactor should be operated in a manner that the overall reaction is exothermic, but at a low value of oxygen to fuel ratio where the higher hydrogen yields and concentrations are favored. The partial oxidation process of the ATR is a fast reaction and provides the necessary endothermic energy for the steam reformation process. The ATR is a thermodynamic model using parameters from Chan and Wang (2000).

***CO cleanup***

As in the IM fuel processor, the IH processor consists of shift and PROX units; however, an additional high temperature shift reactor is necessary due to the higher levels of CO emitted by the ATR fuel processor. The HTS and LTS models used here are detailed models incorporating kinetics (based on Podolski and Kim, 1974 for the HTS and Amadeo and LaBorde, 1995 for the LTS), mass transfer and heat transfer. These models also assume a decreasing (currently fixed) temperature profile that helps ensure better CO cleanup. They are thermally integrated with the steam generator in a

counterflow arrangement. Provisions are also made for water/steam injection into the reformate stream prior to its entry into the HTS and LTS units. This helps maintain the requisite S/C ratios that were determined to be the optimal values based on stand-alone testing of the HTS and LTS units. The selectivity in the PROX unit is based on Kahlich, et al (1997).

***Airbleed***

Air bleed is used to meet the requirements of CO tolerance in the stack. The airflow is considered as 3% of the dry reformate flow exiting the PROX based on an estimated concentration of 100 ppm of CO in the H2 exit flow.

***Steam Generator***

The steam generator uses heat from the anode exhaust burner and shift reactor units to generate steam used in the steam reformation process of the autothermal reaction. The steam generator is assumed to be the slow step in the fuel processor system, relative to the air compressor, which is assumed to respond instantaneously. Currently, the steam generator is assigned a time-constant of 0.01s which is a fairly aggressive number but can be adjusted based on the specific steam generator specifications.

## Steady State Analysis – IM and IH

In this section, the primary focus is on the issues of energy efficiency and transient response of the fuel processor. In the fuel processor modeling four different efficiencies are used to better understand the fuel processor performance:

FP Overall Efficiency: fuel processor efficiency over the cycle, including H2 utilization and air bleed losses. This is defined as

$$\frac{(\text{H2\_consumed @ stack} * \text{LHV\_H2})}{(\text{Fuel\_into\_fuel\_processor} * \text{LHV\_fuel})}$$

FP Efficiency: amount of hydrogen produced divided by the amount of fuel in.

$$\frac{(\text{H2 produced by FP} * \text{LHV\_H2})}{(\text{Fuel\_into\_fuel\_processor} * \text{LHV\_fuel})}$$

H2 Air Bleed Efficiency: amount of hydrogen in the anode inlet divided by the amount of hydrogen at the FP-PROX exit. Air bleed is used to meet the requirements of CO tolerance in the stack. For both systems (IM and IH), the airflow is considered as 3% of the H2 flow exiting the fuel processor (CO Clean up unit for the IM and Prox for the IH) based on an estimated concentration of 100 ppm of CO in the H2 exit flow.

$$1 - \frac{(\text{H2 lost due to airbleed})}{(\text{H2 produced by FP})}$$

H2 Utilization Efficiency: amount of hydrogen used up in the stack divided by the amount of hydrogen available for electric power generation (ie. net hydrogen available at the anode after accounting for the air bleed losses).

$$\frac{\text{(H2 consumed by the stack)}}{\text{(H2 produced by FP - H2 lost due to airbleed)}}$$

One of the primary differences between the IM and the IH cases is the presence of the air compressor (for the ATR) in the IH case. The power for this should logically come from the overall fuel cell system (and would represent a parasitic load along with the cathode side compressor parasitic load). For the purposes of consistency and clarity, it does not make too much sense to modify the IHFP efficiency value using this figure.

** NOTE: unless otherwise specified, the efficiencies shown below refer to the FP Overall Efficiency.*

## Steady State Results and Discussion

### *a) IM efficiency v. power level*

Figure 45 shows the IM fuel processor overall efficiency at 85 % H2 utilization efficiency and 98.2 % air bleed efficiency as a function of the power. In this case power is expressing the amount of hydrogen consumed by the stack on a LHV basis. The numbers for the IM H2 Utilization Efficiency and the IM Air Bleed Efficiency come from the analysis of the simulation results.

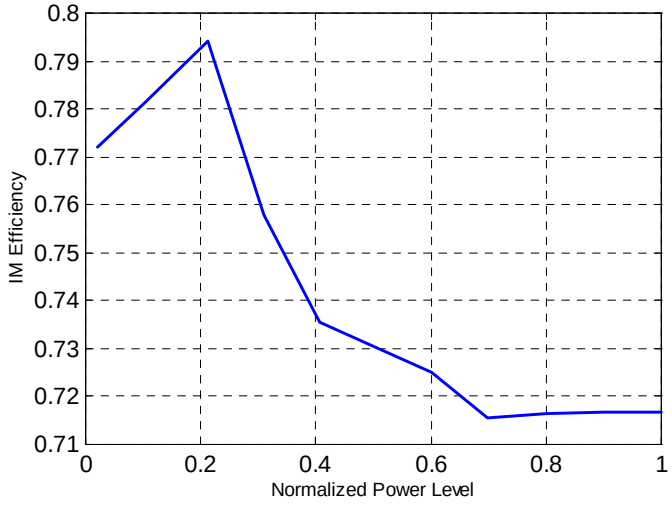


Figure 45 - IM Overall Efficiency versus Normalized Power

### *b) IH efficiency v. power level (not incl. compressor)*

Figure 46 shows the IH fuel processor overall efficiency @ 85 % utilization efficiency and 97 % air bleed efficiency as a function of power. Here again power is

representing the amount of hydrogen consumed by the stack and the numbers for the IH H2 Utilization Efficiency and the IH Air Bleed Efficiency were determined by the analysis of the simulation results. It can be seen that the IH overall efficiency is pretty much flat (note the y-axis scale) over the entire range of operation.

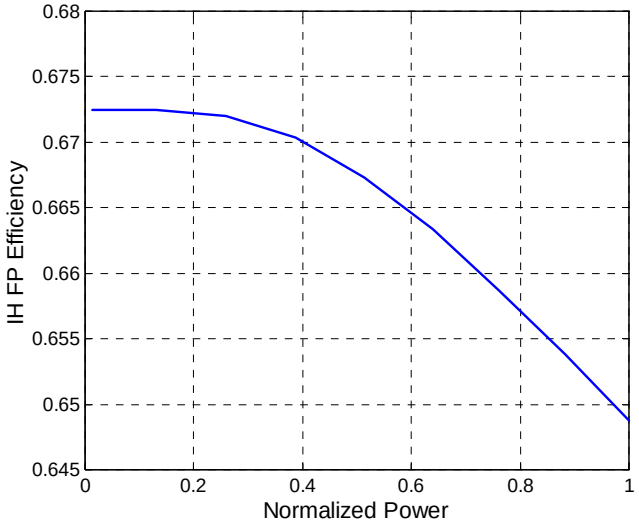


Figure 46 - IH Overall Efficiency versus Normalized FP Power Level

***c) IH compressor consumption v. power level***

Figure 47 is showing the IH compressor power requirement as a function of the power level. It is important to remember that this is the compressor used to supply air to the IH fuel processor and that power (x-axis) is proportional to the amount of hydrogen consumed by the stack.

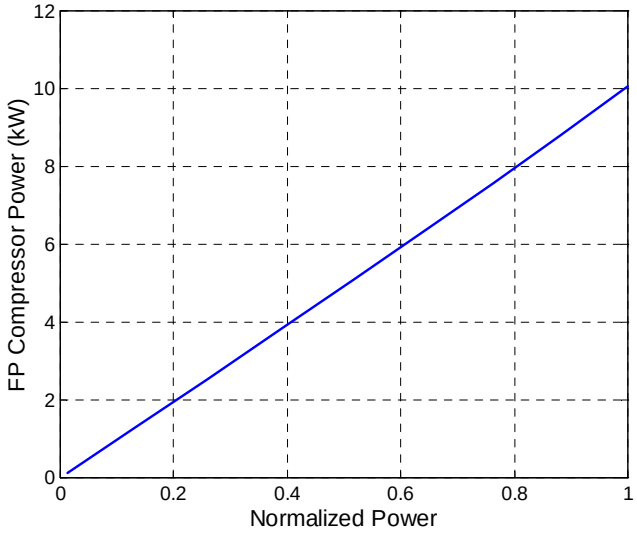


Figure 47 - IH Compressor Consumption versus Normalized FP Power Level

***d) IM step response (100% of full power)***

The IMFP step response is governed by a number of different factors. The main factor is the second order response due to the thermal lag in getting the energy to the reformer from the burner. The second factor is what we term as the volumetric response due to the presence of both the thermal energy available in the thermal mass of the reformer and the hydrogen available in the volume of the reformer. This can be approximated for some FP configurations as a first order effect in terms of hydrogen flow rate. The third factor is one that comes purely from the pneumatic effect of assuming constant pressure in the system. This effect is a zeroth order effect and results in an immediate step response of the exit flow equal to the value of the number of moles coming into the fuel processor. In our current formulation, a reduced version of the full fuel processor model is used to represent the IMFP characteristics. This reduced model tries to take into account the three effects described above. The results from this model correspond exactly to the full model results under steady state conditions. Under the FUDS driving cycle, (see the appendix) the difference between the reduced model predictions and the full model predictions is less than two percent. The typical full fuel processor response to a step increase in demand is shown below in Figure 48 and it can be seen that the response in terms of hydrogen flow (available for conversion at the anode assuming air bleed losses and 85% utilization) is less than 2 seconds. It should be noted that this is the response using a feed-forward controller and not the backpressure controller.

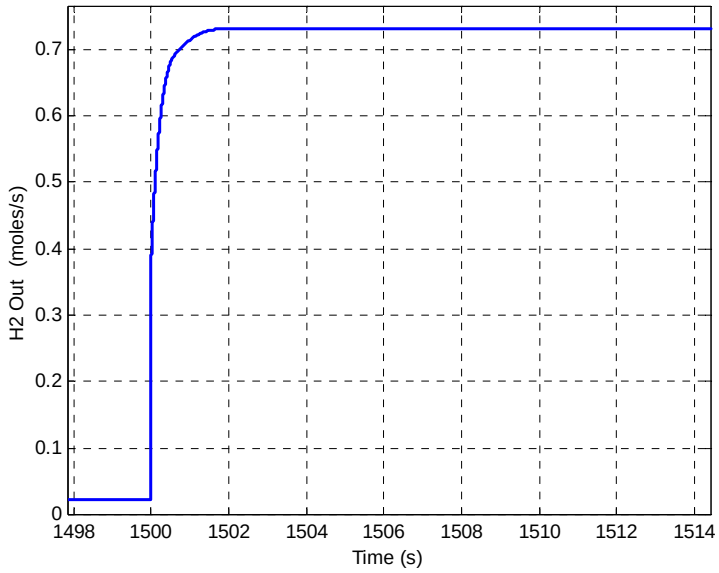


Figure 48 - IM step response (100% of full power)

***e) IH step response (100% of full power)***

Figure 49 shows the step response of the IH case when looking at the IH fuel processor response. This response is account for the 85% hydrogen utilization and 3% air-bleed and effectively shows the amount of hydrogen available for electric power production. It is important to point out that the step response in this case is dependent to

the steam generation. A plot showing the steam generation unit response can be seen in the appendix. The IH FCVSim model considers the steam generation time constant to be around 0.01 s ; this parameter can be adjusted based on the specific ATR steam generator characteristics.

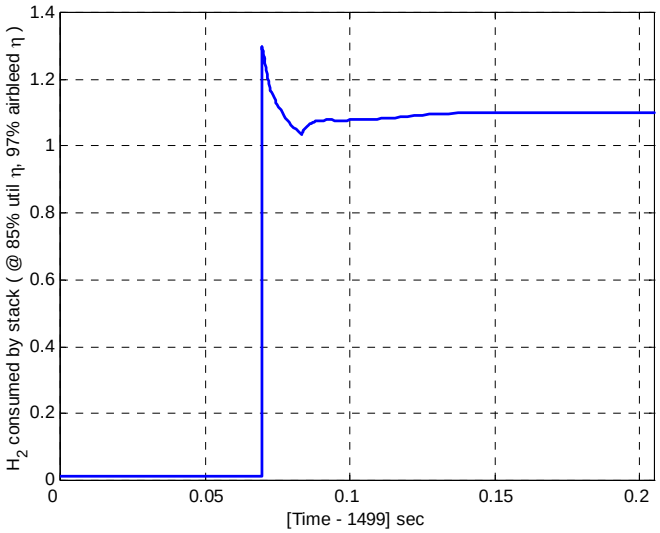


Figure 49 - IH step response (100% of full power)

## Dynamic Analysis - IM and IH

At this point it is important to analyze the potential impacts on the dynamic behavior of the fuel processor.

It was quickly realized that even with a relatively fast fuel processor, the small time lag needed for the supply of the hydrogen required to meet the current demand at the stack exceeded the FP's ability to deliver the proper amount of hydrogen. It was concluded that some method of controlling the utilization within the stack would be desirable.

For the IM fuel processor the method chosen was backpressure (BP) control. By using the volume within the FP and fuel cell stack as 'hydrogen storage', the pressure within the system could be varied quickly enough to account for variations in the hydrogen requirement and availability. The BP control uses the utilization within the stack as a control variable and tries to maintain hydrogen utilization of around 85%.

The controller for the IH fuel processor also uses a utilization set point of 85%; however, a modified form of a utilization-based control strategy is used. If backpressure control were used, the pressure variations that control the volume of hydrogen in the fuel processor would send a feedback to the air compressor and it was thought that this would not be a desirable operating mode. The primary feature of this control strategy is that as the utilization approaches and exceeds 85%, the controller rapidly ramps up the hydrogen request to the fuel processor regardless of the immediate demand of the fuel cell system (in terms of power demand). This helps ensure that the stack is never starved of hydrogen and thus cause any catastrophic loss in power but on the other hand it adversely impacts the overall drive-cycle efficiencies. The IH FCVSim model does NOT consider the use of a buffer as the default option. However it is an option in the model. The effect of the use of a hydrogen buffer is illustrated in the drive cycle results section.

## Drive Cycle Results and Discussion

As mentioned before, in the fuel processor modeling, four different efficiencies are used to better understand the fuel processor performance:

FP Overall Efficiency: fuel processor efficiency over the cycle, including H2 utilization and air bleed losses. This is defined as

$$\frac{(\text{H2\_consumed @ stack} * \text{LHV\_H2})}{(\text{Fuel\_into\_fuel\_processor} * \text{LHV\_fuel})}$$

FP Efficiency: amount of hydrogen produced divided by the amount of fuel in.

$$\frac{(\text{H2 produced by FP} * \text{LHV\_H2})}{(\text{Fuel\_into\_fuel\_processor} * \text{LHV\_fuel})}$$

H2 Air Bleed Efficiency: amount of hydrogen in the anode inlet divided by the amount of hydrogen at the FP-PROX exit. Air bleed is used to meet the requirements of CO tolerance in the stack. For both systems (IM and IH), the airflow is considered as 3% of the H2 flow exiting the fuel processor (CO Clean up unit for the IM and Prox for the IH) based on an estimated concentration of 100 ppm of CO in the H2 exit flow.

$$1 - \frac{(\text{H2 lost due to airbleed})}{(\text{H2 produced by FP})}$$

H2 Utilization Efficiency: amount of hydrogen used up in the stack divided by the amount of hydrogen available for electric power generation (i.e. net hydrogen available at the anode after accounting for the air bleed losses).

$$\frac{(\text{H2 consumed by the stack})}{(\text{H2 produced by FP - H2 lost due to airbleed})}$$

**Comparison of Efficiencies and Fuel Economy using FUDs, HIWAY, and US06 Drive Cycles:**

***a) IM Fuel Processor***

Table 13 - Efficiency comparisons for the IM

| | IM FUDS | IM HIWAY | IM US06 |
|---|---|---|---|
| **FP overall eff** | 68 | 73 | 66 |
| **FP efficiency** | 88 | 91 | 78 |
| **H2 airbleed eff** | 98 | 98 | 98 |
| **H2 utilization eff** | 79 | 81 | 86 |
| **Vehicle Efficiency (%)** | 26 | 31 | 27 |

Analyzing Table 13 and Figure 50, one can see that the efficiencies vary with the drive cycles, except the air bleed efficiency, which is the same for all drive cycles. The H2 Utilization and the FP efficiency numbers vary significantly across drive cycles.

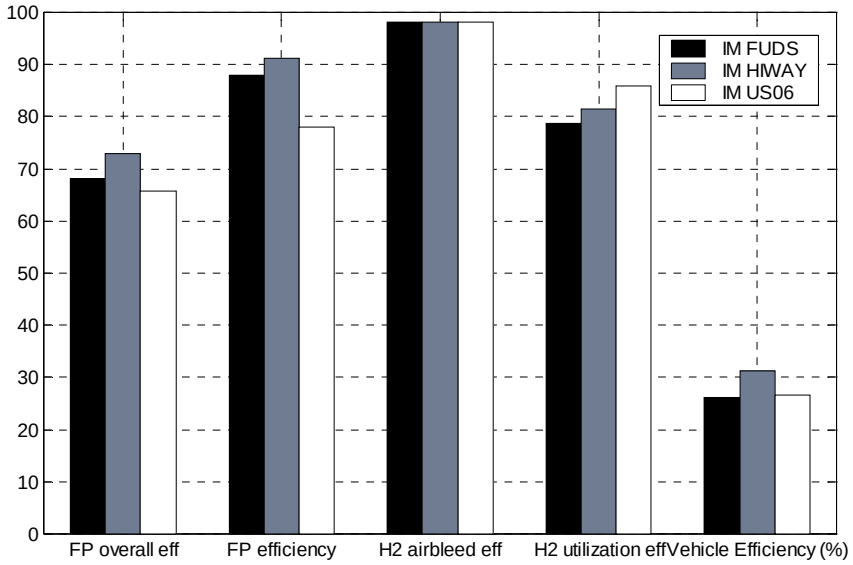


Figure 50 – IM FP Efficiencies for Different Drive Cycles

***b) IH Fuel Processor***

The corresponding results for the IH FP are as shown below. The trends seen here are similar to the ones seen in the IM case. The principal effect on the overall fuel processor efficiency is that due variations in the intrinsic fuel processor efficiency and the utilization efficiency.

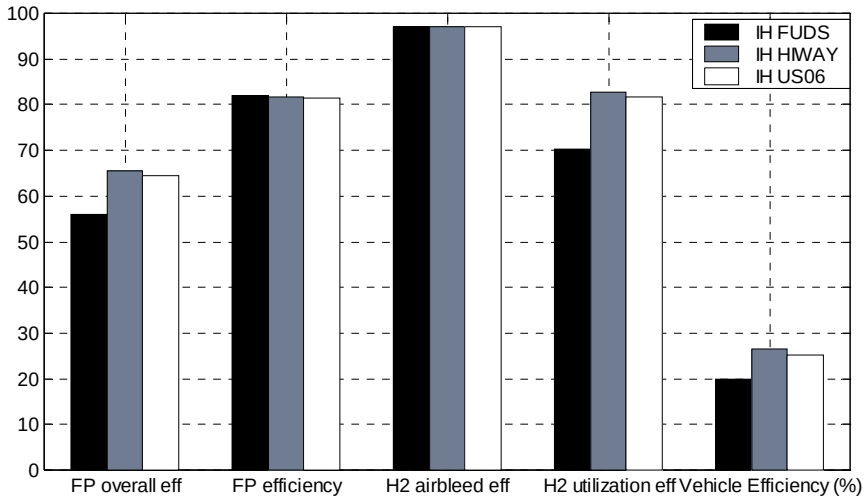


Figure 51 : IH FP Efficiencies for Different Drive Cycles

The corresponding numerical values are shown in Table 14 below.

Table 14: Numerical values for IHFP efficiencies for different drive cycles

| | IH FUDS | IH HIWAY | IH US06 |
|---|---|---|---|
| **FP overall eff** | 56 | 66 | 65 |
| **FP efficiency** | 82 | 82 | 81 |
| **H2 airbleed eff** | 97 | 97 | 97 |
| **H2 utilization eff** | 70 | 83 | 82 |
| **Vehicle Efficiency (%)** | 20 | 27 | 25 |

However, unlike the IM case, here the intrinsic FP efficiency is fairly constant over all the drive cycles. As in the IM case, the effect of air bleed seems independent of the drive cycle type (it is however slightly higher than that for the IM case). The only other factor that strongly influences the overall fuel processor efficiencies is utilization efficiency. The one other significant feature of the results shown above is that the overall fuel processor efficiency is better in the US06 cycle than the FUDs cycle. (Note: The plots comparing these two vehicles for different drive cycles are included in the Appendix).

Since the utilization efficiency plays such an important role in both the IM and the IH cases, it might be useful to recall the physical meaning of utilization efficiency. When averaged over a drive-cycle, the utilization efficiency gives us a measure of the ability of the stack to use the hydrogen available to it. So a higher value of utilization implies better

use of the hydrogen by the stack. The quantity (1-util) gives us the fraction of the hydrogen flow that ends up in the anode exhaust.

However, the presence of hydrogen in the anode exhaust need not have that severe an impact on the overall system efficiency if one can utilize the hydrogen in the FP burner for providing either the endothermic heat requirements or for superheating the steam and the fuel. But there is a limit to how much energy is needed for this process and if a lot of hydrogen makes its way to the burner, for practical reasons, some of it will have to be flared to prevent either reformer catalyst deactivation (IM case) or steam blanketing of the ATR catalyst (due to excess steam production in the IH case).

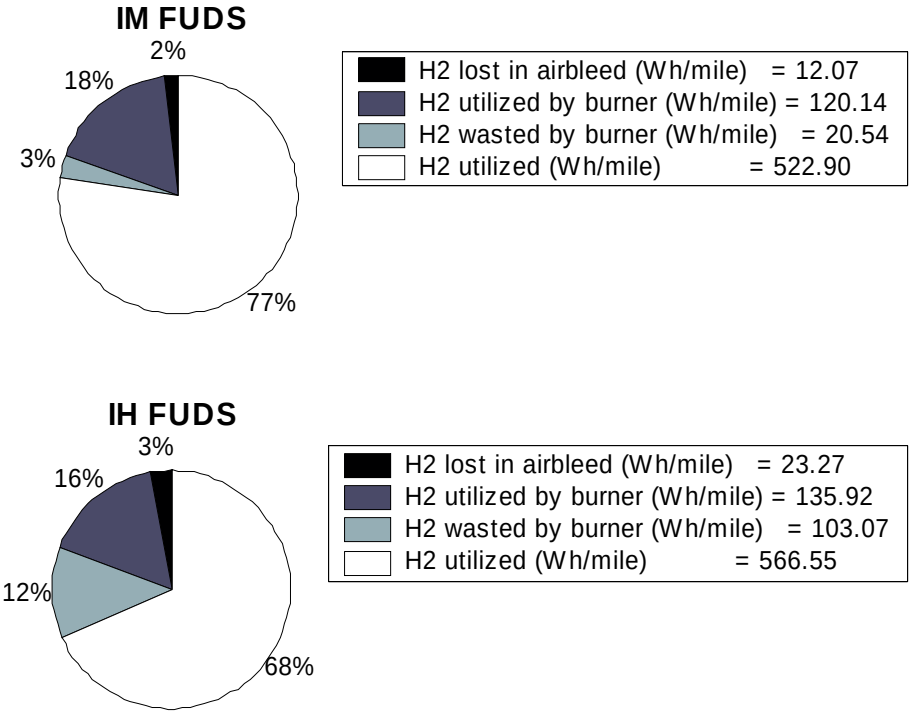


Figure 52: IM and IH fuel processor hydrogen inventory for the FUDS cycle. The total hydrogen produced is a) IM – 675.64 Wh/mile, b) IH – 828.81 Wh/mile

Figure 52 shows the differences in the use of the anode hydrogen exhaust from the stack. While the burner in the IM case is able to use most of the hydrogen (~85%) in the IH case, only slightly more than half of the anode exhaust is used up. Contrary to what one might think at first, the differing nature of the reactions in the case of IM (endothermic with fuel and steam generation requirements) and the IH case (ATR – nominally exothermic), is not the primary reason for the inability to use the hydrogen. This point should become clearer when we look at the corresponding results for the US06 cycle.

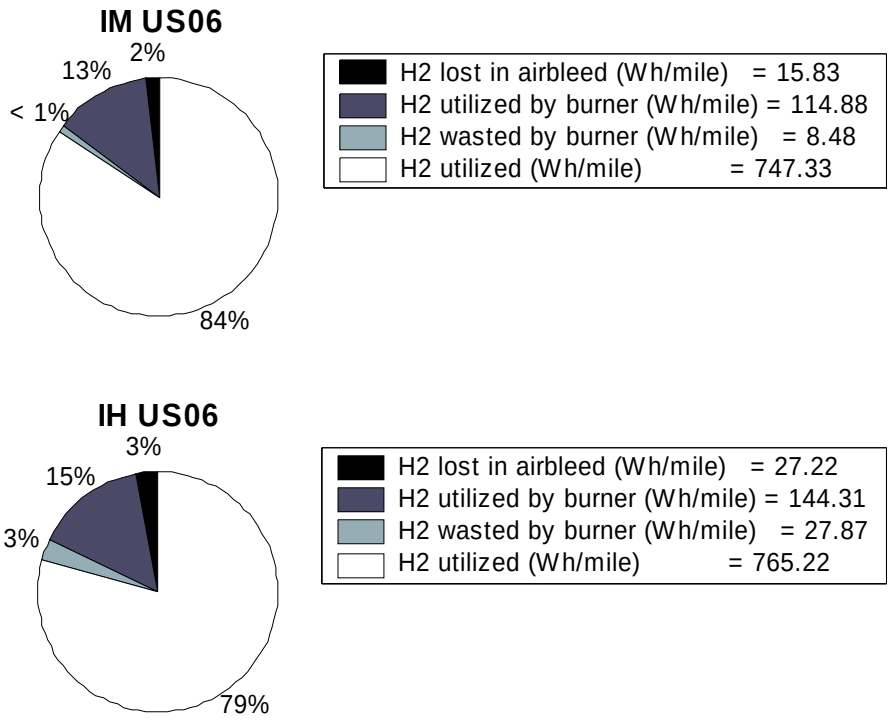


Figure 53: IM and IH fuel processor hydrogen inventory for the US06 cycle. The total hydrogen produced is a) IM – 886.51 Wh/mile, b) IH – 964.62 Wh/mile

One can see that in this case of a higher power cycle, there is better ability to utilize the hydrogen in the anode exhaust gas and not waste it. The IM burner is able to use up 93% of the anode hydrogen exhaust and the IH burner is able to use up 84% of the anode exhaust - a considerable improvement over its rather dismal performance in the FUDS cycle. The question here would be whether the increased ability is due in some way to the increased demands for thermal energy from the burner or due to better control on the amount of hydrogen in the anode exhaust.

Table 15: Utilization efficiency in the two cycles

| H2 utilization eff | FUDS | US06 |
|---|---|---|
| IM | 79 | 86 |
| IH | 70 | 82 |

In order to understand this issue, it might be useful to revisit the issue of utilization efficiency (Table 15). The lower the utilization efficiency value, more of the hydrogen makes its way to the burner. It can be seen that for the US06 cycle, relatively minor fractions of the hydrogen makes its way to the burner whereas in the FUDS case, a larger fraction of the hydrogen supplied to the stack gets sent to the burner. The reason

for this is closely tied to the nature of the controller for the IM and IH cases and the nature of the drive cycles themselves.

The fuel processor fuel supply controllers are designed from the viewpoint of being able to aggressively meet the drive cycle requirements and prevent stack failure due to stack hydrogen starvation. In the FUDS cycle, though the average power is smaller, there are a lot more up-down transients than in the US06 cycle where the average power is higher. The downturns hit the fuel processor utilizations particularly hard due to the fact that the stack load drops instantly to zero while the fuel processor is still at a high power level and is able only (relatively) slowly to drop-down to low operating power levels. What this indicates is that large number of down-transients have a negative effect on the overall fuel-processor efficiency.

This impact is seen more strongly for the IH, which does not have a backpressure controller to help it approximately phase match the supply and demand. Instead the controller tries to operate at a higher average power level in an attempt to keep the utilization below 85%.

In order to see the impact of better control schemes, it might be useful to assume that an external hydrogen buffer could be made to operate with the IH fuel processor (while assuming that the pressure fluctuations have no effect on the operation of the fuel processor – an assumption that could be true if the fluctuations were kept below a level determined during the characterization of the fuel processor).

Table 16 - Efficiencies for the IH with and without an external buffer ; FUDs Cycle results

| FUDs Cycle | IH without buffer | IH with buffer |
|---|---|---|
| **FP overall eff** | 56 | 62 |
| **FP efficiency** | 82 | 82 |
| **H2 air bleed eff** | 97 | 97 |
| **H2 utilization eff** | 70 | 78 |
| **Vehicle Efficiency (%)** | 20 | 22 |

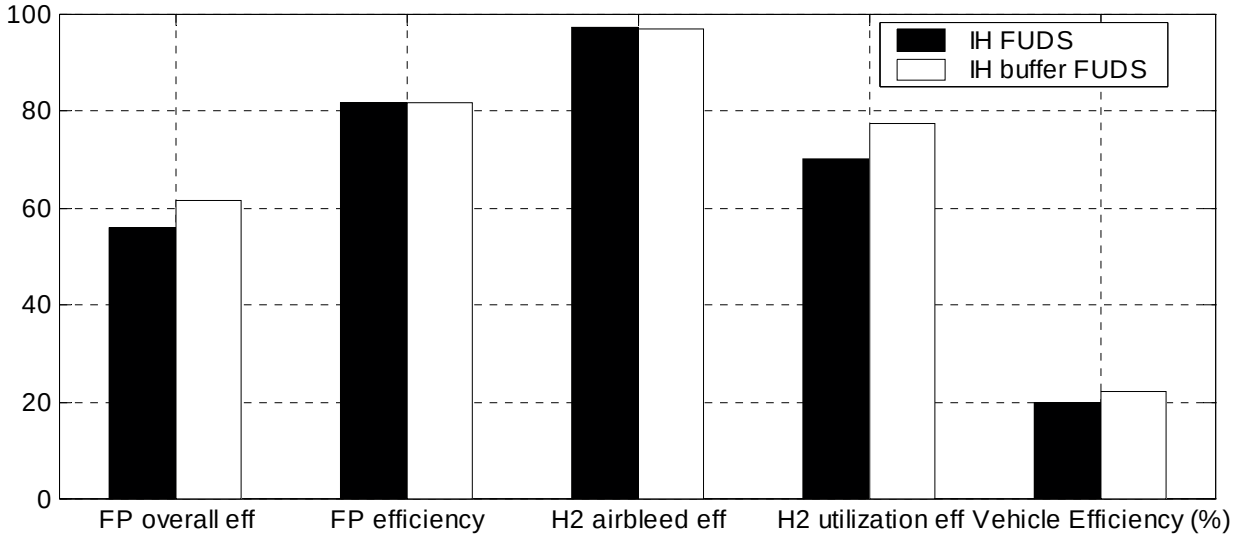


Figure 54 - Efficiencies for the IH - FUDS Cycle

Table 16 and Figure 54 show the comparison between an IH case with a buffer and without a buffer. In this case, the use of a buffer increases the H2 Utilization efficiency and consequently the FP overall efficiency also increases. There is comparatively little impact on the air bleed or intrinsic fuel processor efficiencies. This shows the maximum possible improvements that could be achieved by focusing on designing an appropriate controller for this drive-cycle. However, since vehicles are designed to operate effectively on all the drive-cycles, the redesign would have to ensure that the proper vehicle performance was achieved under all conditions.

** NOTE: The IH without the buffer is the default vehicle option. At present, based on our analysis and feedback from our experts, IH reformate buffering doesn't appear to be a practical solution to the problem of excess anode hydrogen flow.*

Additional results comparing the IM with the IH (buffered and unbuffered) are shown in the appendix.

#### 4.1.4.3 Air Supply

**Description**

The cathode flow stream of the fuel cell system is controlled with the use of a compressor device, though other components play important roles in the flow stream loop.

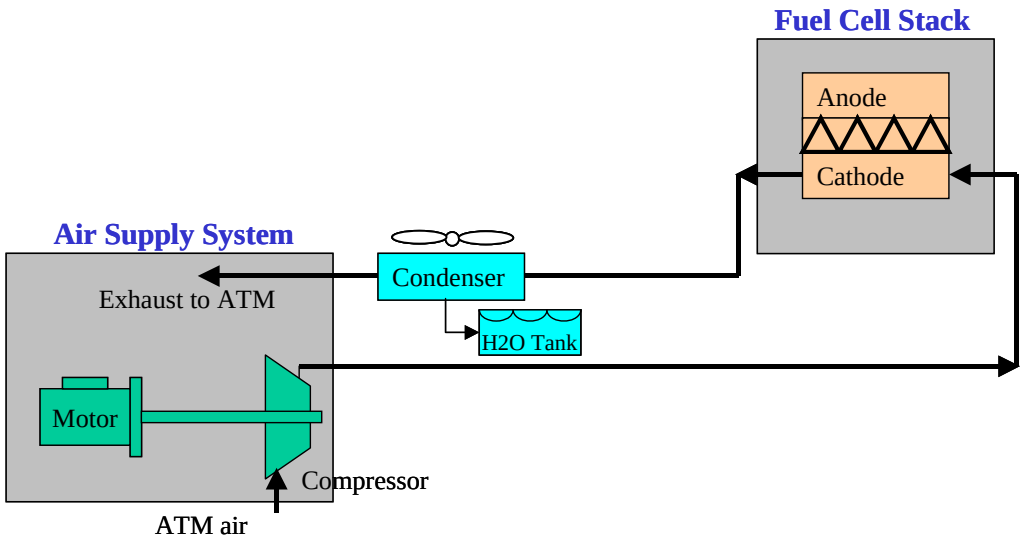


Figure 55: The Air Supply System in the fuel cell engine

Figure 55 above shows the components that interact with the cathode stream. The air supply system includes a compressor with a variable speed electric motor. Compressed air is sent directly into the cathode of the fuel cell stack where oxygen is depleted for power generation.

The gross power of the fuel cell stack is directly dependent on the partial pressure of oxygen ($p_{oxygen}$) at the cathode catalyst reaction sites. Each single value of $p_{oxygen}$ corresponds to a single cell voltage value at each particular current density. However, $p_{oxygen}$ is a function of both the total air pressure and the air mass flow rate, and can be achieved through different combinations of the two. For this reason, a compressor that can provide variable flow and pressure is required.

The following equation shows the relationship between the air flow rate (g/s) provided from the compressor and the current generated in the fuel cell stack (amps) at the catalyst reaction sites.

$$\dot{m}_{a\_comp} = \frac{I_{stack}\, 4.76 MW_{air}\, (n\_cells) SR}{4F} \qquad (10)$$

where SR is the stoichiometric ratio of air is ratio of ***moles of $O_2$ in the air per second*** supplied to fuel cell stack vs. ***moles of $O_2$ per second*** utilized at the corresponding stack. F is the Faraday's constant (96,484 C/mole) and n_cells is the number of active cells in the fuel cell stack.

All of the system configurations require such an air management sub-system. For the DH, IM, and IH systems, the air system is essentially the same, where the air system/cathode loop is independent from the fuel/anode loop (This is contrary to some developments, for example, that combine the anode and cathode exhaust streams and heat the combined stream in a burner.) The only major difference between the three systems (in terms of the air management) is that the IH system requires a second means of air supply for use in the fuel processing sub-system. This is accomplished with a second, independent compressor for this study (see Figure 20).

In addition to the interaction with the fuel cell stack, the air system also interacts with water and thermal management components. Following the stack reactions, it is necessary to recover liquid water from the stack exhaust stream. This stream consists of excess oxygen, the unused nitrogen, and water liquid and vapor. If the amount of liquid water is not sufficient for system water requirements, a condenser is necessary.

For the simulations in this study, a screw-type, positive displacement compressor from Vairex Corp. was chosen that has a maximum $r_c$ (pressure ratio) capability of 2.5 and a maximum air mass flow rate of 105 g/s at an $r_c$ of 1.8 (assuming STP conditions). The performance maps used in the model adequately account for the associated limitations of the particular technology (maximum and minimum performance regions). Additionally, a variable speed motor and controller map was utilized to determine the electric efficiency for the corresponding compressor shaft speed and torque. The motor operates with a current draw from the fuel cell stack and the same voltage as is produced at the stack. Control of the back-pressure acting on the compressor and control of the motor shaft speed allow for the manipulation of the desired air flow into the fuel cell stack. An expander (turbine) device was not used in these simulations.

## System Steady Analysis

One unique feature of the model is the optimization procedure between the fuel cell stack performance, the parasitic load of the air supply technology utilized, and the parasitic loads of the condenser and radiator for the WTM system. The optimization in the model determines the air system operating scheme such that the net system electric power is maximized for each value of the stack current density. A full description of this optimization procedure can be found in references in Section 5.4 [General System section: Friedman 1999, and Friedman 2001].

The defined net electric power is simply the stack gross electric power minus the parasitic loads of the air system electric motor (calculated from the air system model during the optimization process) and the WTM radiator and condenser loads. Equations 11 and 12 below specifically define these relationships.

$$P_{stack} = (VI)_{stack} \quad ; \quad P_{as\_motor} = \frac{(P_{sh\_comp})}{\eta_{as\_motor}} \tag{11}$$

$$P_{net} = P_{stack} - P_{as\_motor} - P_{rad} - P_{cond} \tag{12}$$

Different $r_c$ / air mass flow combinations lead to different water states (%vapor vs. %liquid) in the fuel cell exhaust. Both of these factors have ramifications on condenser and radiator loads and will affect pump and fan (parasitic) electric loads. For this reason, the condenser and radiator loads are taken into consideration when determining the optimum air system control strategy (see Equation 12 above).

As stated above, performance maps were incorporated into the model to determine the air compressor parasitic load. The following figure summarizes the performance of the screw-type compressor. The efficiency values plotted incorporate the mechanical losses in the compressor device as well as the isentropic efficiency of compression. Therefore, the resulting power is expressed at the shaft of the motor.

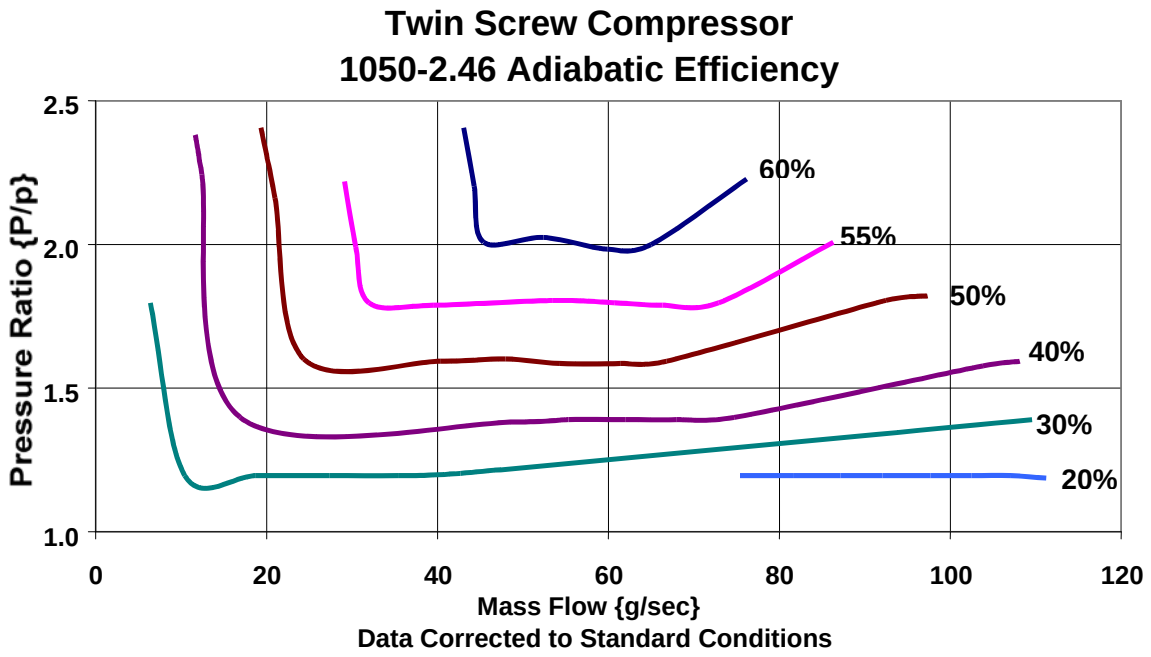


Figure 56: Vairex Screw Compressor Efficiency ($\eta_{\_comp}$)

The following equation can be used to calculate the shaft power given the information in the figure above. For this calculation, $T_1$=298K, $c_p$=1.005kJ/kg-K, and $k_c$=1.4.

$$P_{c\_shaft} = \frac{\dot{m}_a c_{pc} T_1 \left( r_c^{\frac{kc-1}{kc}} - 1 \right)}{\eta_{comp}} = \frac{P_{c\_isentropic}}{\eta_{comp}} \qquad (13)$$

The output performance control schemes from the optimization process represent a simulated steady-state operation. In other words, assuming instantaneous response of all mechanical components and gas streams, when an electric power is demanded of the fuel cell system, the optimization model provides a defined air pressure and mass flow rate at which to operate the system in order to maximize system efficiency.

Some of the results from the steady-state optimization are summarized in Figure 57 and Table 17 below. Figure 57 shows, given a variable $r_c$ and air flow operation, the ratio of the electric power for the compressor to the gross power from the fuel cell stack. This ratio is then plotted for the complete range of the stack's gross power capability.

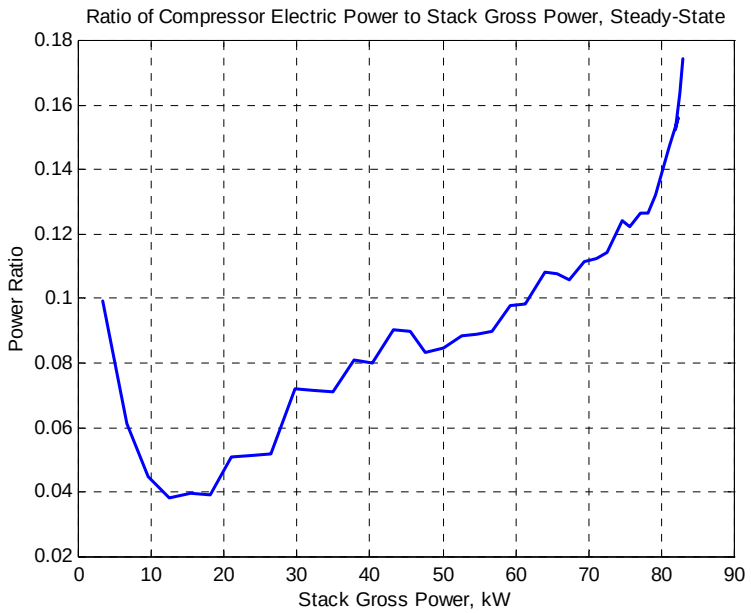


Figure 57: Air Supply and Stack Power Ratio – DH System

When optimized, the relative power for the compressor can be quite low in the partial load regions. Near full load operation, the compressor is forced to operate in a less efficient region of performance, and the power ratio begins to increase. The rapid increase in the power ratio at the very low load region occurs because the compressor has a minimum idle flow that it must provide (technology limited) regardless of the stack output power requirements for other loads.

Table 17: Air Supply and related System Parameters

*Note: All values are those that occurred at the **peak net power***

| | Net Power | Stack Power | Comp Power-e | Current density | Air mass flow | Air press at comp | Air Stoic Ratio |
|---|---|---|---|---|---|---|---|
| DH | 66.5 | 82.3 | 12.9 | 925 | 88 | 2.01 | 1.65 |
| IM | 75.0 | 90.0 | 12.3 | 775 | 82 | 2.10 | 1.40 |
| IH | **70.5** | 99.5 | 13.8 | 650 | 96 | 1.91 | 1.38 |

* All power values are in units of kW.

** Power-e = electrical power

Over the range of system net power load, the pressure and air flow demands vary, as stated previously. Generally, the air mass flow steadily increases from the minimum flow (~ 5 g/s) to the peak value shown in Table 17. The pressure, however, does not exhibit as steady of a ramp characteristic. Though, overall, the pressure increases, the optimized line decreases slightly at times for increasing load.

Table 17 shows specific values for all three systems at the peak load condition only. For all three systems, the peak pressure was similar. This is not the case for the air flow. As can be expected for a larger stack power, the IH system's peak air flow is greater than that of the DH system. However, the IM system shows a reduced peak flow

compared to that of the DH while occurring at a higher stack power. This can partly be explained by the slight increase in pressure for the IM system, but also by the reduced stoichiometric ratio (SR). At a SR of 1.40, a larger percentage of the flow is actually utilized in the stack, resulting in less total flow demanded.

## Transient Analysis

In reality, systems do not respond instantaneously. In general, there are two primary system characteristics that may result in a transient delay from the time the compressor motor is supplied with sufficient electrical power (relative to a demanded air pressure and air mass flow) to the time that the air pressure and flow reach the fuel cell stack cathode reaction sites. First, there is a time associated with changing the state of the air in the entire physical volume of pipes and cathode channels. This may be thought of as "charging" the system. The time delay will be relatively larger, for example, if the system needs to be changed from a low pressure (i.e. 1.2 atms) to a higher pressure (i.e. 3.0 atms). The second time delay is associated with the inertia of the compressor shaft movement. Specifically, an increase (from a steady state operation) in the rotational speed of a spinning object cannot occur instantaneously.

These simulations include a simple time delay feature that retard the supply of air pressure and air mass flow relative to the demanded stack current.

*Vehicle Drive Cycle Operation*

Over the course of a full drive cycle, the compressor motor consumes a portion of the total energy produced by the stack. Figure 58 shows the relative energy levels of each system type for three different drive cycles. The trends for any given drive cycle are expected: the DH system exhibits the lowest energy demand, and the IH system shows the highest energy demand. Note that for the IH and IM systems, this does not include the air supply requirements for the fuel processors.

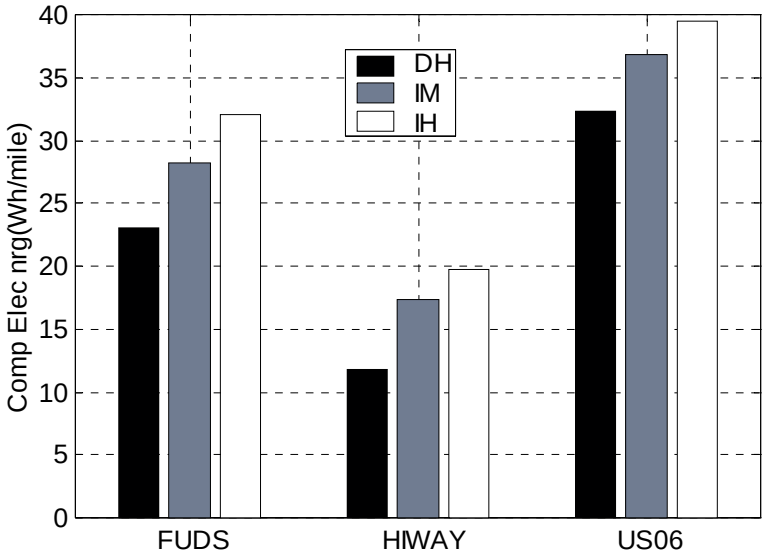


Figure 58: Air System electric energy, per drive cycle and system type

In Figure 58, the energy values are normalized with respect to the distance of each drive cycle. This makes it possible to compare the marginal energy demand between drive cycles. Here, once again, the results are expected. The US Hiway driving cycle is a lower power cycle due to less vehicle acceleration demands. The US06 cycle, on the other hand, is known to be the aggressive acceleration cycle of the three. Table 18 summarizes the numerical values from Figure 58 and also shows the ratio of the air compressor energy to that of the fuel cell stack.

Table 18: Drive cycle energy, Air System and Fuel Cell Stack

| | Comp Elec Energy (Wh/mile) | Comp/Stack Energy Ratio, % | Gross Stack Energy (Wh/mile) |
|---|---|---|---|
| DH FUDS | 23 | 7.4 | 310 |
| DH HIWAY | 12 | 4.7 | 248 |
| DH US06 | 32 | 8.0 | 404 |
| IM FUDS | 28 | 8.6 | 330 |
| IM HIWAY | 17 | 6.6 | 262 |
| IM US06 | 37 | 8.6 | 425 |
| IH FUDS | 32 | 8.8 | 365 |
| IH HIWAY | 20 | 7.0 | 281 |
| IH US06 | 39 | 8.7 | 452 |

This data expresses the aggregated power over the entire drive cycle (in other words, energy). However, it is worth noting that the power demand profile can be quite unsteady over the cycle. In other words, the demanded pressure and air flow profile can look quite sporadic and therefore require a responsive compressor motor and controller.

#### 4.1.4.4 Water and Thermal Management

**Scope**

For the purposes of this report, the water and thermal management (WTM) subsection refer to the primary heat transfer component (radiator) and primary water recovery unit (condenser) within the fuel cell system. These two components are analyzed in the context of the system and the impact they have as a parasitic power draw on the stack. The WTM views all other components in the system in the context of heat generation and water balance. The integration of the thermal management of the fuel processor is covered in that subsection independently.

## WTM system - Basic Elements

This section briefly describes the basic elements of a WTM system for fuel cell vehicles. The descriptions of several of the elements in the system (stack, fuel processor) are described from a WTM-centric viewpoint. In other words, the descriptions are greatly simplified to account for only the aspects that affect the WTM. The basics elements of the WTM system are similar for all three systems analyzed unless otherwise noted.

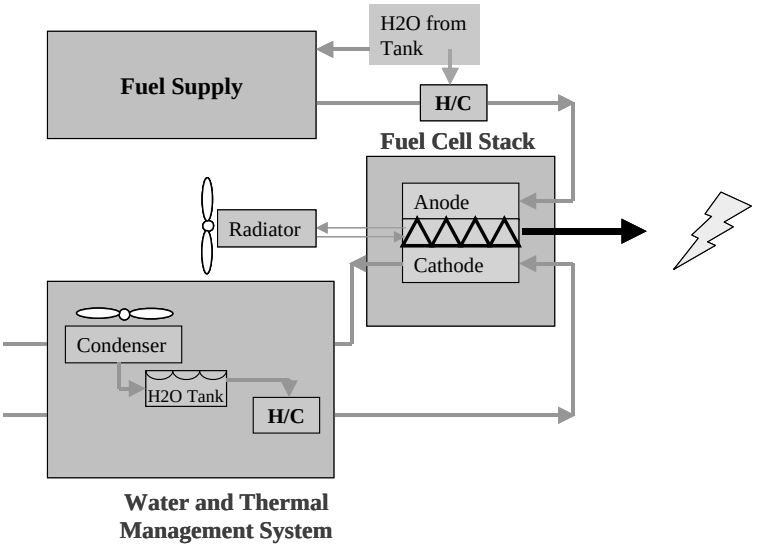


Figure 59: WTM System Diagram

## Fuel Cell Stack

From the perspective of the WTM, the stack is viewed a heat source and a water production component. Each aspect is first discussed independently, then as how they are interrelated.

### *Stack as heat source*

The stack can produce heat by two primary mechanisms: 1) the inefficient conversion of fuel energy into electrical energy and 2) the condensation of water inside the stack. The combination of these two heat sources is what determines the load on the radiator.

The amount of heat produced by the inefficient conversion of fuel energy is directly related to the stack efficiency. These inefficiencies are generally associated with the term 'stack losses'. The stack losses can be further broken down into three components: 1)anode overpotential, 2)cathode overpotential, and 3) resistive losses.

The stack efficiency is defined by Equation 14. This equation states that the efficiency is defined as the gross electrical power produced by the stack divided by the lower heating value of the fuel (H2) used in the stack. It is important to note that the stack efficiency is based on the fuel used within the stack as opposed to the fuel supplied to the stack. This has important implications, especially when talking about reformate systems, as all the fuel for these systems is not consumed inside the stack. The lower heating value is used for this equation because it is initially assumed that the water exits

the stack in vapor form. This is not always the case it is necessary to adjust this number as discussed in the next section.

$$Stack\_eta = \frac{P\_gross}{M\_dot\_H_2 * LHV_{H2}} \tag{14}$$

With the definition of stack efficiency given in Equation 14, the amount of heat generated can be written as shown in Equation 15. We see that we can reduce the amount of heat generated within the stack by increasing the efficiency of the stack.

$$Q_{stack\_ineff} = P\_gross(\frac{1}{Stack\_eta} - 1) \tag{15}$$

Even though the stack is substantially more efficient than an internal combustion (IC) engine, the amount of heat that has to be dissipated through the cooling circuit is much greater in the fuel cell. This is because relatively little heat is carried away in the exhaust of the fuel cell (<10%) as opposed to the IC engine (>33%). Additionally, because the stack generally has a narrow window of optimal temperature operation, the flow rates of the coolant can be quite high.

***Stack as Water Supply***

As was previously mentioned, all of the water condensed for the system is done at the exhaust of the stack cathode. The cathode exhaust consists of nitrogen, residual oxygen, and water. The water in the cathode exhaust can be from four different sources:

1. Water production due to the reaction of hydrogen and oxygen.
2. Net water dragged from the anode to the cathode
3. Ambient humidity in the air
4. Water used for cathode humidification (assumed to be zero for this case).

The water in the cathode exhaust can exit in either vapor or liquid form. If the water exits in liquid form, the amount of heat rejected due to condensation has to be accounted for in the calculation of the heat load of the stack. This amount of heat due to condensation is equal to the amount of water condensed multiplied by the heat of vaporization as shown in Equation 16.

$$Q_{stack\_cond} = \dot{M}_{H2O\_liquid} \times H_{fg\ -H_2O} \tag{16}$$

The amount of water that condenses within the stack is a strong function of the cathode operating parameters of air pressure and air mass flow rate (or stoichiometry). The interaction of these parameters is discussed further in the report.

***Stack as heat storage***

In a vehicle system, it is likely that the radiator fan will be sized for a specific peak load. This is generally thought about in terms of continuous peak power or grade-ability. This peak power is usually not the maximum power the system can produce.

Therefore there will be situations when the radiator is not able to remove all the heat that the stack produces. When this occurs, the stack acts like a thermal storage medium. The rate at which the stack stores heat is a function of the weight of the stack and the specific heat of the stack. The equation for rate at which the stack stores heat is as follows:

$$\dot{Q} = M_{stack} \times Cp_{stack} \frac{dT}{dt} \quad (17)$$

By integrating this differential equation, we can determine the rate at which the temperature of the stack rises when all the heat cannot be removed by the coolant. Additionally, when the stack is above it's operating temperature and operating below the maximum heat removal of the coolant, we can calculate how long it will take to cool the stack back down to the operating temperature.

Major Assumptions:

1. All heat loss through coolant loop (No stack heat loss to ambient).
2. All water condensed in stack is immediately available to the system.
3. The effects of cathode and anode flooding have not been modeled.

### Radiator

The vehicle radiator has the primary function of maintaining the stack at its operating temperature. As we saw in the previous section, the heat load is given by the combination of the following:

- Heat rejection due to inefficiency
- Heat rejection due to water condensation

The total heat that must be rejected by the radiation is the combination of Equations 15 and 16. Therefore the total heat rejection requirement is given by Equation 18.

$$Q_{rad} = Q_{stack} = P\_gross\left(\frac{1}{Stack\_eta} - 1\right) + \left(\dot{M}_{H2O\_l} \times H_{fg}\right) \quad (18)$$

Because of the substantial heat generation that must be carried away from the stack and the low temperature differential between the coolant and ambient temperature, fuel cell vehicles will require large radiators. The radiator used in this model is a radiator with an area of 0.5 $m^2$ and a variable speed fan. The sizing of the radiator was done so that the worst-case system (IH) could operate at a system net power of 35kW (not including FP compressor) continuously with a fan output of less than 3 kW (see Figure 63) and still maintain a stack temperature of 80°C. The radiator model is based on a lookup table that uses empirical data generated from a modern standard brazed aluminum, single-pass radiator with 33 tubes (Ricardo, 2000). The characteristics of the radiator [(Q/A-ITD) vs. (kg/s)] is shown in Figure 60 and are assumed to be valid for varying frontal areas.

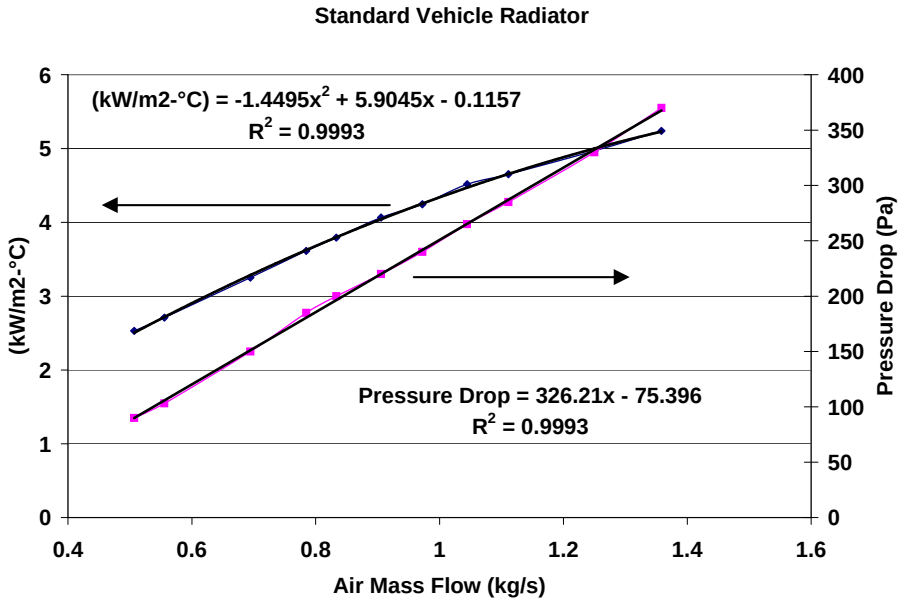


Figure 60: Vehicle Radiator Specs

Major Assumptions:

1. No ram-air effect (all air flow due to radiator fan). Including ram-air will reduce the load on the condenser fan.
2. Temperature difference of coolant at 5°C maintained. Will require variable flow rate coolant pump (not modeled here).
3. Constant fan efficiency of 50%. This is a conservative assumption. A real fan would have an efficiency map based on torque and speed.

## Condenser

The purpose of the condenser is to condense the net water that is needed by the system. The condenser in this model is placed only at the cathode exhaust. As stated previously, the cathode exhaust contains water from three sources: 1) water production do to the reaction of hydrogen and oxygen, 2) net water dragged from the anode to the cathode, and 3) water present in ambient air used for compression.

First, the model calculates the water required for the system. Given the cathode conditions some amount of that water may or may not condense within the stack. The condenser must condense the difference between the system requirement and the amount condensed within the stack.

The model of the air-air condenser that is used for this purpose is based on a cross flow heat exchanger with an area of .33 $m^2$ and a variable speed fan. The condenser was sized such that it could maintain water neutrality for the IH system (worst-case) at a peak gross stack output power of 70 kW with a fan power requirement of approximately 2 kW. The condenser heat transfer coefficient on the cathode side is calculated using an equation for film-wise condensation in vertical tubes (Chato, 1962). The condenser heat transfer coefficient on the air-side is calculated from Kroger and is strongly affected by the air mass flow rate (Kroger, 1984). The overall heat transfer is calculated using the E-NTU calculation method that is finally used to determine the condenser fan power.

Major Assumptions / Implications

1. All water condensed at cathode exhaust (no anode exhaust condenser). While this is not an issue for the DH system because of fuel re-circulation, the other systems (IH, IM) can lose significant water through the anode exhaust.
2. No ram-air effect (all air flow due to condenser fan). Including ram-air will reduce the load on the condenser fan.
3. Constant fan efficiency of 50%. This is a conservative assumption. A real fan would have an efficiency map based on torque and speed.

## Anode Humidification

Proton exchange membrane fuel cells require a well-humidified membrane in order to facilitate the conduction of the hydrogen proton from the anode to the cathode (Monaghan, et. al.). If water is not supplied to the anode side of the fuel cell, membrane drying will result, causing a significant increase in the proton resistivity of the membrane. It is therefore considered beneficial and necessary to humidify the anode stream to avoid membrane drying of the cell. Several methods of humidification that are currently being considered are direct water injection, membrane humidification, and 'wicking' water directly into the stack. In this model, the method of humidification is considered to be direct water injection.

The amount of water required to humidify the anode stream is greatly dependant on the system considered. The following is a brief description of the anode water requirements for each system.

### *DH*

For the model it is assumed that the DH is humidified to 100% relative humidity (RH) prior to entry into the stack. Because of re-circulation of the anode stream (no exhaust to ambient), the water requirement for the anode is equal to the water dragged from the anode to the cathode. This value is calculated from a separate stack model that yields values for net water drag from approximately 0.1 to 0.3 moles/ mole H2 consumed (reference).

### *IM*

The IM has several anode humidification and cooling requirements. The boundary condition of an anode stream humidified to 100% RH at 80°C prior to entry to the stack sets the total anode water requirement. It is found that this can be accomplished by cooling the fuel processor exhaust stream with water injection to the stack operating temperature (80°C).

### *IH*

The IH also has several anode humidification and cooling requirements. The boundary condition of an anode stream humidified to 100% RH at 80°C prior to entry to the stack sets the total anode water requirement. Similar to the IM case, there is substantial opportunity for balancing the humidification and cooling requirements of the IH fuel processor. These aspects of thermal management are not covered in this section.

### Cathode Humidification

There is a disagreement in the literature on whether cathode humidification is necessary in a fuel cell vehicle. Some authors claim that it improves membrane humidification and thermal management of the air supply (Pischinger (2001), etc.), while others indicate that it might not be necessary in a well designed system and may even make water and thermal management more difficult (Wilson (2000), etc.). For this analysis, it is assumed that the system is designed in such a way that cathode humidification is not necessary. While the model does have the capability to calculate the cooling possible through humidification, this feature was removed for these results.

### WTM / System Optimization

Before the WTM system is put into the vehicle model, it is used to determine the optimal cathode (air) side operating strategy of the compressor. Because the WTM system is strongly affected by the air pressure and flow rate (stoichiometry), it can have a significant impact on the optimization scheme.

The optimization of a fuel cell system can be thought of as maximizing the net power of the system based on controllable operating parameters. The WTM loads are dependant on the system operating parameters (cathode pressure and cathode stoic) and it is important to include them while performing an overall system optimization. An equation for the cathode optimization that includes the major system components is shown in Equation 19.

$$P_{net\_opt}(\mathrm{Pr}_{air,}\dot{m}_{air}) = MAX\,(P_{stack\_gross}(\mathrm{Pr}_{air,}\dot{m}_{air}) - P_{air\_system}(\mathrm{Pr}_{air,}\dot{m}_{air}) - P_{radiator}(\mathrm{Pr}_{air,}\dot{m}_{air}) - P_{condeser}(\mathrm{Pr}_{air,}\dot{m}_{air}))$$ (19)

While trying to devise optimal operating schemes (on the cathode side) for the system, the intention is to determine a pressure ratio and mass flow rate that maximizes the Pnet_opt mentioned above. The resulting curves for the air side operating parameters are shown in Figure 61 and Figure 62. While it is beyond the scope of this report to discuss the full optimization procedure, the reader is encouraged to read Friedman (2001) for additional information.

It is also important to note that the position of the optimal pressure and stoic ratio is strongly influenced by the size and design of the WTM and air supply components. Increasing or decreasing the size or heat transfer coefficient of the radiator or condenser, as well as changing the operating characteristics of the air supply is likely to shift the optimal operating points. In this way, the optimal sizing of the system is part of the overall optimization process. The optimal sizing of components (other than fan motors) is not discussed here.

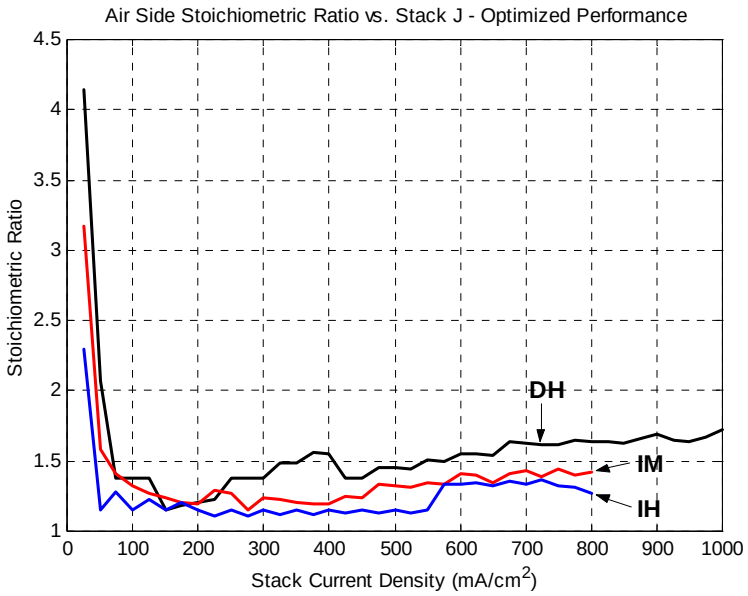


Figure 61: Optimized Cathode Stoichiometric Ratio

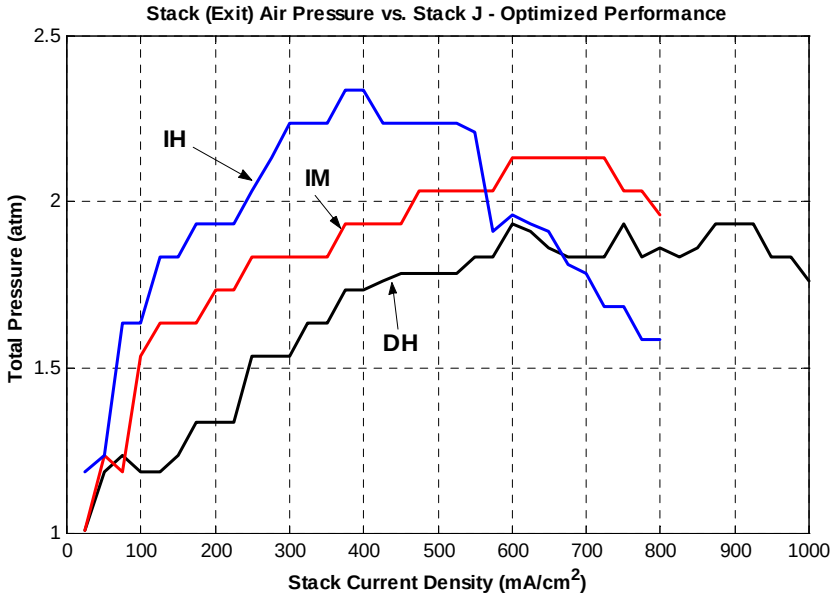


Figure 62: Optimized Cathode Pressure Ratio

## WTM System Control

All of the primary input and output variables are calculated for the steady-state case in a separate detailed 'config' model. There is, however, some amount of system control available at the vehicle-level, which allows for some 'dynamic' water and thermal management. The control algorithms are relatively simple, allowing for maximum power levels for the condenser and radiator fans. The control incorporated in the vehicle model for the condenser and radiator is as follows:

***Radiator Control***

If the radiator power required to maintain the nominal stack temperature exceeds the "P_rad_max" value, the stack temperature will begin to rise. In this situation, the radiator power will continue to stay at "P_rad_max" and continue to remove the maximum allowable heat until the stack temperature falls back within the nominal stack temperature plus a deadband ("wtm.stack.deadband", default = 0.5°C).
The basic logic for the thermal management block is as follows:

Table 19: Radiator Control Logic

| ***Condition*** | ***Radiator Power*** | ***Heat Rejected*** |
|---|---|---|
| Power_rad < P_rad_max<br>WTM_STACK_TEMP < T_stack - wtm.stack.deadband | Power_rad | Q_rad<br>(thermally neutral) |
| Power_rad > P_rad_max | P_rad_max | Q_rad @ P_rad_max<br>(stack temp rises) |
| Power_rad < P_rad_max<br>WTM_STACK_TEMP > T_stack + wtm.stack.deadband | P_rad_max | Water_avail_rad<br>(water level rises) |
| WTM_STACK_TEMP < T_stack - wtm.stack.deadband | Zero | Zero (stack temp rises) |

* Note: The effect of increasing stack temperature on fuel cell stack performance has not been modeled in this vehicle model.

***Condenser Control***

The "P_cond_max" input variable (default = 1 kW) dictates peak available power from the condenser-cooling fan. If this is exceeded during the drive cycle, the condenser will continue to condense the amount of water it is capable of at the "P_cond_max" power level. In this situation, the "WTM_H2O_INT" output variable indicating the water tank level will begin to drop. As soon as the required condenser power drops below the "P_cond_max", the condenser will remain on full power until the water level comes back within the water level deadband ("wtm.water_tank.deadband", default = 0.1 moles) of the original water level ("wtm.water_tank.level", default = 2 moles). Additionally, there is the possibility of condensing water in either the stack or expander in excess of the system requirement. If the water level rises above the initial tank level plus the deadband, the condenser will shut-off and will not draw any power until the water level is drawn back within the deadband. By modifying these parameters, it is possible to investigate water tank, and condenser fan sizing for the given condenser modeled. The logic is given in table form in Table 20.

The basic logic for the water management block is as follows:

Table 20: Condenser Control Logic

| ***Condition*** | ***Condenser Power*** | ***Water Condensed*** |
|---|---|---|
| Power_cond < P_cond_max<br>WTM_H2O_INT <<br>wtm.water_tank.deadband | Power_cond | WTM_H2O_NEEDED<br>(water neutral) |
| Power_cond > P_cond_max | P_cond_max | Water_cond @<br>P_cond_max<br>(water level drops) |
| Power_cond < P_cond_max<br>WTM_H2O_INT > (-)<br>wtm.water_tank.deadband | P_cond_max | Water_avail_cond<br>(water level rises) |
| WTM_H2O_INT ><br>wtm.water_tank.deadband | Zero | Zero (water level falls) |

* Note: The effects of flooding on the stack have not been modeled due to the complex nature of water within the stack. From the model, it is possible to determine the amount of liquid water condensed in the stack but not its effect on performance.

The above logic allows the user to roughly determine (through iteration) the following aspects of the system:

1. Maximum radiator fan power requirement for a given cycle (given a peak allowable stack temperature).
2. Water storage requirement for a given drive cycle (given peak condenser fan power).
3. Condenser power requirement for a given drive cycle (given maximum allowable water storage).

## Optimized WTM Results

The optimization process was briefly discussed in the preceding sections. One of the key products of the optimization process is the optimized control lines for the air pressure and mass flow rate (or stoic ratio) of the air supply system.

Because the WTM components are significantly influenced by these parameters, it is important to understand the differences in the optimized control parameters and their impacts on the WTM components before beginning a discussion of the dynamic results. The optimized control parameters for the air system are outlined in Section 4.1.4.3 and are used for generating the plots in the following section.

### *Radiator Power vs. Stack Net Power*

From the radiator power vs. stack net power graph in Figure 63, we see that if the radiator was always required to remove all the heat generated by the stack the radiator fan power would quickly become a dominant parasitic load on the system. During the optimization process, the radiator is limited to a maximum parasitic draw of 3 kW. If it was necessary for the radiator to remove all of the heat of the stack up to maximum net power, the radiator would either be the primary power draw, or it would have to have an area that is not likely to fit under the hood of the vehicle. Another interesting element of Figure 63 is the IM radiator power is the most for any given net power with the DH and

IH being nearly equal. Given that the anode losses are highest for the IH, one might expect it to have the highest radiator load. However, we must remember that the IH system has the largest cell area, resulting in lower current densities for a comparable power and therefore, lower cathode overpotential and cell resistance. The other factor, stack condensation makes the comparison even more difficult. See the following reference in Section 5.4 (WTM: Badrinarayanan, 2001).

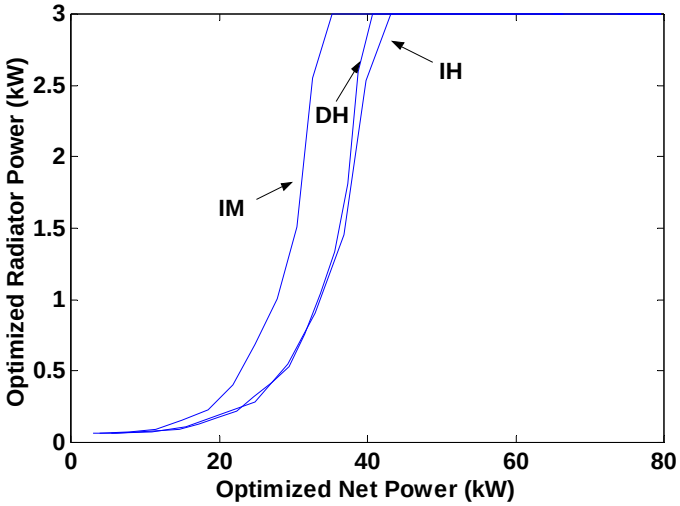


Figure 63: Radiator Power vs. Optimized Net Power

In Figure 64 we see the optimized condenser loads for the three systems. The highest condenser load is for the IH system (except at very low net powers). Both the IM and DH have relatively low condenser loads throughout the cycle. One of the reasons that the IH load is relatively high is because the anode humidification water requirement is highest for the IH for any given current. Based on the assumptions that the anode is humidified to 100% RH at 80°C, and that the dry H2 concentration is around 30%, this represents a significant loss of water to the environment (there is no condenser on the anode exhaust). For this reason, it may be beneficial to try and capture the water in the anode exhaust if possible (not analyzed here).

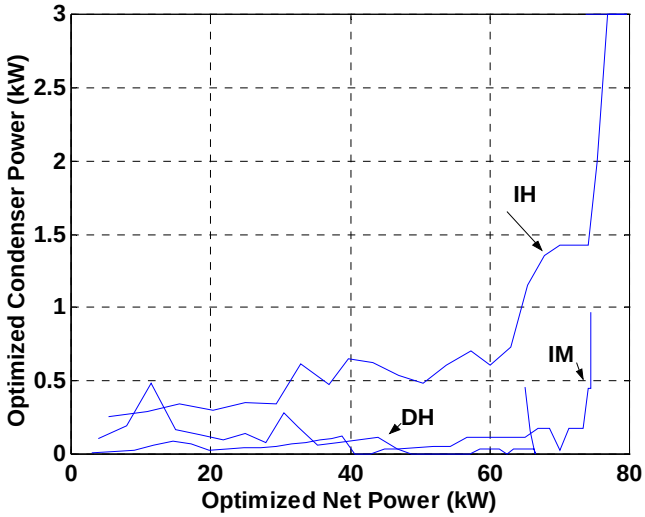


Figure 64: Optimized Condenser Power vs. System Net Power

## System Results – Dynamic

While steady state results are good for characterization and understanding, the system operates within a dynamic vehicle. It is therefore desirable to see how the WTM system operates over a dynamic driving cycle as well as what is the WTM load integrated over the cycle. The three cycles chosen for this analysis are the federal urban driving schedule (FUDs), the low powered HIWAY cycle, and the more aggressive US06 cycle.

### WTM water balance

Before we investigate the WTM loads on the system, it is important to understand where the water is condensed in the system. As was stated earlier, the radiator has to remove all of the heat from the stack including 1) the heat due to inefficiency and 2) any heat of condensation due to water condensing within the stack. Any increase in the condensation load on the stack will have a direct impact on reducing the load on the condenser. It is also important to note that this shift is not equal. See the following reference in Section 5.4 (WTM: Badrinarayanan, 2001).

Figure 65 shows the water needed, water condensed in the stack, and water condensed within the condenser for the FUDs cycle. We see that during the relatively low powered FUDs cycle, most of the needed water is condensed within the condenser. Additionally, the water requirement is greatest for the IH system and least for the DH system.

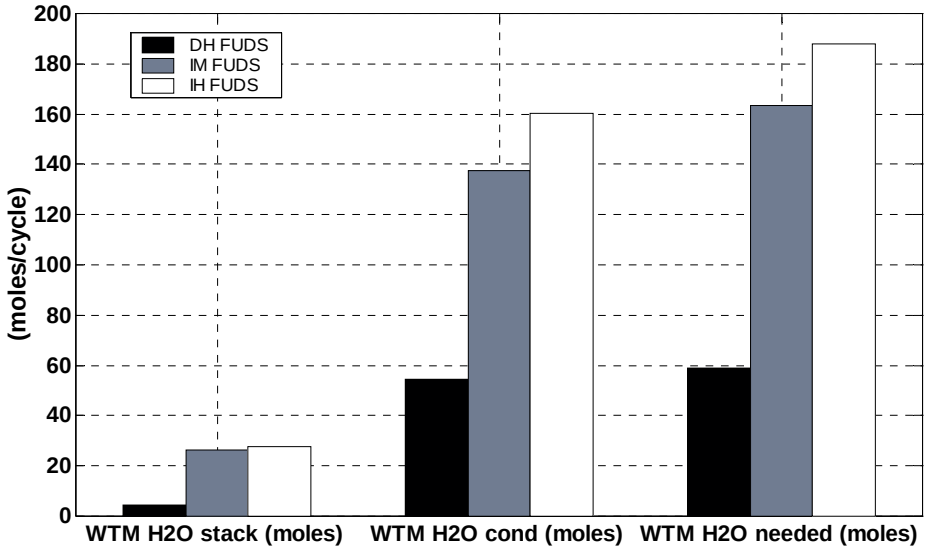


Figure 65: Water Condensation Location (FUDS)

Figure 66 shows the same water requirements for the higher-powered US06 cycle. Here we find that the highest water requirement is for the IM system with the lowest being for the DH system. Additionally, most of the IM water is condensed within the stack, which will have an effect of increasing the radiator load as we will see in the next section.

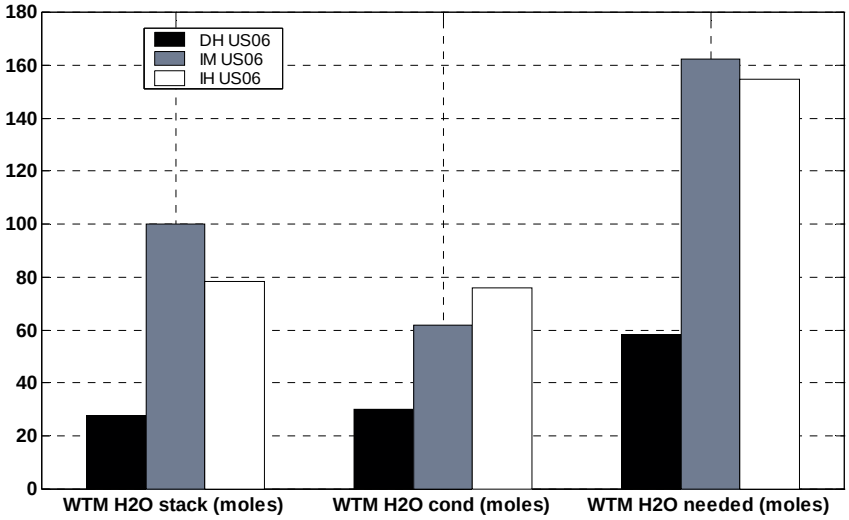


Figure 66: Water Condensation Location (US06)

***WTM Parasitic Loads***

Now that we understand the where the water is condensed, the next step is to look at the WTM parasitic loads on the system. In Figure 67 and Figure 68, the energy use of the two primary WTM components, the condenser and radiator, are compared over the FUDS and US06 cycles. The graph in Figure 67 shows a similar radiator load for the three systems, and an increasing condenser load from the DH to IH systems. The increasing condenser load agrees well with the chart in Figure 65. The parasitic load of the condenser is directly related to the amount of water that it needs to condense.

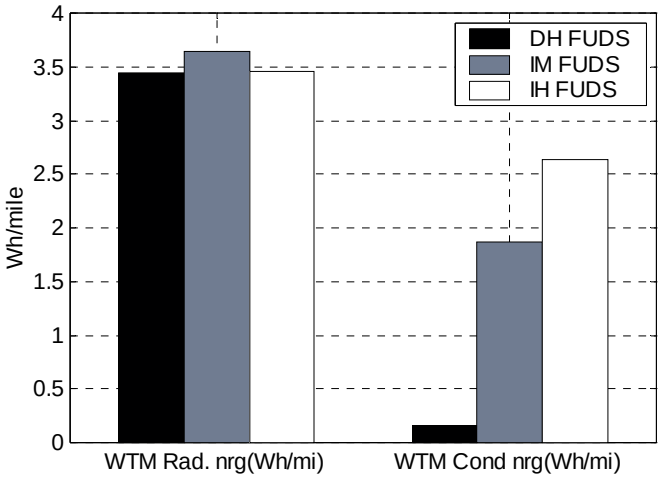


Figure 67: WTM Loads (FUDS)

In Figure 68 we see that, for the US06 cycle, the IM system has a significantly higher radiator parasitic load compared to the DH and IM systems. This is due to two factors. The first factor to note is that the IM system has the highest stack losses of the three systems during the US06 cycle (for further explanation see Section 4.1.4.1). Secondly, as shown in Figure 66, the IM system condenses a significant fraction of the required water in the stack. This combination of increased heat generation due to stack inefficiency and increased condensation load inside the stack lead to a significantly higher load for the IM system during the cycle.

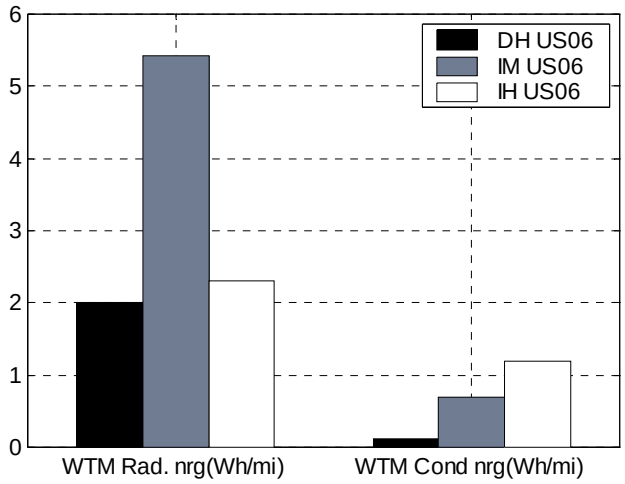


Figure 68: WTM Loads (US06)

It should be noted that the parasitic loads of the WTM system are small in comparison with the other auxiliaries of the fuel cell system (air supply, etc.). It is important to note that this is for an optimized system (one in which the WTM and air supply loads are minimized in comparison to the stack output) and with relatively large heat-transfer areas. It would be relatively easy to design a system that had substantially larger loads than the ones shown here.

***Additional Drive Cycle Info***

For the fuel cell system designer, there are several questions that might be of interest regarding the WTM system within the vehicle. How big of a condenser fan is required to maintain water neutrality for a given cycle? How big of a radiator fan is required to maintain the stack temperature over a given cycle? For a given condenser fan size, how big of a water tank is needed to make up any shortfall for a given cycle?

The values in Table 21 show the peak parasitic fan powers for the condenser and radiator over the FUDs, Highway, and US06 cycles. Those indicated by an asterix (*) are when the vehicle model limited the peak power based on the input parameters. The maximum allowable parasitic loads for the three systems are given in Table 22. For these cases, the amount of water lost or stack temperature increase will be investigated.

Table 21: Peak Parasitic WTM Loads

| | Peak Parasitic Load (Watts) | | | | | | | | |
|---|---|---|---|---|---|---|---|---|---|
| Drive Cycle | Condenser | | | Radiator | | | Total | | |
| | DH | IM | IH | DH | IM | IH | DH | IM | IH |
| FUDs | 25 | 170 | 131 | 160 | 760 | 181 | 165 | 765 | 241 |
| US06 | 57 | 253 | 1000* | 900 | 2000* | 2070 | 912 | 2250* | 3050 |
| Highway | 70 | 170 | 131 | 90 | 230 | 105 | 98 | 272 | 197 |

Table 22: Maximum Allowable WTM Parasitic Loads

| | Peak parasitic load (kW) | | |
|---|---|---|---|
| WTM Component | DH | IM | IH |
| Radiator | 2 | 2 | 3 |
| Condenser | 1 | 1 | 1 |

In several cases during the US06 cycles, the peak parasitic loads were limited by the maximum allowable parasitic power for the components. In these cases it is interesting to investigate the resulting increase in stack temperature (when radiator parasitic load is greater than the limit) and the resulting decrease in water supply (when condenser parasitic load is above limit). The maximum water loss is equal to the starting water level minus the lowest water level over the cycle. This could be considered the minimum water storage required for the cycle.

Table 23: Dynamic Peak Stack Temp and Water Loss

| Drive Cycle | Peak stack Temp (°C) | | | Max Water Loss (moles) | | |
|---|---|---|---|---|---|---|
| | DH | IM | IH | DH | IM | IH |
| US06 | 80 | 88 | 80 | 0 | 0 | 0.17 |

## Summary

Even though the parasitic loads from an optimized WTM system are small in comparison with other auxiliary loads (air supply), it is still important to consider them both during optimization as well as in the vehicle simulation. Additionally, a well-designed WTM system will avoid additional problems such as stack over-temperature and loss of water neutrality. In this model we have assumed a WTM system that provides for all the water and cooling needs of the system. Given extreme operating conditions (extended peak power, high ambient temperatures), it is possible that even a well-designed system will have difficulty maintaining the required system operating specifications.

The summary values in Table 24 show the aggregated parasitic loads for the WTM components over the FUDS, US06 and Highway cycles.

Table 24: WTM Drive Cycle Energy Use

| | WTM Rad. nrg(Wh/mi) | WTM Cond nrg(Wh/mi) |
|---|---|---|
| DH FUDS | 3.44 | 0.16 |
| DH HIWAY | 1.38 | 0.13 |
| DH US06 | 2.01 | 0.11 |
| IM FUDS | 3.63 | 1.86 |
| IM HIWAY | 1.54 | 1.37 |
| IM US06 | 5.42 | 0.68 |
| IH FUDS | 3.45 | 2.63 |
| IH HIWAY | 1.41 | 1.45 |
| IH US06 | 2.30 | 1.18 |

#### 4.1.4.5 Hydrogen Storage (DH only)

**Description**

The goal of our modeling process is to determine the hydrogen storage and delivery characteristics that may affect the system performance, and to feed this information into the system model. The hydrogen tank size is modeled to provide feedback to the user of the physical volume needed for storage, and to model the tank's mass for vehicle considerations.

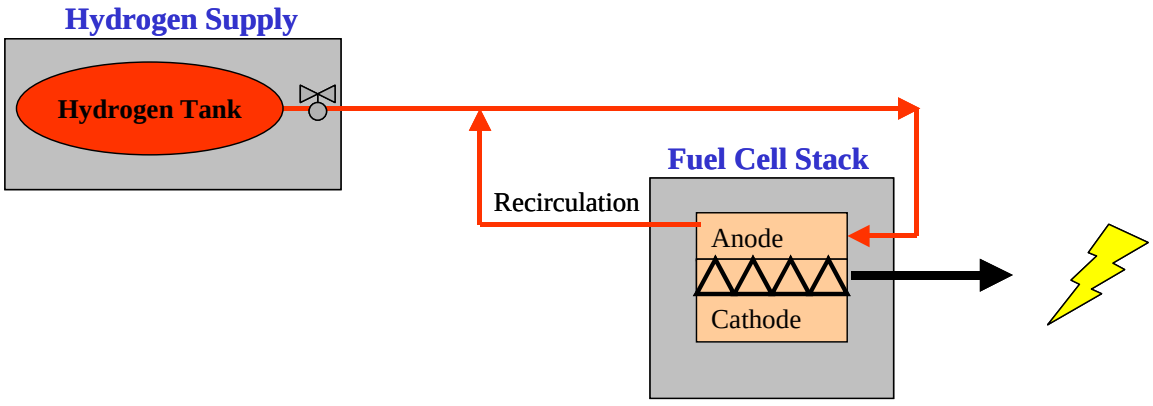


Figure 69: The Hydrogen Supply System in the Fuel Cell Engine

Figure 69 shows the storage tank and the recirculation loop for the unused hydrogen as it exits the stack. An ejector pump is assumed to provide the recirculation for the hydrogen.

Modeling of the compressed hydrogen tank size began by using the PNGV requirements for range as a guideline for the amount of hydrogen that would be required. However, this estimate was then revised due to a self-imposed packaging constraint of 180 liters.

The initial analysis of storage requirements needed for a fuel cell vehicle using direct hydrogen is explained as follows. A value of 5.3 kg of hydrogen was determined by running the DH vehicle model. The formula for determining the estimated mpg for a new vehicle by the automakers (a combination of the FUDS and Highway driving cycles) was used to determine the amount of hydrogen for the PNGV range goal of 380 miles. This required a value of 5.3 kg or a volume of 230 L, which is more than our constraint.

A tank volume of 180 L, yields 4.13 kg. Using this amount of hydrogen, a reduced range of 300 miles was calculated with the energy content of a gallon of gasoline (121,330kJ/gallon) and a gram of hydrogen (120kJ/gram). The tank pressure is assumed to be 5000 psi, with 4.13 kg of hydrogen, which gives the required volume of 180 L at 300 K.

## Assumptions And Model Notes

1. The DH model includes a recirculated hydrogen loop. An ejector pump is assumed for this recirculation; therefore, no parasitic load is required (venturi effect). Transient effects are not taken into account with respect to hydrogen delivery to the system.
2. Other useful output parameters include the hydrogen gas temperature, which may be useful for future WTM calculations. Additional information includes the tank pressure and mass of hydrogen in the tank at any given time during the simulation.

## Pressure and Temperature Considerations

### *Pressure Calculations*

The Solver function in Excel was used to take the Redlich-Kwong (RK) equation and calculate the tank volume at 5000 psi and 300K for 5.3 kg of hydrogen. The volume is 230 liters. The equation is broken down into the following parameters: $p$ is in Pa, $v$ is m^3/kmol and R is 8314.34kPa*m^3/(kmol*K). The remaining constants (critical values for hydrogen) are shown in Table 25 with the RK equations below.

Table 25: Critical Values for Hydrogen

| | Value | Units |
|---|---|---|
| Critical Temp | 33.18 | K |
| Critical Pressure | 1315 | kPa |

$$p = \frac{\overline{R}T}{\overline{v} - b} - \frac{a}{\overline{v}(\overline{v} + b)T^{1/2}} \tag{20}$$

$$a = .42748 \frac{\overline{R}^2 T_c^{5/2}}{p_c} \tag{21}$$

$$b = .08664 \frac{\overline{R}T_c}{p_c} \tag{22}$$

***Temperature Calculations***

The actual temperature was calculated using enthalpy tables for hydrogen.[11] The enthalpy 1890.047 BTU/lb was listed for hydrogen at 5000 psi and an initial temperature of 300K. This enthalpy was then used to calculate a new temperature at a pressure of 4000 psi. This was done for successively lower pressures using the initial enthalpy value. The temperatures at a constant enthalpy value for the following pressures were plotted in excel and a cubic equation was determined. The pressures were: 5000, 4000, 3500, 3000, 2400, 1000, 45 and 14.7 psi. The cubic equation is shown below. Y is temperature in Kelvin and X is pressure in psi. Temperature *increases* with pressure drop and is shown by the graph. (Figure 70).

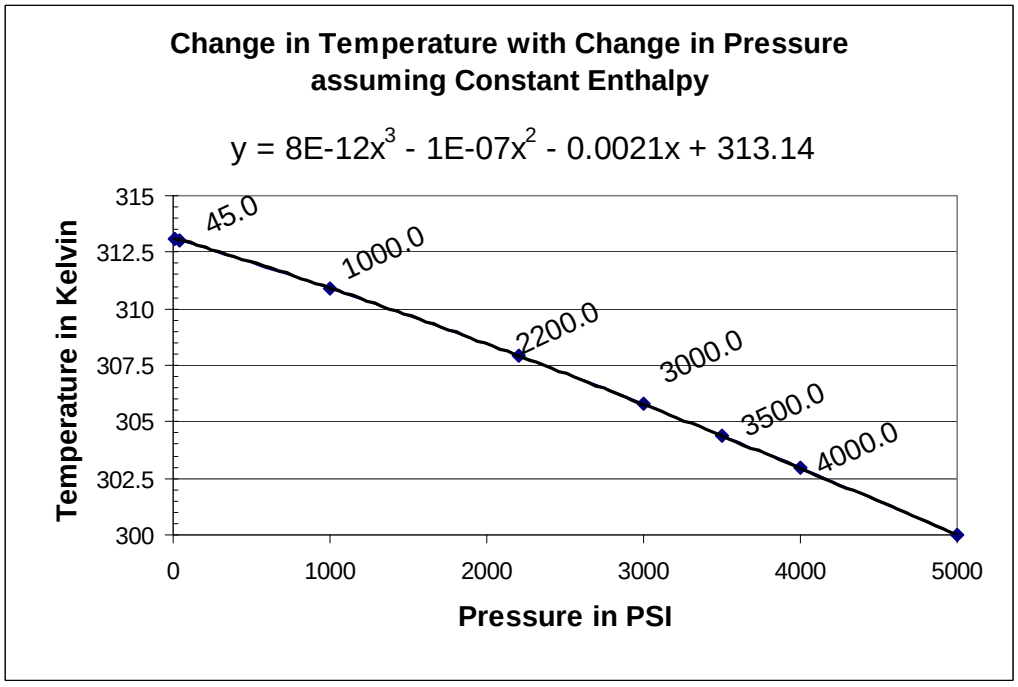


Figure 70: The Hydrogen Temperature as a Function of Pressure

[11] McCarty, D.R, "Hydrogen Technological Survey-Thermophysical Properties", Cryogentics Division, Institute for Basic Standards National Bureau of Standards, Boulder Colorado. Scientific and Technical Information Office, Washington, DC 1975

## 4.2 Upstream Fuel Analysis (WTT)

***Fuel Upstream Emissions and Energy Requirement for Fuel Cell Vehicles Operation in 2010 at California South Coast Air Basin***

### 4.2.1 Goals and Methodology

Since 1998 the UCDavis Fuel Cell Vehicle Modeling Program has been investigating and promoting a new concept to incorporate uncertainties in environmental life cycle analysis (LCA). A LCA must include an inventory phase to account for the amount of emissions generated by certain technology use and it may also include another phase for the assessment of the environmental impact generated by the emissions released. There is considerable disagreement between existing life cycle inventories (LCI) of fuels and vehicles and the existing methodologies can easily be manipulated to support specific advocacy positions. A detailed analysis showed opportunities for improvement in the way of treating the input subjectivities inherent in this kind of analysis (Contadini et al., 2000a). Based on this, the first goal of the project is methodological and it is related to the improvement of the LCA concept by incorporating the inventory uncertainties into the calculation.

The incorporation of the uncertainties has been done by, among other things, better treatment of the data coupled with a participatory discussion with the experts of the interested parties, using a variation of the Delphi technique and via the use of Monte Carlo simulation to propagate the uncertainties in the model using probabilistic curves. The expert network comprises of more than 25 international experts from a dozen organizations including car manufacturers, oil and chemical industries, consulting companies, government agencies, NGOs and universities. The details of this participatory methodology are presented in Contadini et al. (2000d). The participatory discussion is very time consuming but is absolutely essential for the acceptability of the study final results.

Another goal of the project is the ability to perform environmental life cycle analysis of fuels for fuel cell vehicles in different geographic locations. To accomplish this, a flexible model called FUEEM – Fuel Upstream Emissions and Energy Model was developed to assess the fuel upstream activity values from the reservoirs to the vehicle refueling ("well-to-tank"). As stated before the data underlying FUEEM had been derived from expert panel discussions and therefore, the final step of the overall methodology is to test and validate the model results with the interested parties. This present analysis was carried out in order to accomplish this final goal.

### 4.2.2 Scope

To test FUEEM and the proposed new methodology, a Life Cycle Inventory (LCI) is conducted for three Fuel Cell Vehicle Technologies concepts, hypothetically operating in South Coast California Air Basin (SCAB) in the year 2010. The analyzed vehicle concepts are Direct Hydrogen Fuel Cell Vehicle (DHFCV), Indirect Methanol Fuel Cell Vehicle (IMFCV) and Indirect Hydrocarbon Fuel Cell Vehicle (IHFCV). Since Fuel Cell Vehicles (FCVs) are a relatively new technology, the time frame of 2010 is discussed and adopted as the reference. It is assumed that there is a well-established market for fuel cell vehicles in 2010. This is based on the inference that if the technology

becomes reality by that time, all the fuel upstream business associated with fuel cell vehicles will be in place and based on more solid technologies (in economical terms) when compared to possible alternative technologies during a transitional period. This scenario will of course depend on the analyzed region but the main point is that from a fuel infrastructure point of view, it is unlikely that FCVs will have a high market share earlier than 2010 and beyond 2010 the uncertainties related to the fuel upstream business become very high and hence impossible to analyze.

SCAB is chosen because of its well-known air quality problems, its high probability of initiating fuel cell vehicle introduction, the availability of large data sets and at least two previous fuel LCI studies (Unnasch, 1996 and Ogden, 1999) that can be used for comparison purposes.

The requested fuels for the vehicles (hydrogen, methanol and hydrocarbon) are all based on the natural gas pathway. Natural gas is the "most feasible" feedstock to produce hydrogen in areas where electricity is expensive, such as California, USA and Europe. A similar conclusion was reached with respect to methanol production when methanol is produced from inexpensive, large and remote NG reserves, such as Chile, Trinidad-Tobago, Malaysia, etc. For direct-hydrocarbon fuel cell vehicles, Fischer Tropsch Naphtha (FTN) is chosen as the hydrocarbon fuel due to the potential need for a clean (sulfur free) and easier-to-reform(saturated hydrocarbon) fuel for FCVs. There is also a sense that future oil price and the social pressure for a cleanest diesel should make viable the use of the high-quality Fischer Tropsch (FT) diesel as a blending stock. Based on that, the establishment of a market for the light fraction (naphtha) of the FT process appears to be very attractive. Of course, this is not to say that a "gasoline-type" fuel from crude oil pathway should not be considered and analyzed in future developments of this methodology.

FUEEM provides the values for the energy consumption disaggregated into fossil fuels and petroleum consumption as well as the total consumption. It also assesses the major urban air criteria emissions and greenhouse gases ($NO_x$, NMOG, CO, $PM_{10}$, $PM_{2.5}$, $SO_x$, $CH_4$, $N_2O$, $CO_2$ and $CO_{2\text{-equivalent}}$) disaggregated into three different areas selected by the analyst. From a practical viewpoint this analysis considers only the total energy consumption and four emissions ($NO_x$, NMOG, CO and $CO_2$). The three areas where the emissions occurs are SCAB (analyzed area), the state of California (without SCAB), next the total emissions generated in the rest of the world (excluding California).

The scope of the study is limited to air emissions since they represent the main concern for the transportation sector, (water and solid waste are not considered at this point). The boundaries for the fuel upstream calculation include all the operational stages of the activities right from feedstock extraction to the final vehicle refueling stage. In particular, the activities or stages include the feedstock extraction, processing, storage and transportation, as well as the fuel production, storage, transportation and distribution. The calculated values in each stage are disaggregated into combustion processes and fugitive emissions values. The secondary fuels and electricity consumed in each activity are also considered from the feedstock extraction to the final use and it is also reported in a disaggregated way.

### 4.2.3 Scenarios

Most of the FUEEM input variables are probabilistic curves and they are expressed here with words such as "the value is around" or "approximately", etc. Higher Heating Values (HHVs) are considered for all thermal energy aggregation. The details of the calculations and all variables assumed not discussed in this report will be presented in Contadini (2001).

South Coast California Air Basin (SCAB) is a high emission control enforcement area and the chosen technologies placed inside the basin somehow reflect these regional policies. Fuel transportation modes and distances, as well as the chosen pathway scenarios for feedstock and fuel production also reflect the regional characteristics. We strongly discourage the extrapolation of the results to other areas or situations.

For a specific pathway, in which the technologies are well defined, a consensus among the experts was achieved without problems. There is also a consensus that in reality the probability of the fuel upstream activities being a mix of technologies is much bigger than that utilizing a single technology path. Based on that, a combination of pathway scenarios should be a better way to calculate the final result. However, it was very difficult to reach a consensus given the various combinations possible, the subjectivity of the topic, the sensitivity of the variables and the advocacy positions of several experts. The combined scenarios presented here are examples that represent the opinion of several experts but should not be used as a final solution. In any case, the single pathway results represent the edges of any combination assumed.

#### Gaseous Hydrogen

Several hydrogen onboard storage technologies are in development to provide pure hydrogen for the vehicle fuel cell stack. High-pressure tank at $3.45 \times 10^4$ kPa (5000 psi) is chosen as the technology of choice for the purposes of this analysis due to its actual stage of development, relative low cost and better energy efficiency compared to the cryogenic liquid option. A fast refueling system will require a fuel station based over-pressurized hydrogen storage at approximately $4.14 \times 10^4$ kPa (~6000 psi), which is about $6.90 \times 10^3$ kPa (~1000 psi) bigger than the vehicle tank pressure. The fuel station storage system uses compressors in cascade powered by electric motors. The natural gas engine option to power the compressors is not considered due to concerns about emissions. Overall around 4 kg of hydrogen per vehicle is considered for each instance of the refueling activity.

The low density of the gaseous hydrogen makes it difficult to store and also difficult to transport. The cheapest way to transport hydrogen is using pipelines from a centralized plant; however, hydrogen pipelines require special design and are more expensive than natural gas pipelines. Based on this, centralized hydrogen plants are expected to be placed as close as possible to the market, using as much as possible existing natural gas infrastructure. On the other hand, the costs of building a centralized hydrogen plant and the necessary infrastructure are high and the hydrogen demand is not expected to be high enough to justify all this investment, at least in the next few years. Decentralized production at the fuel station can be used in the introductory phase and may remain until 2010. Huge mega-plants (270 mtpd - metric tons per day) that can be placed in rural areas to deliver hydrogen to several markets and may even sequester $CO_2$,

require an extensive transmission pipeline network and also a well established and big market demand. Therefore, for the time frame of 2010 this option is not considered.

Based on these considerations three pathways are used in this study:

Pathway 1: Centralized production – This assumes existing typical size plants (27 mtpd) located inside the market area and producing extra-steam for over the fence exportation. The plant uses a half-day production capacity storage at high pressure (around 23 MPa or 3350 psi) for a steady state operational guarantee and recovers part of the compression energy with a turbo-compressor. A pipeline distribution network of about 60 km (37 miles) is set to deliver hydrogen at the fuel stations at a pressure of 6.9 MPa (1000 psi). *NOTE: This is an optimized pipeline design from one analysis considering efficiency and safety issues (Contadini, 2000c).* For emission control the plant uses selective catalytic reduction (SCR) device and a continuous emission monitor system (CEMS).

Pathway 2: Decentralized production – Hydrogen is produced at the fuel stations using small steam methane reformation (SMR) plants (1 mtpd). The plant uses natural gas (NG) at an inlet pressure of 0.14 MPa (20 psi) and a pressure swing adsorption unit (PSA), with an output pressure of 1.6MPa (230 psi). For the emission control it uses catalytic burners and SCR units.

Combined Scenario: For a reduced fleet scenario, centralized plants already established to supply hydrogen for chemical and petrochemical industries can also supply hydrogen to the nearby fuel stations. In this situation a relative high percentage of hydrogen fuel may come from decentralized plants to attend the fuel station that are far from the industrialized area. With the increase of the number of hydrogen vehicles in the area, new centralized plants can be built, reducing the relative percentage of decentralized plants in the area. Based on these ideas, the combined scenario considers a curve for the hydrogen production, establishing that the hydrogen production coming from small plants (pathway 2) is between 20 to 50 % and that the remaining production comes from centralized plants (pathway 1).

### Liquid Fuels Marketing

The major benefits of liquid fuels are the higher energy density compared to gaseous fuels and the relatively ease with which one can transport and store them. The benefits in the transportation and storage of liquid methanol and Fisher-Tropsch Naphtha (FTN) qualify them as possible hydrogen carrier fuels for FCVs. The rationale for these liquid fuels marketing closely parallels that for gasoline. Taking into account the high degree of air quality enforcement in areas such as SCAB and considering the transportation infrastructure in place, the established scenarios for all pathways take into account the following activities:

a. Balance control recovery system for the vehicle refueling and for the fuel station underground tank refueling. The system allows the tank fuel vapor displaced by the refueled new fuel to be transferred from tank to tank until the fuel terminal where the majority of the vapor is recovered.
b. Diesel truck tankers (US class 8b) equipped with vapor collector for the retail distribution stages.

c. Internal floating roof tanks at the fuel terminals which, for the SCAB case, are located close to the port.
d. The port activities include diesel engines and diesel tugboats.
e. The tanker ship size considered is the one equivalent to 150,000 dead weight tons of crude oil. The ship has no air emission control devices and uses bunker fuel (US residual oil 6) as fuel. During the return trip of the vessel, a water ballasting of around 30 % by weight is assumed
f. The bulk fuel storage tanks at the remote areas are dependent on the region air quality enforcement policy assumed in each pathway. Several examples show that the remote plants are likely to be constructed in areas that have already some industrial activities and concentrated industrialized areas are more likely to control local emissions. On the other hand, because of the industrial concentration the plants are able to export steam or electricity, therefore, in this analysis air control device requirements become associated with the steam-exportation possibilities.
g. Finally, it is assumed that the fuel production plants are located next to the ports.

### Methanol

Five pathway scenarios are considered for the methanol analysis. Two different technologies are considered to produce syngas for the methanol synthesis and also two different regional situations for steam exportation with air emission control device requirement. All pathways consider the same fuel marketing activities explained in the previous section (liquid fuels marketing topic).

Pathway 1: A typical size methanol plant of 2,500 metric tons per day (mtpd) using steam methane reformation (SMR) syngas production constructed in a site without industrial concentration. The plant uses no air control device and uses fixed roof tanks for the fuel storage. No extra steam exportation is considered.

Pathway 2: A mega-size methanol plant of 10,000 metric tons per day (mtpd) using a combination of SMR and partial oxidation (POX) for the syngas production constructed in a site without industrial concentration. The plant uses no air control device and uses fixed roof tanks for the fuel storage. No extra steam exportation is considered.

Pathway 3: A typical size methanol plant of 2,500 mtpd using SMR syngas production constructed in a site with industrial concentration. The plant uses a selective catalytic reduction as air control device and it uses internal floating roof tanks for the fuel storage. Extra steam exportation is considered.

Pathway 4: A mega-size methanol plant of 10,000 metric tons per day (mtpd) using a combination of SMR and partial oxidation (POX) for the syngas production constructed in a site with industrial concentration. The plant uses a selective catalytic reduction as air control device and it uses internal floating roof tanks for the fuel storage. Extra steam exportation is considered.

Combined Scenario: Currently the methanol industry has around 20 % to 30 % of over capacity. The future for MTBE (an oxygenated additive for gasoline that uses methanol

as feedstock) is controversial and creates a possibility of an even bigger over capacity in the near future. Existing and relatively older plants use SMR in a less efficient way than the new SMR plants considered in this study. Several experts believe that these less efficient plants are going to be decommissioned by 2010 and that all methanol for FCVs will be produced in existing new plants or in new designed plants. However, some controversies exist about what the new plant designs will be and their market share by the year 2010. Mega-size plants (10,000 mtpd) using combined SMR/POX are more efficient and according to some experts there are several projects already considering this option. Other experts disagree with this scenario believing that short-term new plants (if so) will have similar characteristics (with small efficiency increment) of current typical size plants (2,500 mtpd) using SMR. Some controversies also exist in the extra-steam exportation as stated before. Ultimately, to show an example of pathway combination the present analysis assumes that the composition of the methanol fuel in the market will be around 25 % of each pathway considered (in fact this percentage is considered as a normal distribution curve with a minimum value of 20 % and a maximum value of 30 %).

### Fisher-Tropsch Naphtha (FTN)

Similarly to the methanol analysis, five pathway scenarios are considered for the FTN analysis. Two different technologies using oxygen to produce syngas for the Fisher-Tropsch (FT) synthesis and also two different regional situations for steam exportation with air emission control device requirement are considered. The major problem of FT nowadays is the initial costs of the plant. Great part of the capital investment is related to the oxygen plant. One way to reduce the initial costs is by using air injection instead of oxygen and trading off the plant efficiency, on account of the amount of nitrogen (inert) that must be carried over in the pressurized system. A possible benefit, according to some of the experts is the safety of having no pure oxygen in the plant. On the other hand, several experts believe that the oxygen safety is not an issue and that the economy of the air system, in most of the cases, does not compensate the efficiency losses. High temperature FT synthesis (300 to 350 $^{o}$C) using alkalized iron or fused iron oxide catalysts are not considered in this analysis due to the mix of non-paraffinic components (olefins, aromatics, etc.) that they tend to produce. All of the pathways consider the same fuel marketing activities explained before in the section on Liquid Fuels Marketing.

Pathway 1: A FT plant with capacity of 5,000 mtpd constructed in a site without industrial concentration, using slurry bed low temperature reactor (220 to 270 $^{o}$C) and cobalt catalyst. The plant also uses combined SMR/POX syngas production with pure oxygen injection. The plant has hydrotreating and hydrocraking stages with final cuts around 60% of diesel, 18% of kerosene and 22% of naphtha (by weight). The plant uses no air control device and uses fixed roof tanks for the fuel storage. No extra steam exportation is considered.

Pathway 2: A FT plant with capacity of 5,000 mtpd constructed in a site without industrial concentration, using multi-tubular low temperature reactor (220 to 270 $^{o}$C) and cobalt catalyst. The plant also uses combined SMR/POX syngas production with air injection instead of pure oxygen. The plant has hydrotreating and hydrocraking stages with final cuts around 50% of diesel, 20% of kerosene and 30% of naphtha (by weight).

The plant uses no air control device and uses fixed roof tanks for the fuel storage. No extra steam exportation is considered.

Pathway 3: A FT plant with capacity of 5,000 mtpd constructed in a site with industrial concentration, using slurry bed low temperature reactor (220 to 270 $^{o}$C) and cobalt catalyst. The plant also uses combined SMR/POX syngas production with pure oxygen injection. The plant has hydrotreating and hydrocraking stages with final cuts around 60% of diesel, 18% of kerosene and 22% of naphtha (by weight). The plant uses a selective catalytic reduction as air control device and it uses internal floating roof tanks for the fuel storage. Extra steam exportation is considered.

Pathway 4: A FT plant with capacity of 5,000 mtpd constructed in a site with industrial concentration, using multi-tubular low temperature reactor (220 to 270 $^{o}$C) and cobalt catalyst. The plant also uses combined SMR/POX syngas production with air injection instead of pure oxygen. The plant has hydrotreating and hydrocraking stages with final cuts around 50% of diesel, 20% of kerosene and 30% of naphtha (by weight). The plant uses a selective catalytic reduction as air control device and it uses internal floating roof tanks for the fuel storage. Extra steam exportation is considered.

Combined scenario: For most of the experts, it is possible that a continuum among the technologies presented in the four pathways described above will be the most probable case, but there was no consensus on what form this continuum should take. The possibility to export extra-steam in remote areas produced another controversy since water from the plant and also desalinization of water using extra-energy produced at the plant can be a solution and benefit for arid areas. Ultimately, to show an example of pathway combination, the present analysis assumes that the composition of the FTN fuel in the market will be around 25 % for each pathway considered (in fact this percentage is considered as a normal distribution curve with a minimum value of 20 % and a maximum value of 30 %).

### Natural Gas Feedstock

For Gas-to-Liquids Production: Gas-to-liquids fuels (methanol and Fisher-Tropsch) have the benefit of being able to use the cheapest (sometimes with negative values) natural gas reservoirs located far from the markets. Being liquids at the ambient temperature, methanol and Fisher-Tropsch naphtha (FTN) can be easily transported by sea tankers and be sold as a hydrogen carrier for fuel cell application in developed markets.

Australia, Quatar, Malaysia, Chile and Trinidad Tobago are examples of relatively inexpensive natural gas reservoirs where new gas-to-liquid plants been proposed. In most of the cases these sites have feature some industrial development supported by the local natural gas industry. This study considers Malaysia, as an example of a source at an intermediate distance, in order to facilitate comparison with a previous study (Unnasch, 1996). The maritime distance between Malaysia and LA (about 15500 nautical miles – round trip) can be considered as a conservative assumption compared to the other sites (Chile and Trinidad Tobago). The transportation energy requirement for the Malaysia site represents about 2% of the total energy requirement this requirement would be 1.3% of the total for Chile and Trinidad Tobago sites.

The natural gas extraction characteristics in Malaysia can also be assumed as being representative of the other optional sites. Around 30% of the natural gas is extracted in wells associated with light oil and 70% come from the non-associated gas wells. One interesting characteristic of these NG sites is that, in general, they are close to the coast and most of the industrial complexes have been developed near the port areas. This study assumes a 20-mile pipeline transporting natural gas from the processing plants to the gas-to-liquid plants. Natural gas turbines drive the pipeline.

For Hydrogen Production: For the hydrogen case the situation is completely different. Bulk liquid hydrogen is not an economical solution due to the high-energy requirement of the liquefying process and also due to the necessary use of special ships to maintain cryogenic temperatures and to consume hydrogen boiled-off.

Being unable to benefit from the inexpensive natural gas from abroad, the hydrogen plants are forced to use a much more expensive gas of the California market. By 2010 it is assumed that around 50% of the marginal demand will be supplied by Texas and 50% by Canada. This assumption is similar to the one used by the California Energy Commission (Unnasch, 1996).

The Canada NG characteristic is around 60 % produced in non-associated wells, 15 % produced in wells associated with light oil and 25 % produced in wells associated with heavy oil. Pipelines along with the compressors (50 % reciprocating engines and 50 % turbines) take care of the gas transportation and distribution. The length of the pipeline inside the basin (SCAB) is around 80 Km (50 miles). Around 640 Km (400 miles) are placed in the California State and around 2,170 Km (1,350 miles) are placed in the rest of the world (USA and Canada).

The Texas NG characteristic is as follows; 85 % produced in non-associated wells, 14.7 % produced in wells associated with light oil and 0.3 % produced in wells associated with heavy oil. Pipelines along with the compressors (50 % reciprocating engines and 50 % turbines) take care of the gas transportation and distribution. The length of the pipeline inside the basin (SCAB) is around 80 Km (50 miles) and around 2,170 Km (1,350 miles) are placed in the rest of the world (USA crossing the California State board directly into SCAB). For small consumers such as fuel stations a distribution pipeline of around 60 Km (37 miles) is also added.

## Electricity

All the system upgrade and new generator implementation to produce electrical energy in the South Coast Air Basin (SCAB) has been considered by the California Energy Commission (CEC) using natural gas combined cycle turbines. This technology has been assumed in this analysis for SCAB and also for the eventual electricity used in Malaysia where the gas-to-liquid plants are considered. For the California State electricity mix the probabilistic curves were extrapolated from the literature and the production technology share is around 19 % coming from coal, 31 % coming from natural gas and 3 % from oil. For the USA mix the share is around 52 % coming from coal, 22 % from natural gas and 2 % from oil. For the Canada mix the share is around 16 % coming from coal, 5 % from natural gas and 2 % from oil. The high voltage transmission lines losses are between 3 to 7%. For short distances and small consumers

such as fuel stations a low voltage distribution line is considered with losses between 2 to 4 %.

### 4.2.4 Results

All the results expressed here consider 90% of confidence level and energy content in high heating values (HHV).

#### Energy Requirement / System thermal efficiency

Considering the combined scenarios the Methanol (MeOH) upstream efficiency, defined in terms of energy delivered per energy required upstream, can rely between 62.9 and 64.5% (1.54 to 1.59 $GJ_{req\text{-}upst}/GJ_{fuel\text{-}deliv}$). The most probable value (mode) is the efficiency of 64.1% (1.56 $GJ_{req\text{-}upst}/GJ_{fuel\text{-}deliv}$) and the average(mean) of the possible cases for methanol is 63.7% (1.57 $GJ_{req\text{-}upst}/GJ_{fuel\text{-}deliv}$). The combined scenarios for Hydrogen (H2) and Fisher-Tropsch Naphtha (FTN) have the same efficiency if only the mean (57.1% for 1.75 $GJ_{req\text{-}upst}/GJ_{fuel\text{-}deliv}$) or the mode (57.5% for 1.74 $GJ_{req\text{-}upst}/GJ_{fuel\text{-}deliv}$) is considered. However, the hydrogen case has 33 % of possibility of having a better upstream efficiency than the FTN and 29 % of chances of having a worse efficiency when all the cases are observed. Hydrogen is better between the efficiency of 58.1 % and 60.2 % (1.66 to 1.72 $GJ_{req\text{-}upst}/GJ_{fuel\text{-}deliv}$) and worse between the efficiency of 54.3 % and 55.9 % (1.79 to 1.84 $GJ_{req\text{-}upst}/GJ_{fuel\text{-}deliv}$). For almost 40 % of the cases one cannot say which system (hydrogen or FTN) is more efficient. Figure 71 shows this idea and the distribution characteristics in terms of total energy required.

Figure 72 shows the dependency of the energy requirements (average values) on the energy sources. One can notice that the results confirm the expectancy of eliminating the dependency on petroleum but it also maintain the dependency in non-renewable sources (fossil-fuel) since all scenarios considered are natural gas based fuels.

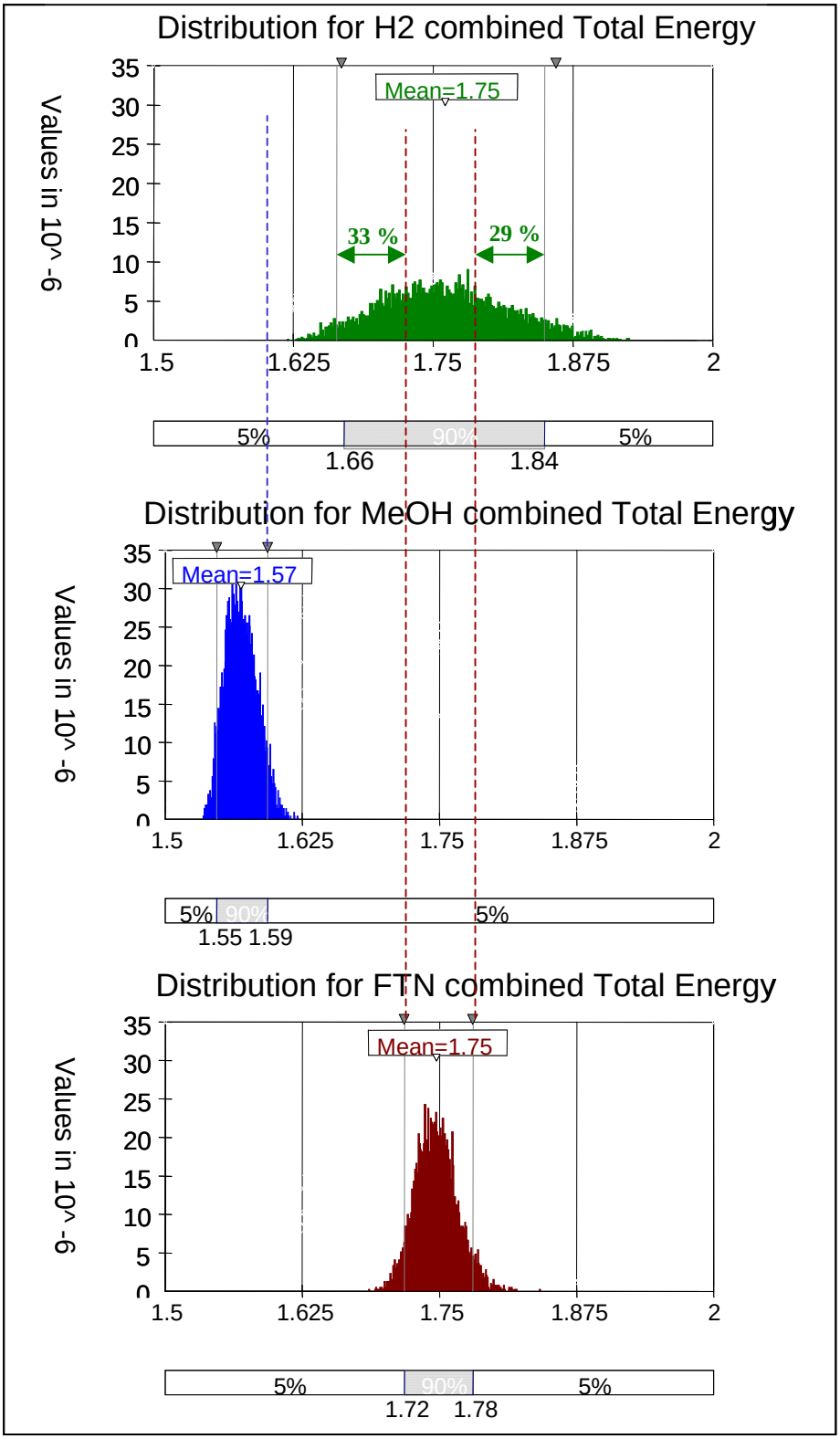


Figure 71 – Total Energy Requirement for the Combined Scenarios ($GJ_{req.-upstream}/GJ_{fuel-delivered}$) - HHV

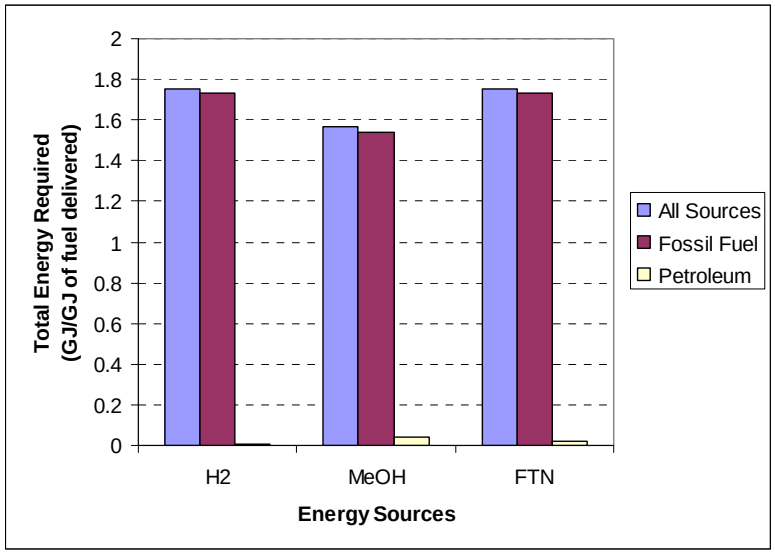


Figure 72 – Energy Sources Dependency based on the Average Values (Combined Scenarios)

### Criteria Emissions in SCAB

An important observation is that the criteria emissions for the liquid fuels will not be accounted for in the SCAB region if the fuel ends up being produced overseas (outside the region). In contrast, for example, this study assumed that hydrogen was produced in the SCAB region.

For methanol and FTN all pathways are equal in that the activities that occur inside SCAB (floating roof tanks, diesel trucks, etc.), therefore the combined scenario results do not modify if one changes the combination characteristics.

### Nitrous Oxides (NOx)

Figure 73 shows the $NO_x$ Emissions for the Combined Scenarios in the SCAB area. Observing this figure one can see that emissions from hydrogen scenarios are orders of magnitude bigger than emissions from FTN and MeOH. The bulk of $NO_x$ emissions in the hydrogen scenario come from the reformer furnace in the hydrogen production plant, the electricity production and also from the NG feedstock activities inside the area. More discussion about the hydrogen emissions is done in topic 4.2.5.

The difference in the $NO_x$ emissions between FTN and Methanol reflects the higher energy density of FTN compared to Methanol when similar power is required from the IC engines to transport the same volume of fuel (trucks, port activities, etc.). The heat content of the fuels also account for some of the differences.

### Non-Methane Organic Gases (NMOG)

Figure 74 is representing the NMOG Emissions for the Combined Scenarios in the SCAB area. It shows that the hydrogen scenario emits less NMOG than the other ones. In average it will emit around 3 grams of NMOG per GJ of hydrogen delivered at the fuel station and the range encompass 1.2 to 5 g per GJ of hydrogen delivered. It is important to point out that 90% of these emissions come from NG leaking and venting in

the hydrogen production plants and in the NG pipeline systems. The shape of the distribution curves for methanol and FTN shows that there is a high possibility of the emissions be more concentrated around the mode (most probable value), which is 8.92 $g/GJ_{delivered}$ for FTN and 13.63 $g/GJ_{delivered}$ for methanol. However, there are some possibilities that the NMOG emissions for the FTN reach values as high as16.39 $g/GJ_{delivered}$. It indicates that in 38.3% of the cases FTN emissions can be considered better than methanol.

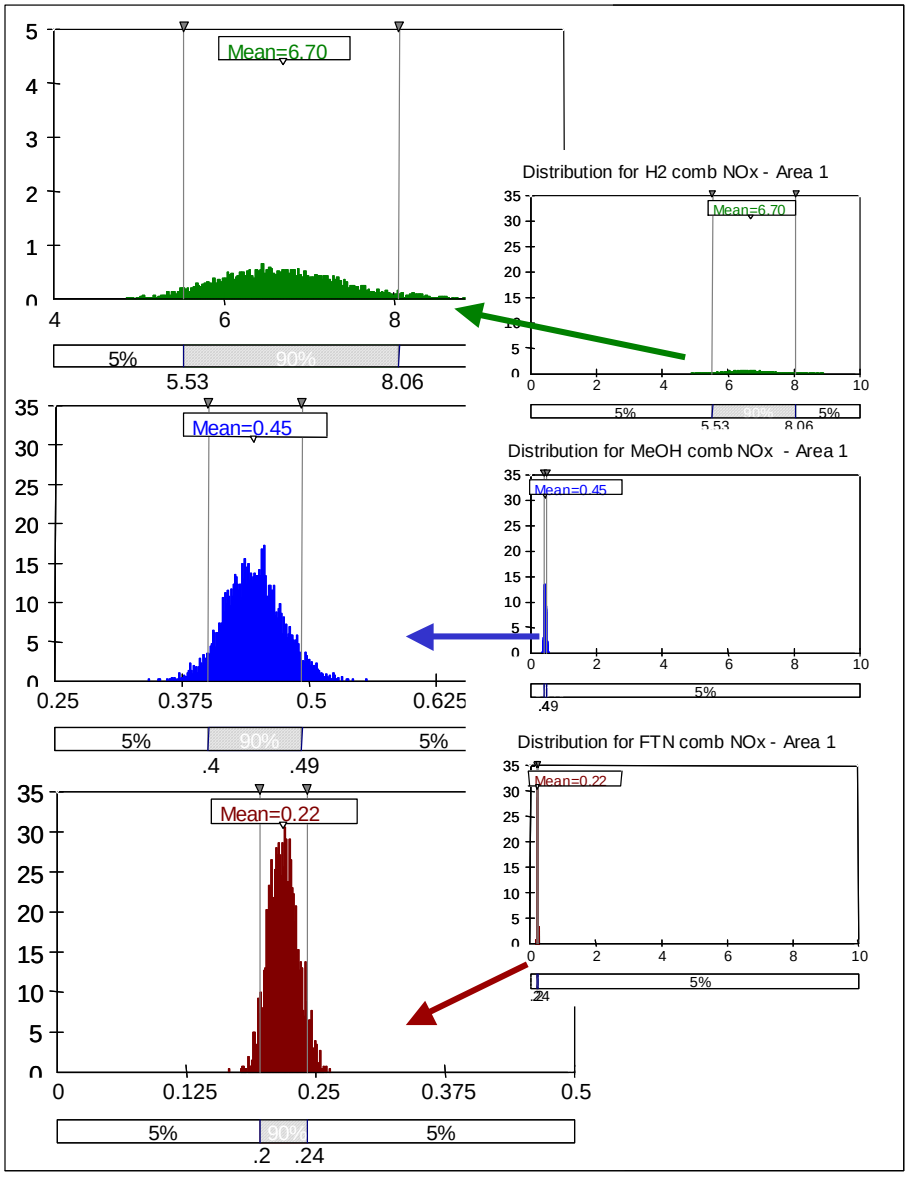


Figure 73 – $NO_x$ Emissions for the Combined Scenarios – SCAB ($g/GJ_{delivered}$)

On the other hand, the methanol emissions can also go as high as 25.04 $g/GJ_{delivered}$ representing that at least for 29.9% of the methanol cases the NMOG emissions are worse than the FTN cases.

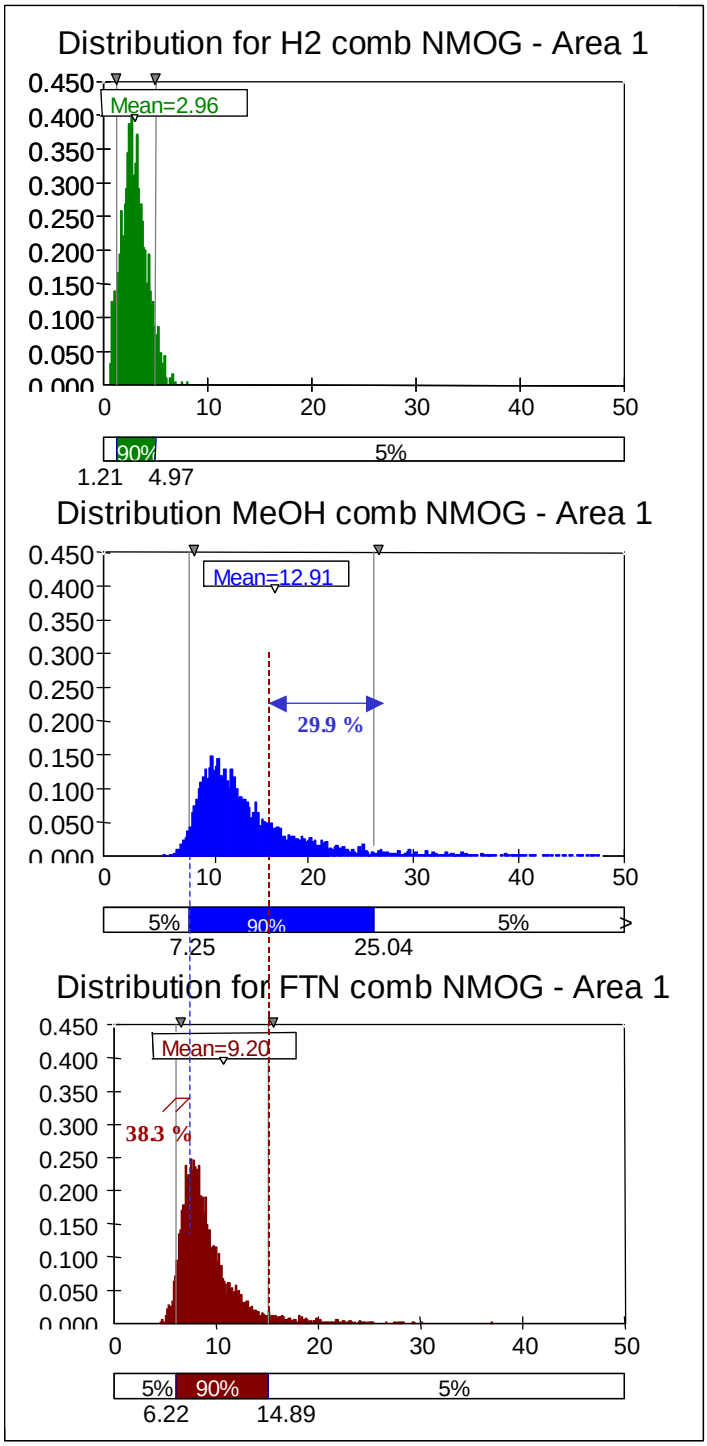


Figure 74 – NMOG Emissions for the Combined Scenarios – SCAB ($g/GJ_{delivered}$) – HHV

Figure 75 shows the NMOG emission sources in the SCAB area. One can see that the biggest source of NMOG emissions is the fugitive emissions, mainly coming from the fuel stations and part of it coming from the port activities. The level of disaggregation in FUEEM makes possible to analyze details in each activity. As an example, the details of the NMOG fugitive emissions in the fuel station are discussed next.

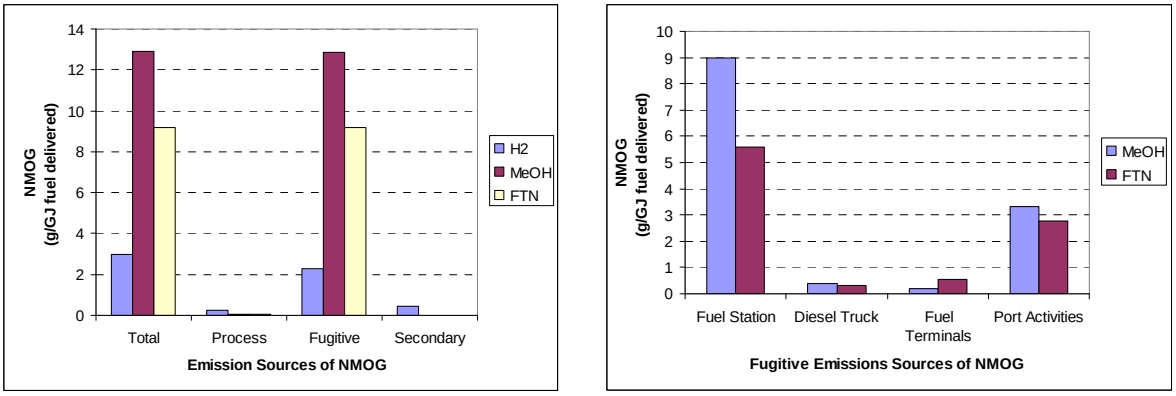


Figure 75 – NMOG Emission Sources – SCAB

Figure 76 shows the average NMOG emissions of a fuel station in more detail. One can notice that the nozzle retention and the refueling spillage are the major sources of emissions. In these sources the difference between methanol and FTN is due to their different energy content and density. Another big source is the vapor tank displacement (disp. Stage II - in the plot). The difference between methanol and FTN is due to the different vapor pressure and energy content of each fuel.

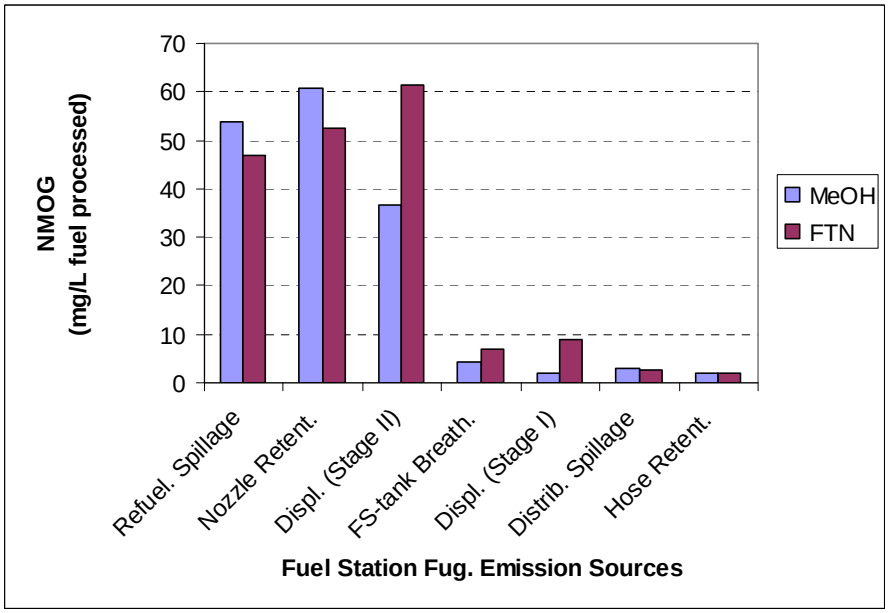


Figure 76 – NMOG Emissions in Fuel Station

## Carbon Monoxide (CO)

Figure 77 illustrates the CO Emissions for the Combined Scenarios in the SCAB area. It can be seen that it has the same behavior as the $NO_x$ emissions and the same discussion done for those emissions applies here.

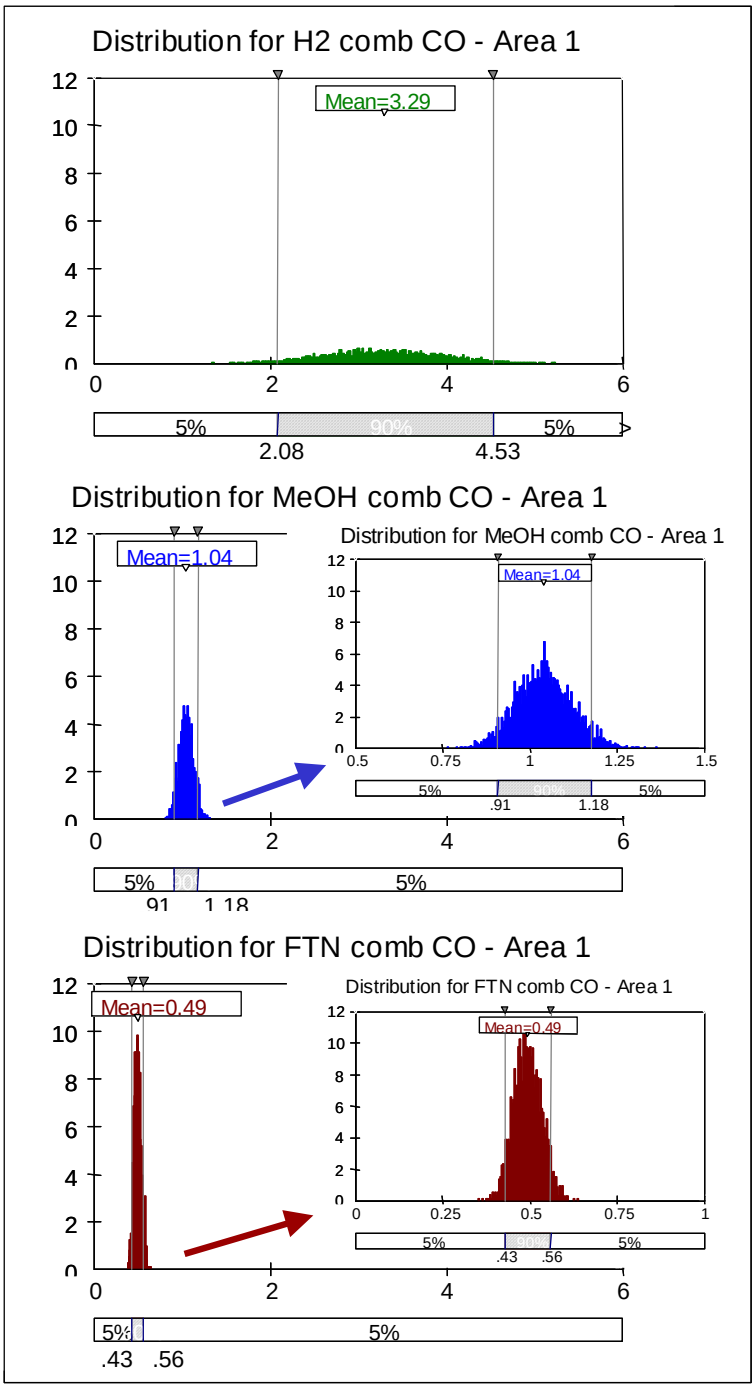


Figure 77 – CO Emissions for the Combined Scenarios – SCAB (g/$GJ_{delivered}$)

## Criteria Emissions in the rest of the California State

Hydrogen pathway only (gas pipelines crossing the state coming from Canada). Liquid fuels coming by ships cross the sea California State board directly into SCAB.

Results (mean):

- ✓ NOx ~ 0.02 g/GJ-$H_{2\text{-delivered}}$;
- ✓ NMOG ~ 0.59 g/GJ-$H_{2\text{-delivered}}$
- ✓ CO ~ 1.91 g/GJ-$H_{2\text{-delivered}}$

## Global Carbon Dioxide (CO2) emissions

Figure 78 represents the Global $CO_2$ Emissions for the Combined Scenarios. It shows that FTN releases less $CO_2$ than methanol, which releases less $CO_2$ than hydrogen. A later evaluation of the FTN mass balance will be done in order to investigate why the range appears to be so small.

Global carbon dioxide of the fuel upstream activities is a combination of the system efficiency above (requesting the combustion of different amounts of fuels) with the carbon content present in the fuel delivered. It is good to point out that most of the carbon in the liquid fuels is going to be released as $CO_2$ in the vehicle operational phase. In contrast, the hydrogen would have released all the carbon content in the feedstock (NG) by the time it is in the vehicle. This is the main reason for the high $CO_2$ emissions of the hydrogen pathway. Another interesting point to keep in mind is that part of the total hydrogen comes from the water in the syngas production and therefore releases no $CO_2$.

Figure 79 presents the $CO_2$ Emissions Sources. The idea is to analyze and show the importance of the secondary calculation in the methodology boundaries. For example, in the hydrogen case, which partially relies on the electricity use, it is really important to include it.

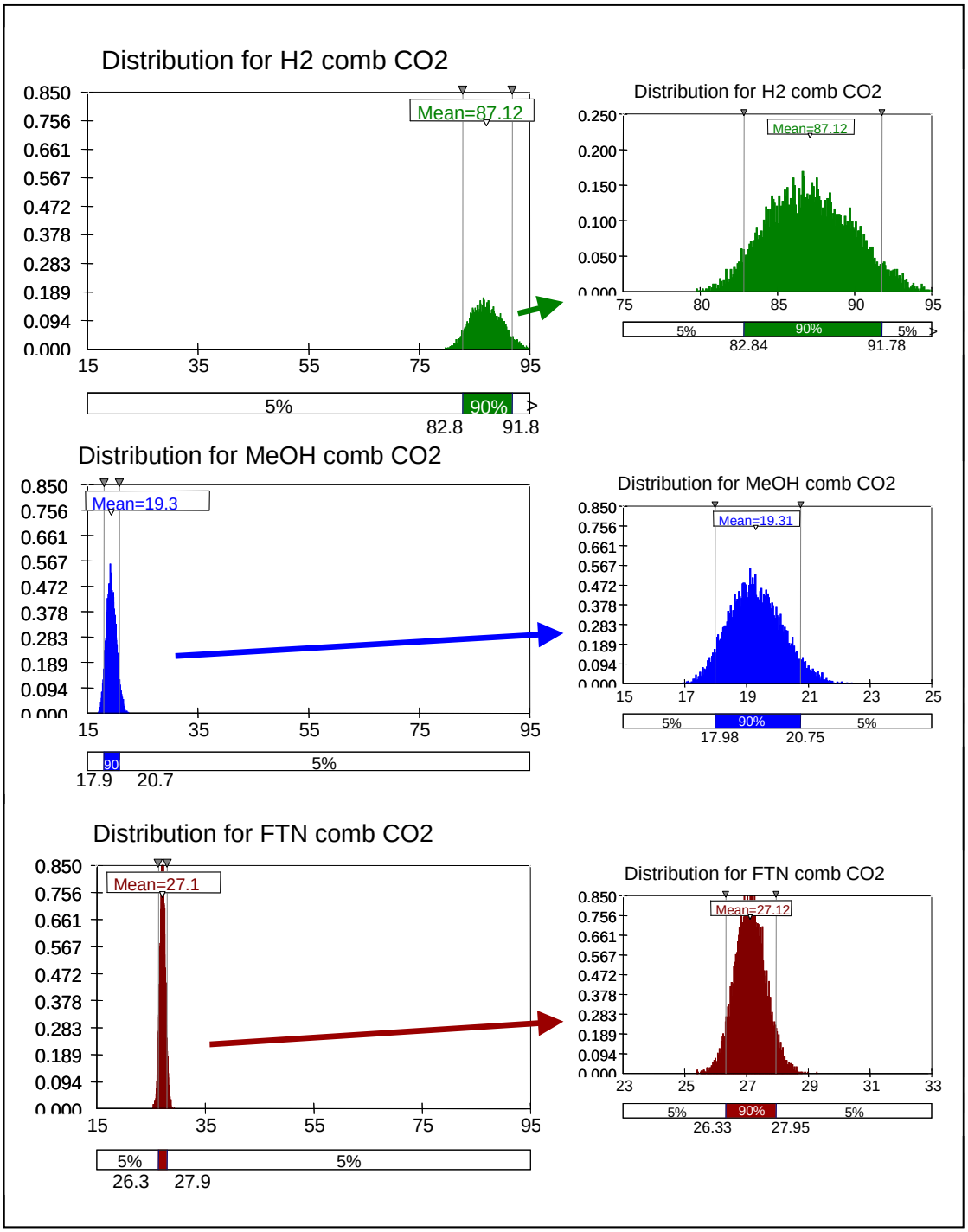


Figure 78 – Global $CO_2$ Emissions for the Combined Scenarios, ($kg/GJ_{delivered}$)

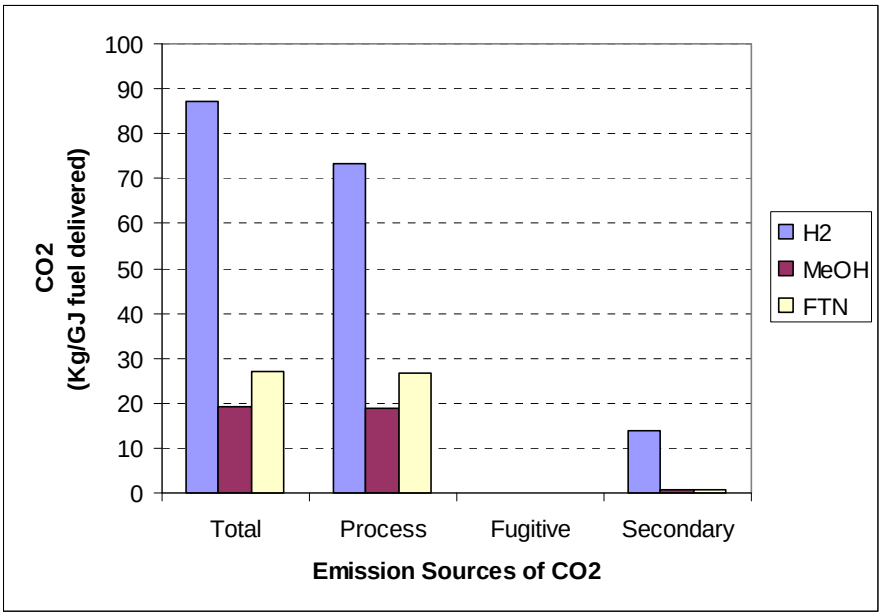


Figure 79 – $CO_2$ Emissions Sources (mean)

### 4.2.5 Scenario Considerations

Scenario considerations can be the very sensitive, especially for cases like the hydrogen pathways where huge differences occur right at the beginning of the chain activities calculation (fuel station).

#### Hydrogen scenarios

Figure 80 shows the total energy requirement for the hydrogen pathways. As one can notice the Pathway 1 (Ptw-1) presents an average value of 1.54 $GJ_{req\text{-}upst}/GJ_{fuel\text{-}deliv.}$ that is smaller than the energy requirement for the Pathway 2 (Ptw-2), which has an average value of 2.10 $GJ_{req\text{-}upst}/GJ_{fuel\text{-}deliv}$. These values correspond to the system efficiency of 64.9% and 47.6% respectively. In fact the Pathway 1 has the efficiency range between 66.6% and 62.9% (1.50 to 1.59 $GJ_{req\text{-}upst}/GJ_{fuel\text{-}deliv}$) representing that it can be comparable with the most efficient of the methanol scenarios (Figure 83). It is good to point out that a mega-size plant (270 mtpd) option, which has a better thermal efficiency, was not considered in this 2010 time frame analysis.

The small reformers located at the fuel stations have the benefit of being modular. This fact can be very helpful in a transitional phase and also for fuel stations far away from possible centralized plant areas. However their thermal efficiencies are an important variable and should be investigated further.

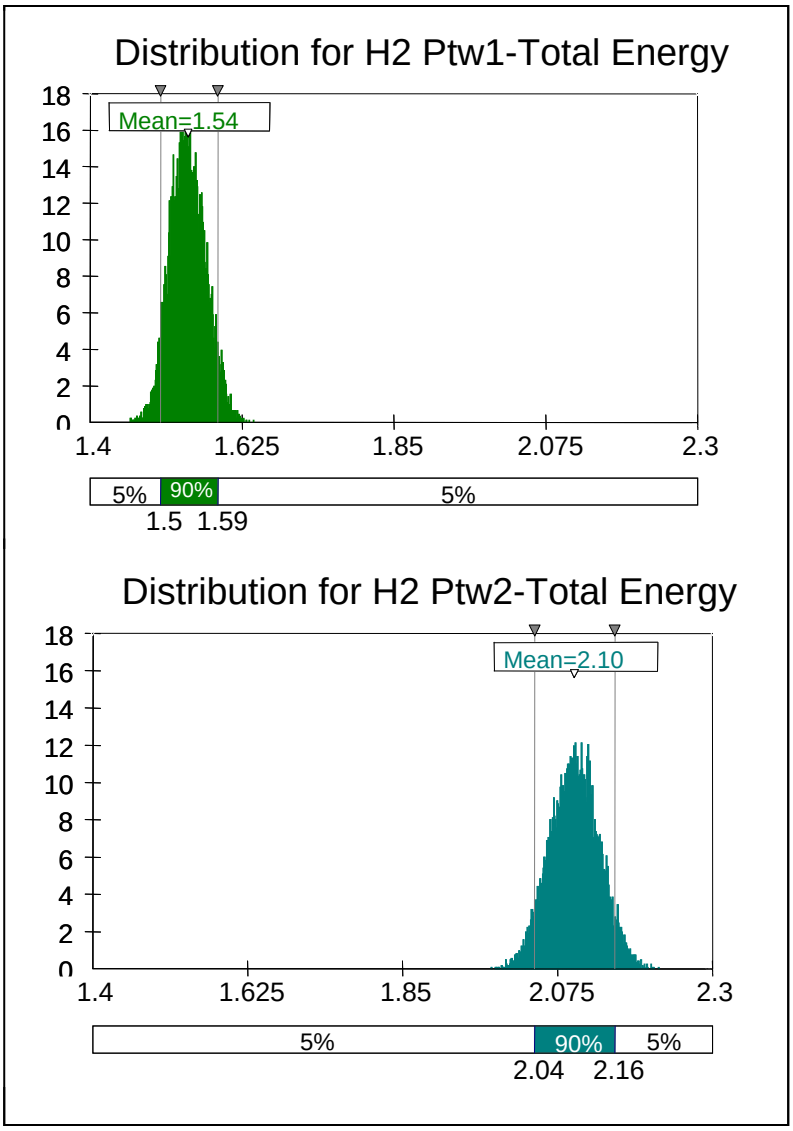


Figure 80 - Total Energy Requirement for the Hydrogen Pathways
($GJ_{req.-upstream}/GJ_{fuel-delivered}$) – HHV

The same discussion presented for the thermal efficiency can be presented for the $CO_2$ emissions (see Figure 81). A more efficient pathway will require less burned fossil fuel and therefore less $CO_2$ is released. Hydrogen production using SMR yield some extra hydrogen from water (steam) in the syngas production and because of that $CO_2$ emissions for hydrogen production is relatively lower than $CO_2$ emissions in the production of gas-to-liquids fuels (MeOH and FTN).

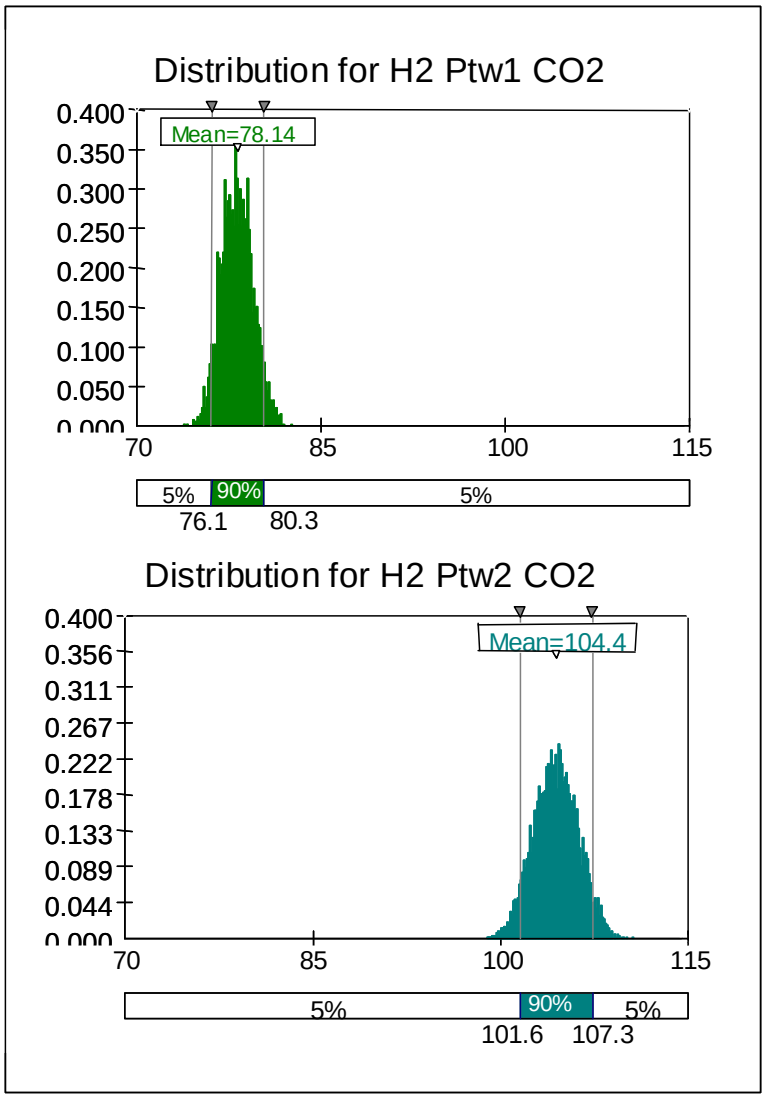


Figure 81 – $CO_2$ Emissions for the Hydrogen Pathways ($kg/GJ_{fuel\text{-}deliv.}$)

The first expectation for NOx emissions was to have lower emissions for the decentralized production pathway since the small reformers at the fuel station may use catalytic burners that have relative low NOx emissions. However, because decentralized plants are less efficient (around 68%) than centralized plants (around 87% considering extra steam exportation), they consume more natural gas per GJ of fuel produced and the extra $NO_x$ emissions generated due to the NG activities cancel out some of the benefits acquired in the burner. On top of that, they also consume a bigger percentage of electric energy, which is also produced inside of the area using NG feedstocks. Finally the electric as well as the natural gas distribution systems for small consumers (like fuel stations) are less efficient than the distribution system for big consumers. The corresponding results are presented in Figure 82.

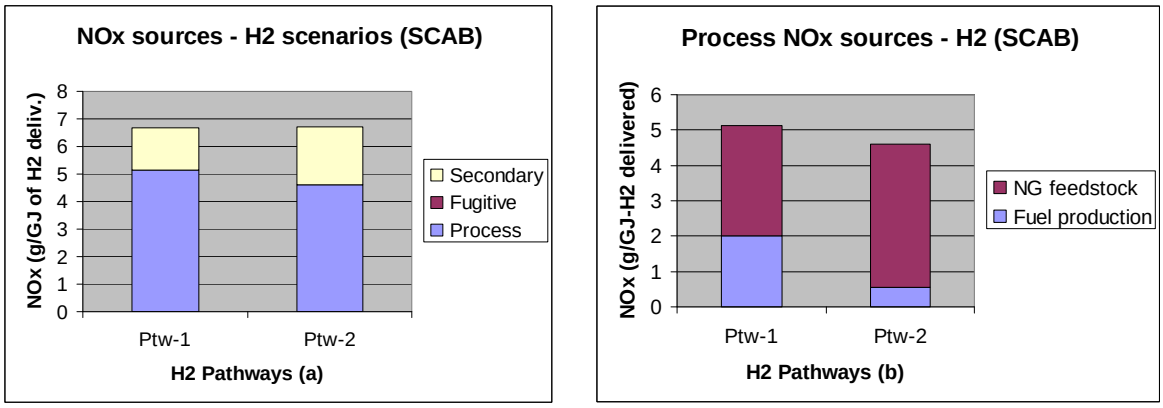


Figure 82 – $NO_x$ Emissions Sources for Hydrogen Pathways

### Gas-to-Liquid Scenarios

Figure 83 shows the total energy requirements for the methanol and Fisher-Tropsch Naphtha pathways.

In both cases the efficiency of the fuel production plant and the possibility for extra steam exportation play the major rules. For methanol a possible mega-size plant using combined SMR/POX can have efficiency around 72% and a typical size plant using SMR and no extra steam exportation can have efficiency around 67%. For FTN, a plant using pure oxygen for syngas production and exporting extra-steam can have the thermal efficiency around 72.5% and, on the other hand, a plant using air can have the efficiency around 54%.

Similar analysis can be done for the $CO_2$ pathway emissions and is presented in Figure 84.

## 4.2.6 Final Comments

Analyzing specific pathways such as the ones presented in Figure 80 and Figure 83 one can see that assessing the uncertainties related to a single technology assumption prove to be very important. On the other hand, when combined technology scenarios are assumed the sensitivity of the final results proves to be even greater depending on the situation.

This conclusion comes to reinforce that the participation of the various stakeholders in this kind of study is very important. This way, reliable and consensual scenarios can be forecasted and accepted by all parties and thus helping generate useful results.

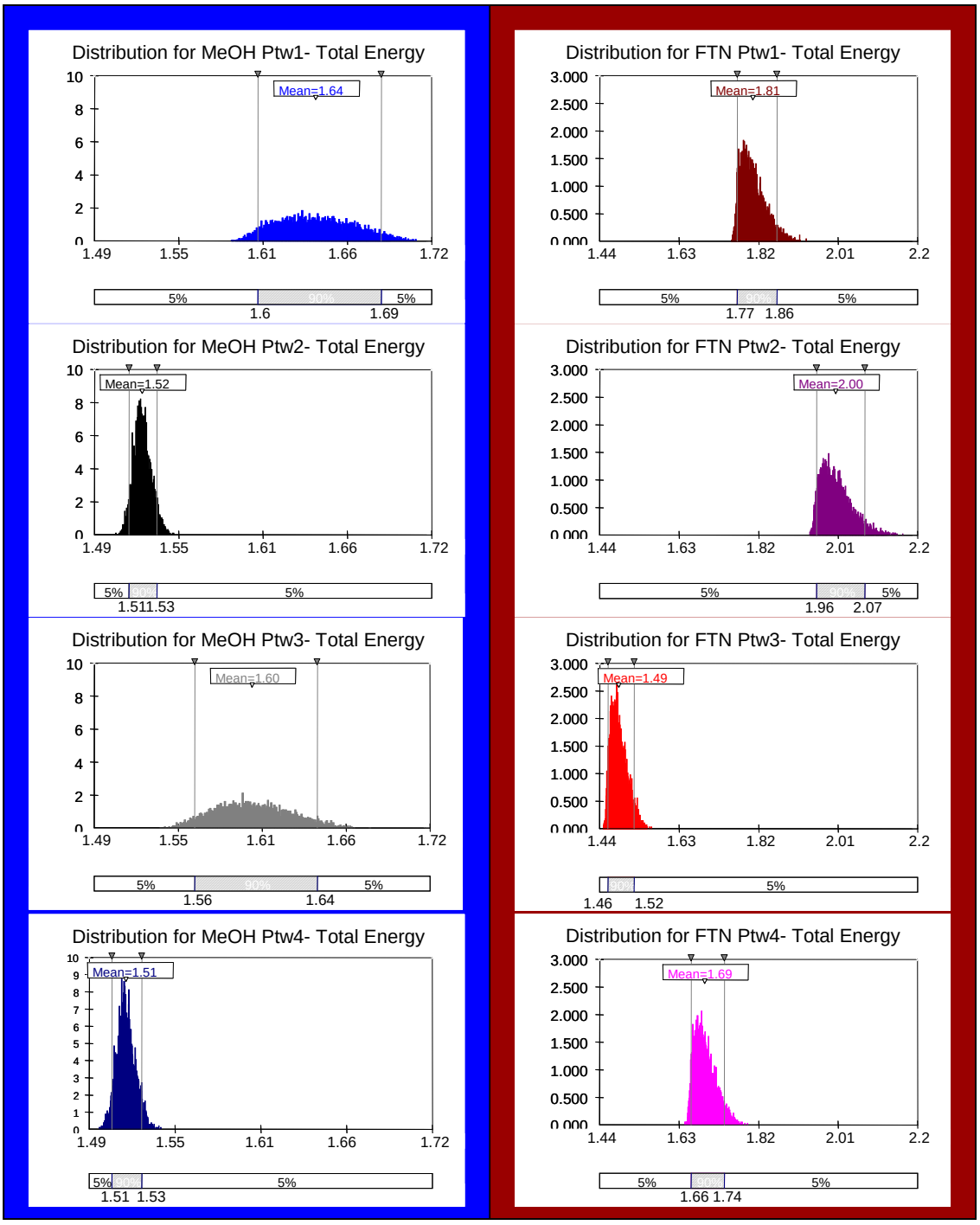


Figure 83 – Total Energy Requirement for Methanol and FTN Fuels

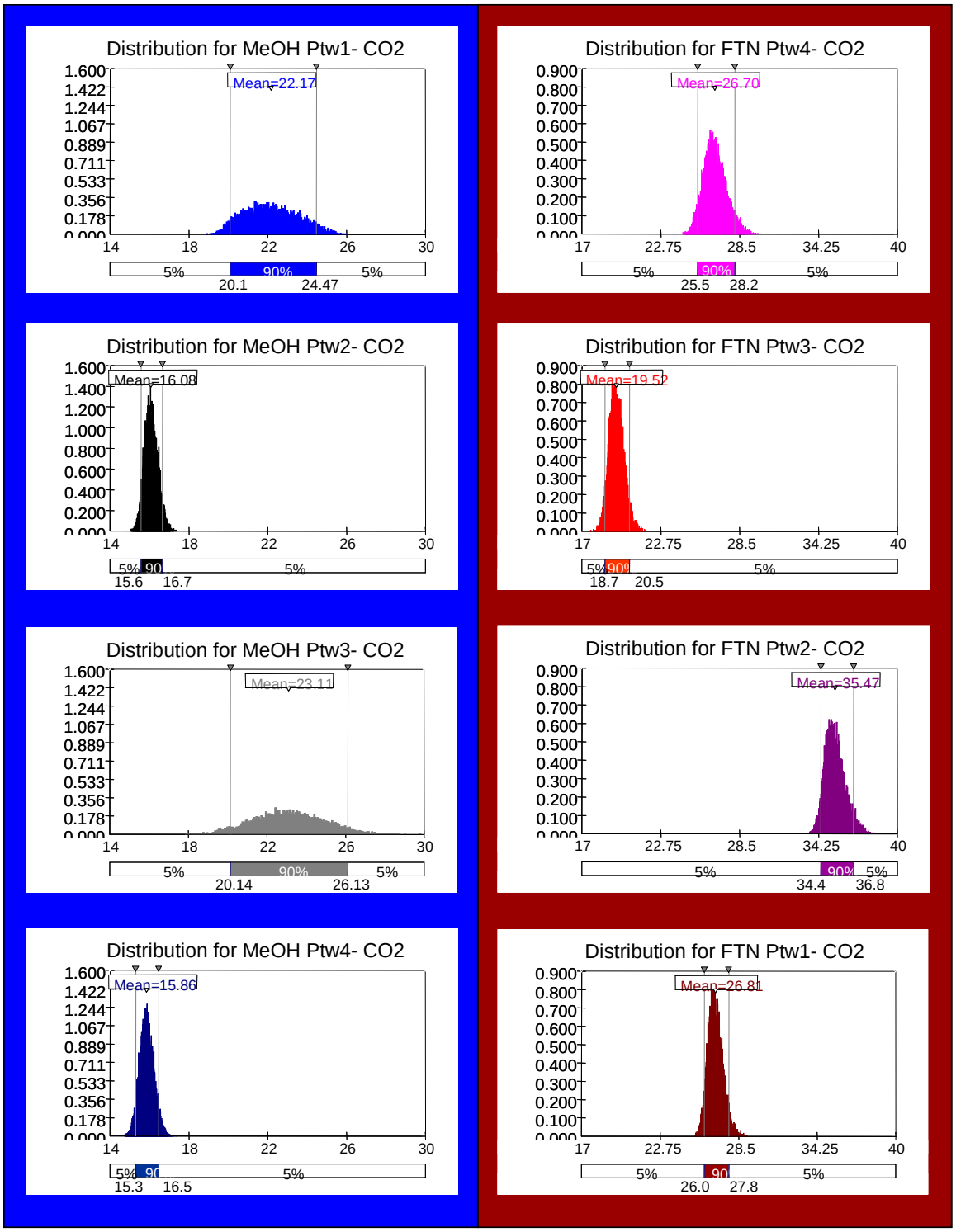


Figure 84 - $CO_2$ emissions for the different pathways of the liquid fuels ($kg/GJ_{fuel\text{-}deliv.}$)

# 5 Appendix

## 5.1 Fuel Cell Vehicle and System Energy Details

Figure A 1 shows detailed energy results for the three vehicle platforms on two driving cycles. The energy values shown in this figure are simply the combination of results shown in Figure 3 and Figure 29 earlier in the report. Note that the term "nrg" in some of the titles refers to "energy".

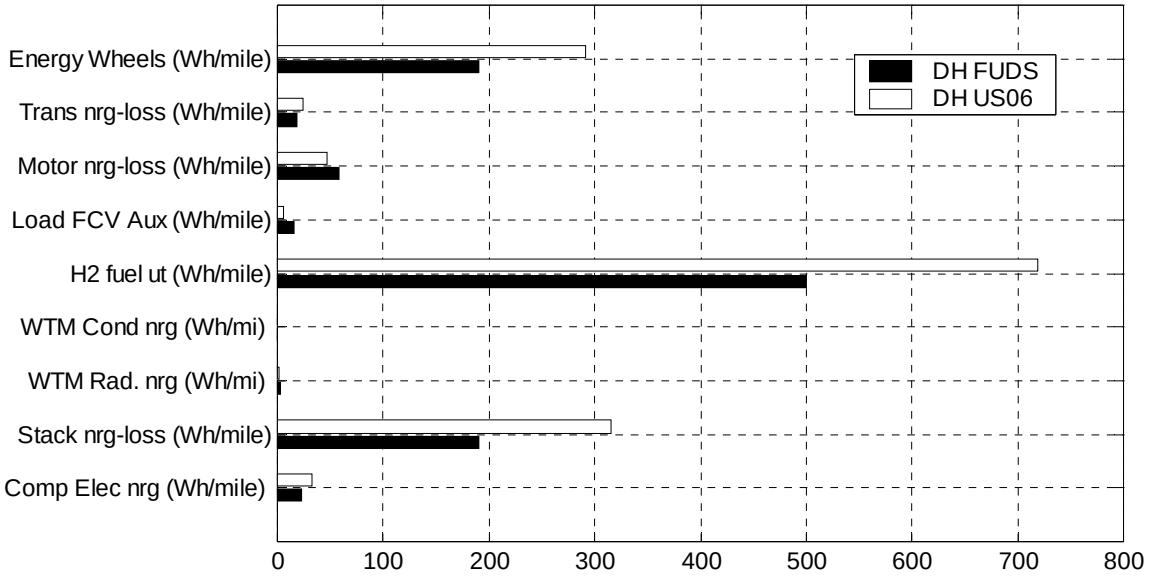


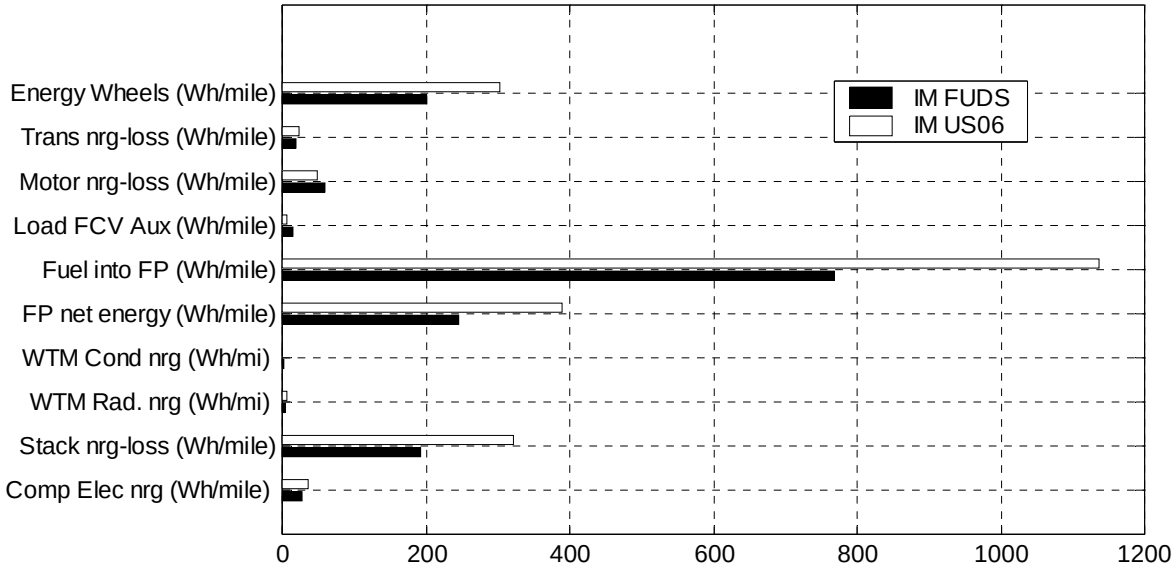

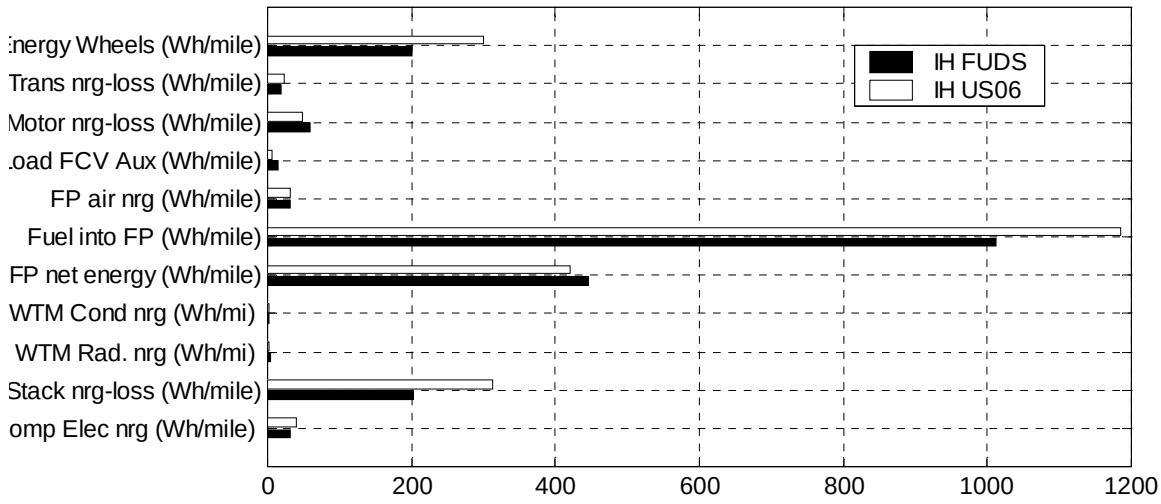


Figure A 1: Drive Cycle results: System total energy comparison - DETAIL

* NOTE 1: Drive Train NRG is the combined energy of the motor and transmission losses along with the energy required at the wheels. Refer to Section 2.1.2.
* NOTE 2: Stack Gross Energy equates to the summation of the other variable values

## 5.2 Fuel Processor Details

### IH Step Response versus Steam Generation

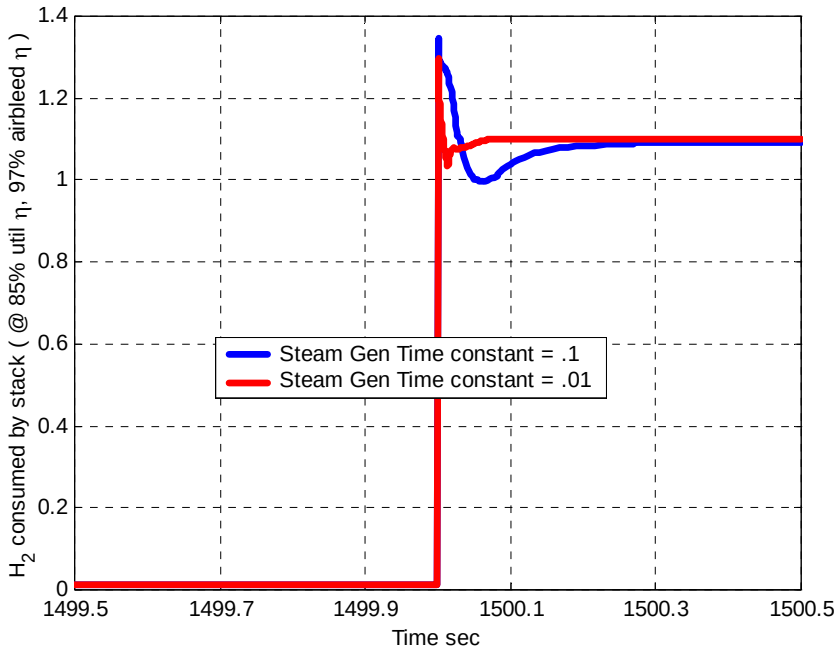


Figure A 2 – Impact of steam generator time constants : IH fuel processor response (scaled to reflect Hydrogen consumed at the stack @ 97% air bleed efficiency and 85 % utilization)

### Further Dynamic Analysis - Drive Cycles Results

***IM Fuel Processor***

***a) Comparison between FUDS, HIWAY, US06, ECE and J-1015 Cycles:***

Table A 1 - Efficiency Comparisons for the IM

| | IM ECE | IM FUDS | IM HIWAY | IM US06 | IM J1015 |
|---|---|---|---|---|---|
| **FP overall eff** | 62.40 | 68.11 | 73.02 | 65.80 | 69.06 |
| **FP efficiency** | 88.71 | 88.01 | 91.26 | 78.06 | 91.69 |
| **H2 airbleed eff** | 98.21 | 98.21 | 98.21 | 98.21 | 98.21 |
| **H2 utilization eff** | 71.62 | 78.80 | 81.47 | 85.83 | 76.68 |
| **Vehicle Efficiency (%)** | 20.05 | 26.23 | 31.29 | 26.70 | 25.36 |

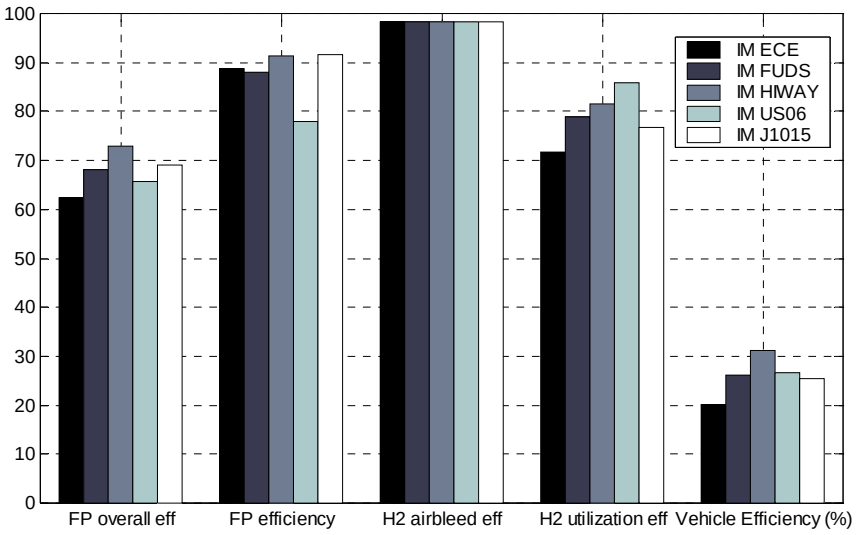


Figure A 3 - Efficiency comparisons for the IM

***IH FP Buffer/no Buffer***

***a) HIGHWAY Cycle***

For the Highway drive cycle the use of a buffer makes a slight difference in the efficiency of the fuel processor as one can see in the Table A 2 and Figure A 4 below.

Table A 2 - Efficiency comparisons for the IH – HIWAY Cycle

| | IH HIWAY | IH buffer hiway |
|---|---|---|
| **FP overall eff** | 65.65 | 65.43 |
| **FP efficiency** | 81.66 | 81.83 |
| **H2 air bleed eff** | 97.18 | 97.11 |
| **H2 utilization eff** | 82.72 | 82.34 |
| **Vehicle Efficiency (%)** | 26.64 | 26.52 |

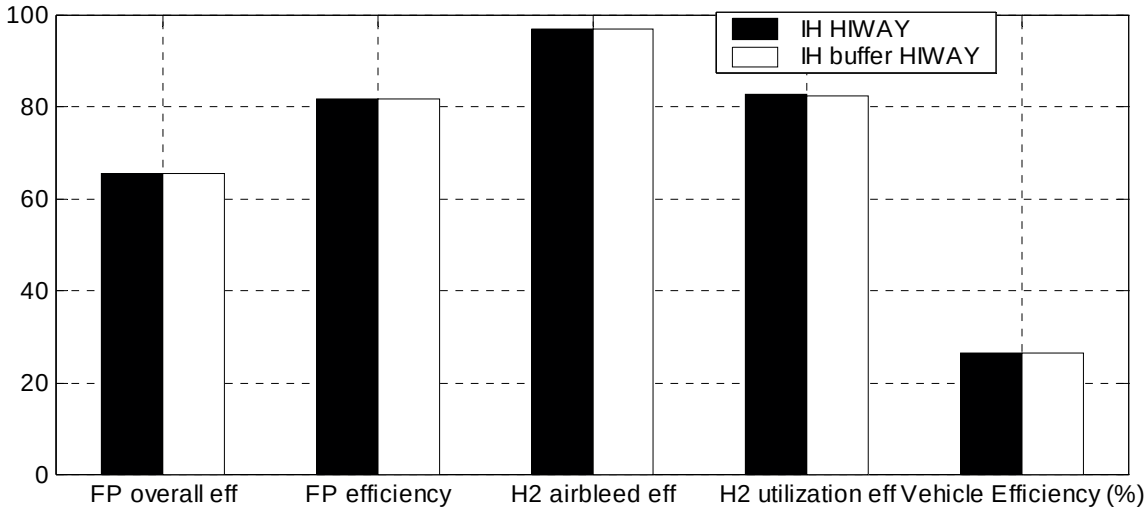


Figure A 4 - Efficiency comparisons for IH - HIWAY Cycle

***b) US06 Cycle:***

In this case the use of a buffer increases the H2 Utilization efficiency and consequently the FP overall efficiency also increases. The values can be seen at Table A 3 and Figure A 5 below.

Table A 3 - Efficiency comparisons for the IH – US06 Cycle

| | **IH US06** | **IH buffer US06** |
|---|---|---|
| **FP overall eff** | 64.58 | 67.33 |
| **FP efficiency** | 81.41 | 81.15 |
| **H2 air bleed eff** | 97.18 | 97.13 |
| **H2 utilization eff** | 81.63 | 85.42 |
| **Vehicle Efficiency (%)** | 25.33 | 26.56 |

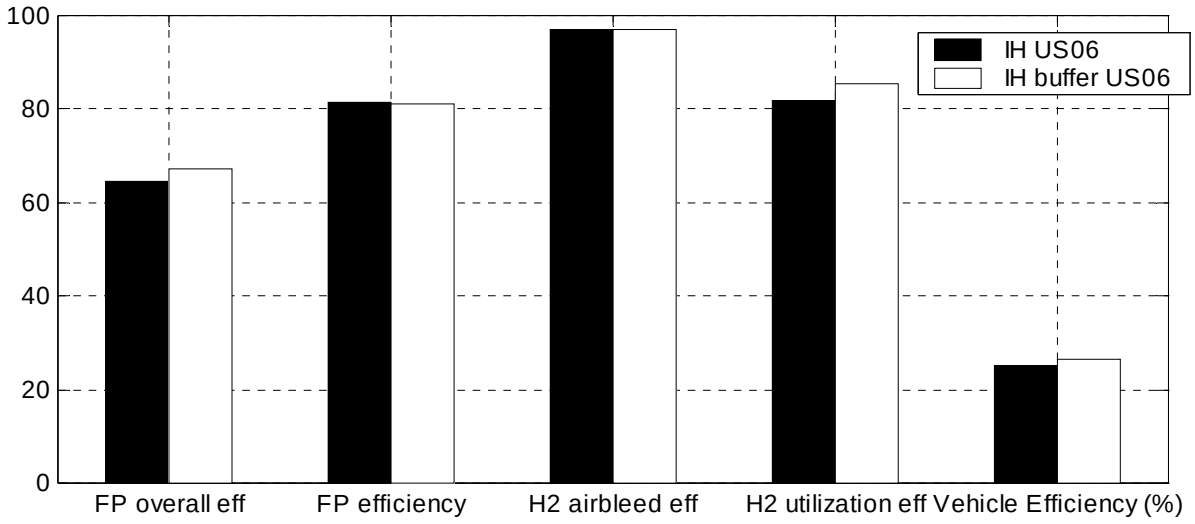


Figure A 5 – Efficiency comparisons for the IH – US06 Cycle

***c) ECE Cycle***

In this case the use of a buffer increases the H2 Utilization efficiency and consequently the FP overall efficiency also increases. The values can be seen at Table A 4 and Figure A 6 below.

Table A 4 - Efficiency comparisons for the IH – ECE Cycle

| | **IH ECE** | **IH buffer ECE** |
|---|---|---|
| **FP overall eff** | 43.79 | 55.24 |
| **FP efficiency** | 82.15 | 82.15 |
| **H2 air bleed eff** | 97.21 | 96.57 |
| **H2 utilization eff** | 54.84 | 69.63 |
| **Vehicle Efficiency (%)** | 12.25 | 16.2 |

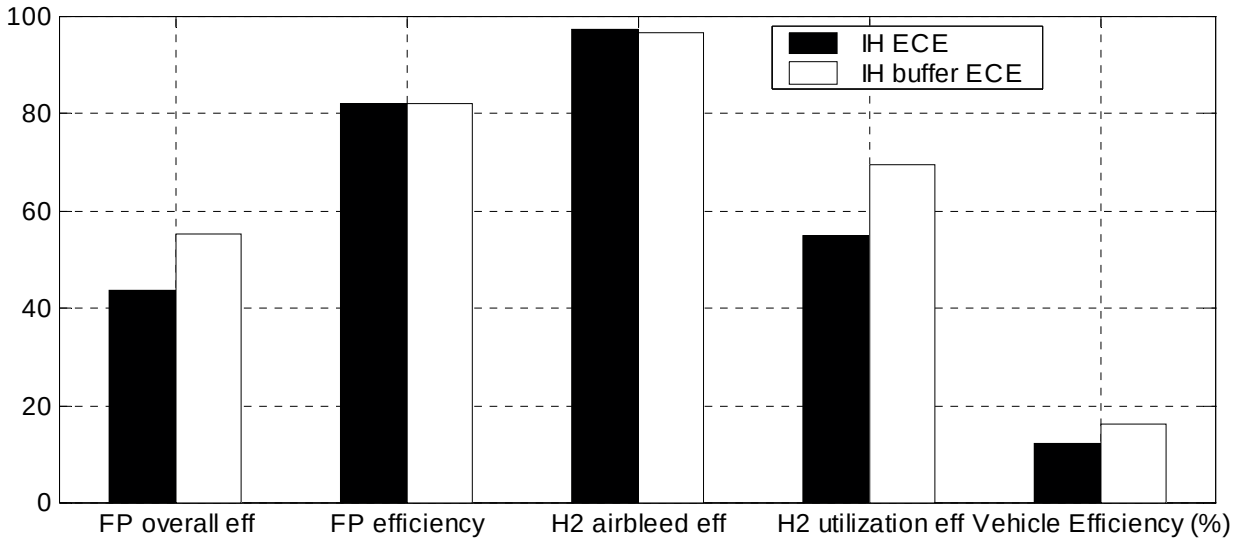


Figure A 6 - Efficiency comparisons for the IH – ECE Cycle

***d) J-1015 Cycle***

In this case the use of a buffer increases the H2 Utilization efficiency and consequently the FP overall efficiency also increases. The values can be seen at Table A 5 and Figure A 7 below.

Table A 5 - Efficiency comparisons for the IH – J-1015 Cycle

| | **IH J1015** | **IH buffer J1015** |
|---|---|---|
| **FP overall eff** | 50.16 | 58.96 |
| **FP efficiency** | 81.97 | 82.05 |
| **H2 air bleed eff** | 97.20 | 96.90 |
| **H2 utilization eff** | 62.96 | 74.15 |
| **Vehicle Efficiency (%)** | 16.58 | 20.05 |

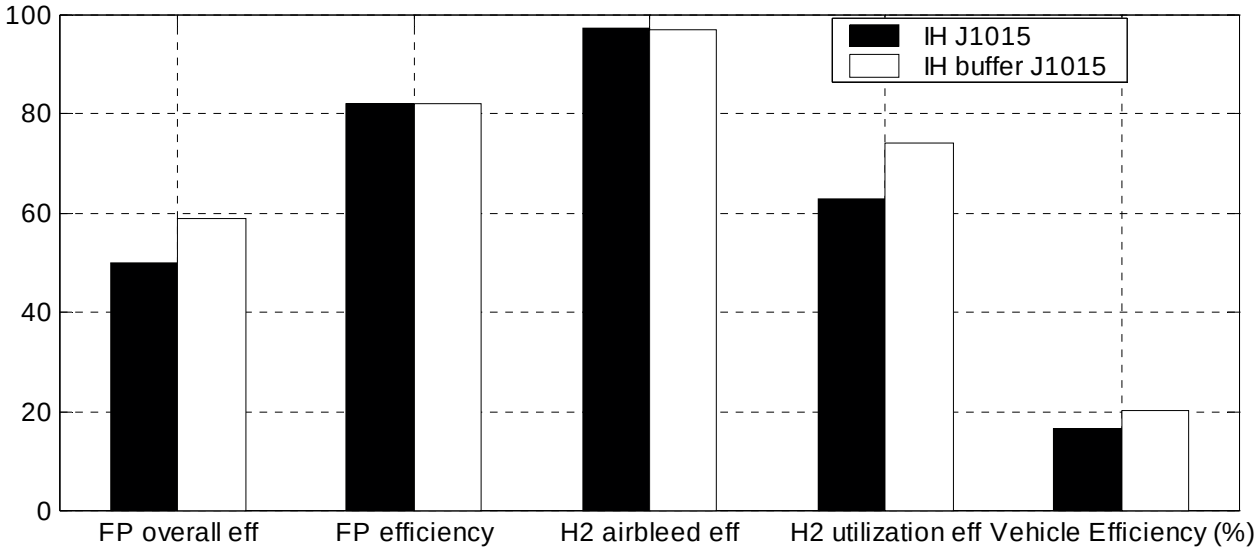


Figure A 7 - Efficiency comparisons for the IH – J-1015 Cycle

***Comparison of the IH and IM***

***a) FUDS Cycle***

Table A 6 - Efficiency comparisons for IH and IM – FUDS Cycle

| | IM FUDS | IH FUDS |
|---|---|---|
| **FP overall eff** | 68.11 | 55.95 |
| **FP efficiency** | 88.01 | 81.85 |
| **H2 airbleed eff** | 98.21 | 97.19 |
| **H2 utilization eff** | 78.80 | 70.33 |
| **Vehicle Efficiency (%)** | 26.23 | 19.87 |

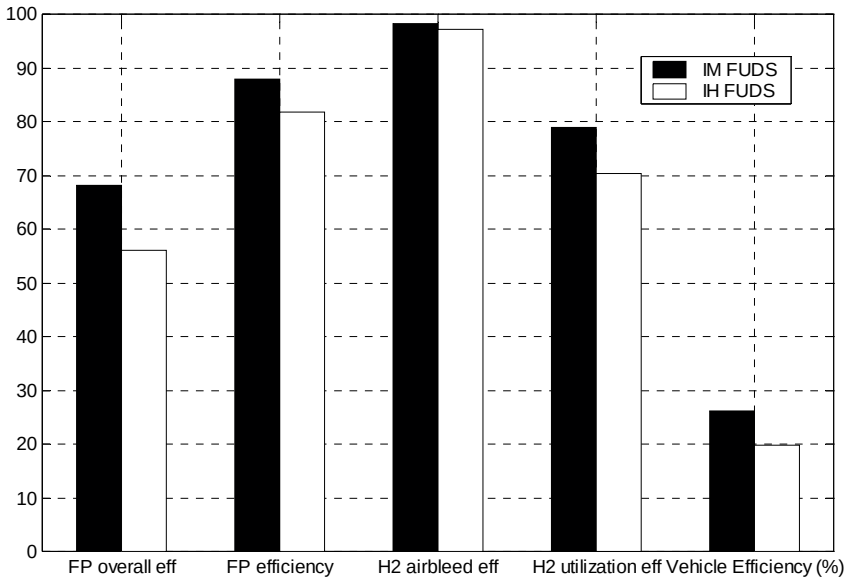


Figure A 8 - Efficiency comparisons, IH and IM – FUDS Cycle

***b) HIWAY Cycle***

Table A 7 - Efficiency comparisons, IH and IM – HIWAY Cycle

| | IM HIWAY | IH HIWAY |
|---|---|---|
| **FP overall eff** | 73.02 | 65.65 |
| **FP efficiency** | 91.26 | 81.66 |
| **H2 airbleed eff** | 98.21 | 97.18 |
| **H2 utilization eff** | 81.47 | 82.72 |
| **Vehicle Efficiency (%)** | 31.29 | 26.64 |

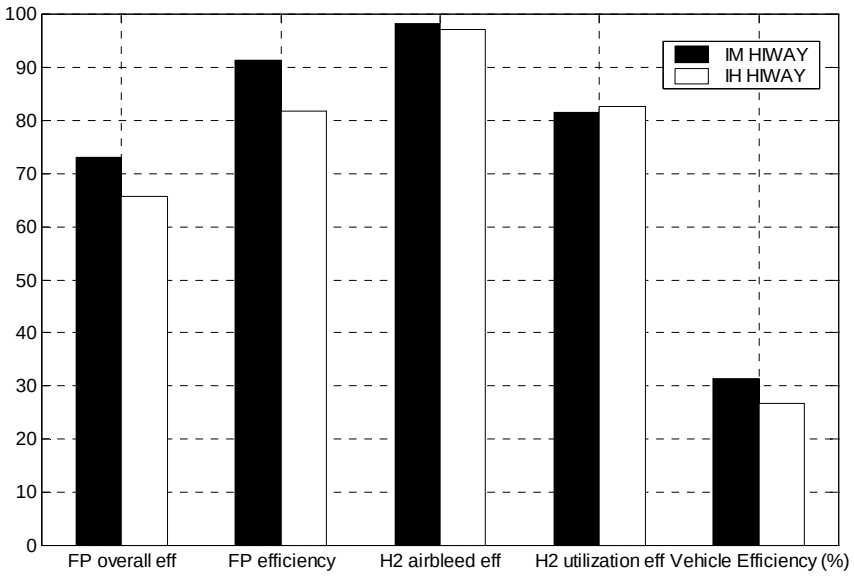


Figure A 9 - Efficiency comparisons, IH and IM – HIWAY Cycle

### *c) US06 Cycle*

Table A 8 - Efficiency comparisons for IH and IM – US06 Cycle

| | IM US06 | IH US06 |
|---|---|---|
| **FP overall eff** | 65.80 | 64.58 |
| **FP efficiency** | 78.06 | 81.41 |
| **H2 airbleed eff** | 98.21 | 97.18 |
| **H2 utilization eff** | 85.83 | 81.63 |
| **Vehicle Efficiency (%)** | 26.70 | 25.33 |

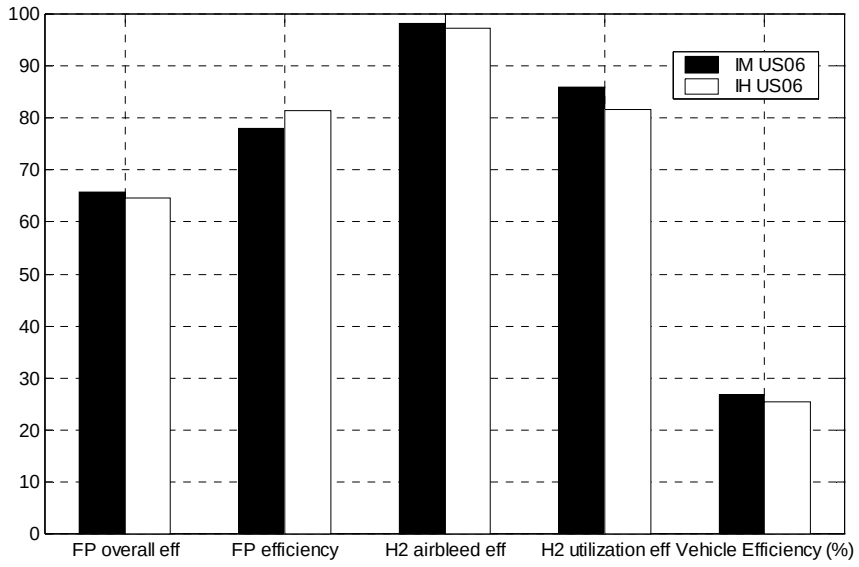


Figure A 10 - Efficiency comparisons, IH and IM – US06 Cycle

***d) ECE Cycle***

Table A 9 - Efficiency comparisons for IH and IM – ECE Cycle

| | IM ECE | IH ECE |
|---|---|---|
| **FP overall eff** | 62.40 | 43.79 |
| **FP efficiency** | 88.71 | 82.15 |
| **H2 airbleed eff** | 98.21 | 97.21 |
| **H2 utilization eff** | 71.62 | 54.84 |
| **Vehicle Efficiency (%)** | 20.05 | 12.25 |

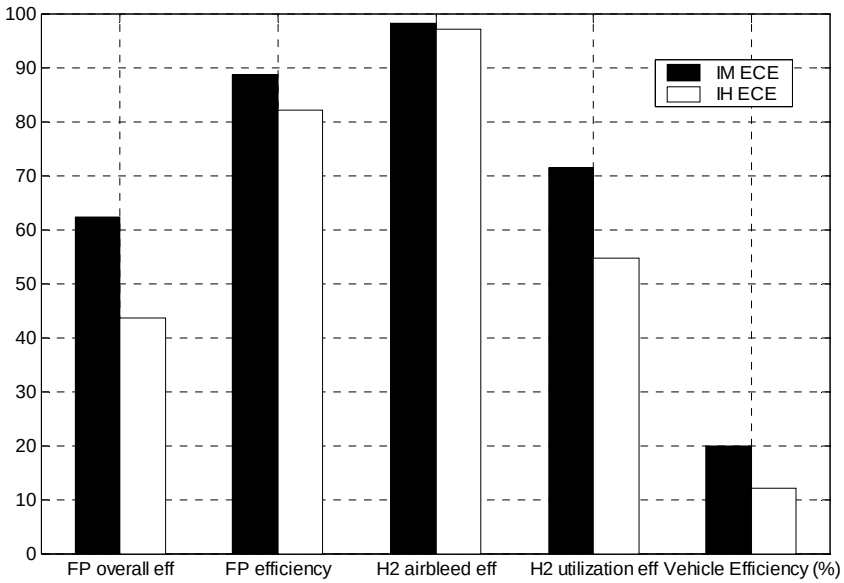


Figure A 11 - Efficiency comparisons, IH and IM – ECE Cycle

***e) J-1015 Cycle***

Table A 10 – Efficiency comparisons, IH and IM – J-1015 Cycle

| | IM J1015 | IH J1015 |
|---|---|---|
| **FP overall eff** | 69.06 | 50.16 |
| **FP efficiency** | 91.69 | 81.97 |
| **H2 airbleed eff** | 98.21 | 97.20 |
| **H2 utilization eff** | 76.68 | 62.96 |
| **Vehicle Efficiency (%)** | 25.36 | 16.58 |

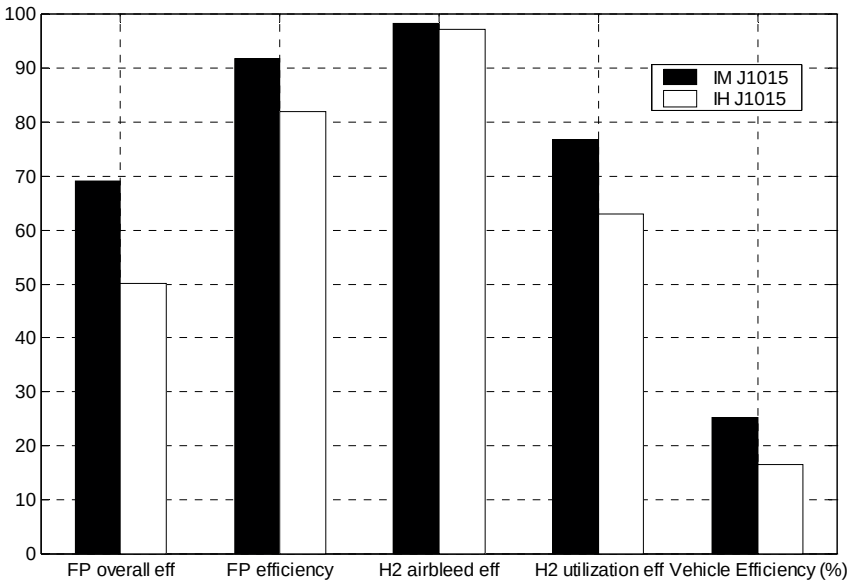


Figure A 12 - Efficiency comparisons, IH and IM – J1015 Cycle

## Full and Reduced Models Comparison for IM and IH

For these comparisons just the FUDS drive cycle has been considered here because it is the most dynamic one. The other drive cycles were run but not included in this report. They can be made available upon request.

### *a) IM Case (FUDS Cycle)*

Table A 11 – Full and Reduced Models Comparison for the IM – FUDS Cycle

| | IM FUDS | IM fullfp FUDS |
|---|---|---|
| **FP overall eff** | 68.11 | 69.46 |
| **FP efficiency** | 88.01 | 89.55 |
| **H2 air bleed eff** | 98.21 | 98.22 |
| **H2 utilization eff** | 78.80 | 78.98 |
| **Vehicle Efficiency (%)** | 26.23 | 26.74 |

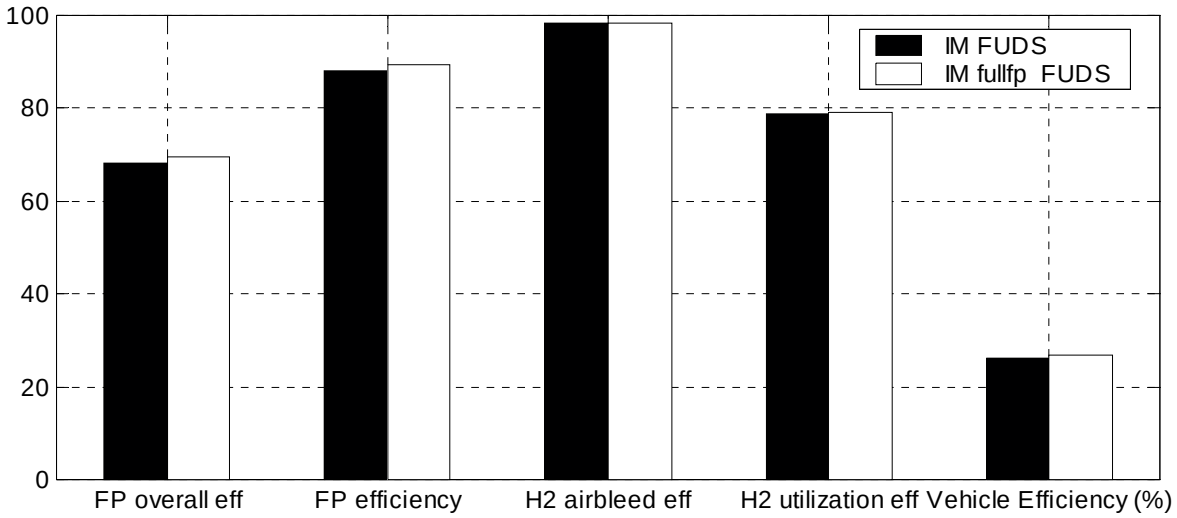


Figure A 13 - Full and Reduced Models Comparison for the IM – FUDS Cycle

***b) IH Case (FUDS Cycle)***

Table A 12 - Full and Reduced Models Comparison for the IH – FUDS Cycle

| | **IH FUDS** | **IH fullfp FUDS** |
|---|---|---|
| **FP overall eff** | 55.95 | 55.98 |
| **FP efficiency** | 81.85 | 81.88 |
| **H2 air bleed eff** | 97.19 | 97.19 |
| **H2 utilization eff** | 70.33 | 70.34 |
| **Vehicle Efficiency (%)** | 19.87 | 19.88 |

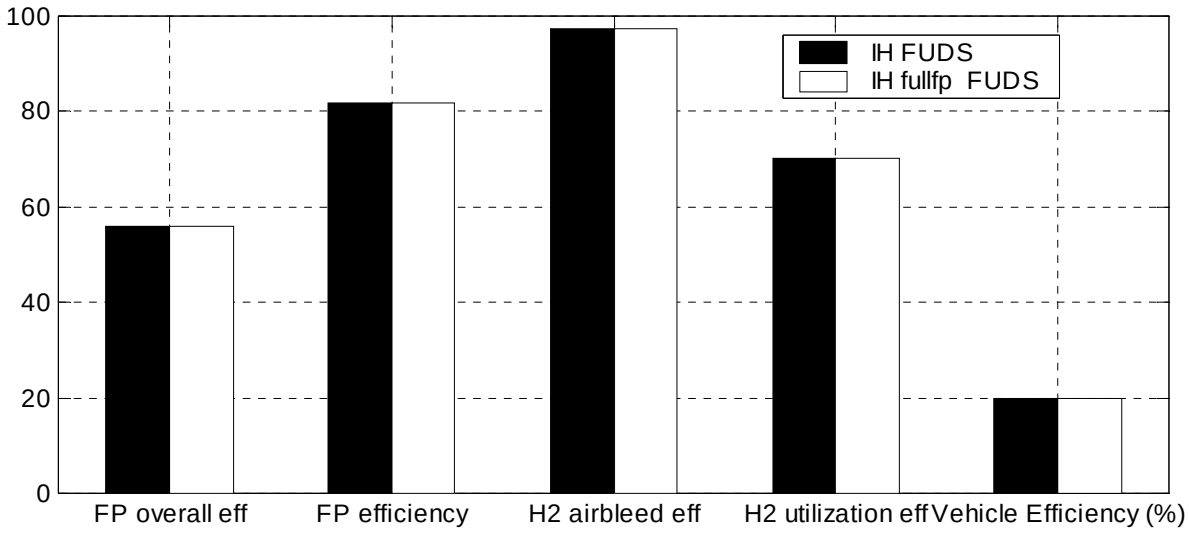


Figure A 14 - Full and Reduced Models Comparison for the IH – FUDS Cycle

## 5.3 Upstream Fuel Pathway

Table A 13 – Fuels Properties

| Fuels | Energy content (HHV) | | Density | |
|---|---|---|---|---|
| | Btu/gal (or scf)[a] | kJ/L (or $m^3$)[a] | lb/gal (or scf)[a] | g/L (or $m^3$)[a] |
| Hydrogen | 324 | 12070 | $5.24 \times 10^{-3}$ | 83.9 |
| Methanol | 64800 | 18062 | 6.63 | 794.5 |
| FT-Naphtha[b] | 116500 | 32472 | 5.76 | 690.3 |

a = For the hydrogen case (standard cubic feet)
b = Average (depend of the composition)

Table A 14 - Total Upstream Energy Requirement – Combined Scenarios

| Total upstream energy requirement – combined scenarios ($GJ_{req\text{-}upstream}$ / $GJ_{fuel\ delivered}$) | | | | | |
|---|---|---|---|---|---|
| Fuels | Mean | Mode | Std Deviat. | $5^{th}$ Percent | $95^{th}$ Percent |
| Hydrogen | 1.75 | 1.74 | 0.06 | 1.66 | 1.84 |
| Methanol | 1.57 | 1.56 | 0.01 | 1.55 | 1.60 |
| FTNaphtha | 1.75 | 1.74 | 0.02 | 1.72 | 1.79 |

Table A 15 - Total Energy Required – combined scenarios (mean)

| **Total Energy Required (GJ/GJ-deliv)** | | | |
|---|---|---|---|
| **Fuels** | **All Sources** | **Fossil Fuel** | **Petroleum** |
| **$H_2$** | 1.75 | 1.73 | 0.01 |
| **MeOH** | 1.57 | 1.54 | 0.04 |
| **FTN** | 1.75 | 1.73 | 0.02 |

Table A 16 – Global CO2 Emissions – combined scenarios (mean)

| **Global CO2 emissions (Kg/GJ-deliv)** | | | | |
|---|---|---|---|---|
| **Fuels** | **Total** | **Process** | **Fugitive** | **Secondary** |
| **$H_2$** | 87.12 | 73.22 | 0.00 | 13.80 |
| **MeOH** | 19.31 | 18.79 | 0.04 | 0.68 |
| **FTN** | 27.12 | 26.52 | 0.04 | 0.54 |

Table A 17 – NMOG Emission Sources in SCAB – combined scenarios (mean)

| **NMOG emis. sources in SCAB (g/GJ-deliv.)** | | | | |
|---|---|---|---|---|
| **Fuels** | **Total** | **Process** | **Fugitive** | **Secondary** |
| **$H_2$** | 2.96 | 0.24 | 2.27 | 0.45 |
| **MeOH** | 12.91 | 0.06 | 12.85 | 0.00 |
| **FTN** | 9.2 | 0.03 | 9.17 | 0.00 |

Table A 18 – NMOG Fugitive Emissions – SCAB – all scenarios (mean)

| SCAB NMOG Fug. Emiss. (g/GJ-deliv) | | |
|---|---|---|
| **Activities** | **MeOH** | **FTN** |
| **Fuel Station** | 8.99 | 5.57 |
| **Diesel Truck** | 0.39 | 0.32 |
| **Fuel Terminals** | 0.2 | 0.55 |
| **Port Activities** | 3.33 | 2.76 |

Table A 19 – NMOG Fuel Station – all scenarios (mean)

| Fuel Station NMOG Fug. (mg/L-proc) | | |
|---|---|---|
| | **MeOH** | **FTN** |
| **Refuel. Spillage** | 53.9 | 46.8 |
| **Nozzle Retent.** | 60.6 | 52.6 |
| **Displ. (Stage II)** | 36.5 | 61.5 |
| **FS-tank Breath.** | 4.4 | 7.0 |
| **Displ. (Stage I)** | 2.0 | 9.0 |
| **Distrib. Spillage** | 2.9 | 2.6 |
| **Hose Retent.** | 2.1 | 1.9 |

Table A 20 – $NO_x$ –Hydrogen pathways – SCAB (mean)

| H2 - NOx - Area 1 (g/GJ fuel-deliv.) | | |
|---|---|---|
| **Sources** | Ptw-1 | Ptw-2 |
| **Process** | 5.14 | 4.59 |
| **Fugitive** | 0 | 0 |
| **Secondary** | 1.53 | 2.14 |

Table A 21 - NOx from Process – Hydrogen pathways (mean)

| H2 - NOx from Process (g/GJ-deliv.) | | |
|---|---|---|
| **Sources** | Ptw-1 | Ptw-2 |
| **Fuel production** | 2 | 0.55 |
| **NG feedstock** | 3.13 | 4.04 |

Table A 22 – Total Energy Requirement – Methanol pathways

| MeOH - Total Energy (GJ-req.upst/GJ-deliv.) | | | | | |
|---|---|---|---|---|---|
| | Mean | Mode | St. Dev. | $5^{th}$ | $95^{th}$ |
| **Ptw-1** | 1.64 | 1.63 | 0.03 | 1.60 | 1.69 |
| **Ptw-2** | 1.52 | 1.52 | 0.01 | 1.51 | 1.53 |
| **Ptw-3** | 1.61 | 1.60 | 0.03 | 1.56 | 1.64 |
| **Ptw-4** | 1.52 | 1.52 | 0.01 | 1.51 | 1.53 |

Table A 23 - Total Energy Requirement – FTN pathways

| FTN - Total Energy (GJ-req.upst/GJ-deliv.) | | | | | |
|---|---|---|---|---|---|
| | Mean | Mode | St. Dev. | 5th | 95th |
| **Ptw-1** | 1.80 | 1.78 | 0.03 | 1.77 | 1.86 |
| **Ptw-2** | 2.00 | 1.98 | 0.04 | 1.96 | 2.07 |
| **Ptw-3** | 1.49 | 1.47 | 0.02 | 1.46 | 1.52 |
| **Ptw-4** | 1.70 | 1.67 | 0.02 | 1.66 | 1.74 |

Table A 24 - - $NO_x$ – SCAB - Combined Scenarios

| $NO_x$ - Area 1 (g/GJ delivered) - Combined Scenarios | | | | | |
|---|---|---|---|---|---|
| | Mean | Mode | St. Dev. | 5th | 95th |
| **$H_2$** | 6.69 | 6.06 | 0.76 | 5.53 | 8.06 |
| **MeOH** | 0.45 | 0.43 | 0.03 | 0.40 | 0.49 |
| **FTN** | 0.22 | 0.21 | 0.01 | 0.20 | 0.24 |

Table A 25 - NMOG – SCAB - Combined Scenarios

| NMOG - Area 1 (g/GJ delivered) - Combined Scenarios | | | | | |
|---|---|---|---|---|---|
| | Mean | Mode | St. Dev. | 5th | 95th |
| **$H_2$** | 2.96 | 3.24 | 1.15 | 1.21 | 4.97 |
| **MeOH** | 12.91 | 10.63 | 6.23 | 7.25 | 25.04 |
| **FTN** | 9.20 | 7.73 | 2.99 | 6.22 | 14.89 |

Table A 26 - CO – SCAB - Combined Scenarios

| CO - Area 1 (g/GJ delivered) - Combined Scenarios | | | | | |
|---|---|---|---|---|---|
| | Mean | Mode | St. Dev. | 5th | 95th |
| **$H_2$** | 3.29 | 3.40 | 0.75 | 2.08 | 4.53 |
| **MeOH** | 1.04 | 0.96 | 0.08 | 0.91 | 1.18 |
| **FTN** | 0.49 | 0.50 | 0.04 | 0.43 | 0.56 |

Table A 27 – Total Energy Requirement – Hydrogen pathways

| Hydrogen - Total Energy (GJ-req.upst/GJ-deliv.) | | | | | |
|---|---|---|---|---|---|
| | Mean | Mode | St. Dev. | 5th | 95th |
| **Ptw-1** | 1.54 | 1.53 | 0.03 | 1.50 | 1.59 |
| **Ptw-2** | 2.10 | 2.07 | 0.04 | 2.04 | 2.16 |

Table A 28 – Global CO2 Emissions – combined scenarios

| CO2 Total Emissions (Kg/GJ delivered) - Combined Scenarios | | | | | |
|---|---|---|---|---|---|
| | Mean | Mode | St. Dev. | 5th | 95th |
| **$H_2$** | 87.12 | 87.2 | 2.72 | 82.84 | 91.78 |
| **MeOH** | 19.31 | 19.0 | 0.84 | 17.98 | 20.75 |
| **FTN** | 27.12 | 27.4 | 0.49 | 26.33 | 27.95 |

Table A 29 – Global CO2 emissions – Hydrogen pathways

| **Hydrogen – Total CO2 (Kg/GJ-deliv.)** | | | | | |
|---|---|---|---|---|---|
| | Mean | Mode | St. Dev. | 5th | 95th |
| **Ptw-1** | 78.14 | 78.40 | 1.30 | 76.06 | 80.34 |
| **Ptw-2** | 104.44 | 103.90 | 1.76 | 101.56 | 107.33 |

Table A 30 – Global CO2 emissions – Methanol pathways

| **MeOH - Total CO2 (Kg/GJ-deliv.)** | | | | | |
|---|---|---|---|---|---|
| | Mean | Mode | St. Dev. | 5th | 95th |
| **Ptw-1** | 22.17 | 21.88 | 1.34 | 20.10 | 24.47 |
| **Ptw-2** | 16.01 | 15.93 | 0.33 | 15.56 | 16.66 |
| **Ptw-3** | 23.11 | 23.08 | 1.81 | 20.14 | 26.13 |
| **Ptw-4** | 15.86 | 15.73 | 0.36 | 15.30 | 16.47 |

Table A 31 – Global CO2 emissions – FTN pathways

| **FTN - Total CO2 (Kg/GJ-deliv.)** | | | | | |
|---|---|---|---|---|---|
| | Mean | Mode | St. Dev. | 5th | 95th |
| **Ptw-1** | 26.81 | 26.52 | 0.55 | 25.99 | 27.77 |
| **Ptw-2** | 35.47 | 34.86 | 0.73 | 34.43 | 36.82 |
| **Ptw-3** | 19.52 | 19.44 | 0.54 | 18.68 | 20.47 |
| **Ptw-4** | 26.69 | 26.47 | 0.81 | 25.45 | 28.15 |

## 5.4 References

**Vehicle Modeling References:**


- Karl-Heinz Hauer, Julius Quissek et. al. Technical Requirements of Fuel Cell Powered Electric Vehicles, Global Powertrain Congress, Detroit
- Karl-Heinz Hauer et. al. , Dynamic Response of an Indirect Methanol Fuel Cell Vehicle, SAE 2000 conference, SAE 2000-01-0370
- Karl-Heinz Hauer et. al., A Simulation Model for an Indirect Methanol Fuel Cell Vehicle, Future Technology and Transportation Conference, SAE 2000-01-3083
- Karl-Heinz Hauer et. al. , Dynamic Interaction Between the Electric Drive Train and Fuel Cell System for the Case of an Indirect Methanol Fuel Cell Vehicle, American Institute Aeronautics and Astronautics Inc.AIAA-2000-3039
- Karl-Heinz Hauer, Dr. Robert M. Moore Dr. Sitaram Ramaswamy, The Hybridized Fuel Cell Vehicle Model of the University of California, Davis, SAE 2001 World Congress, SAE 2001-01-0543
- Karl-Heinz Hauer,An Analysis Tool For Fuel Cell Vehicle Hardware and Software (Controls), Dissertation 2001
- Karl-Heinz Hauer, Badri Narayanan, Numerical Simulation of Two Different Ultra Capacitor Hybrid Fuel Cell Vehicles, EVS 18 (Draft)


**Upstream Pathway References:**


- Acurex Environmental Corporation (1996). Evaluation of Fuel-Cycle Emissions on a Reactivity Basis. 2 volumes. Prepared for CARB. A166-134. Principal Authors: Unnasch, S.; Browning, L. and Montano, M.
- Contadini, J. F.; Moore R. M.; Sperling, D. and Sundaresan, M. (2000a). Life-cycle Emissions of Alternative Fuels for Transportation: Dealing with Uncertainties. Society of Automotive Engineers, Inc.; SAE 2000-01-0597.
- Contadini, J. F.;. Diniz, C. V; Sperling, D. and Moore R. M. (2000b). Hydrogen Production Plants: Emissions and Thermal Efficiency Analysis. Proceedings of the Second International Symposium on Technological and Environmental Topics in Transports. Milan, October.
- Contadini, J. F.;. Diniz, C. V; Sperling, D. and Moore R. M. (2000c). Design and Energy Requirements for Future Marketing Activities of Gaseous Hydrogen Fuel for Fuel Cell Vehicles. Proceedings of the Second International Symposium on Technological and Environmental Topics in Transports. Milan, October.
- Contadini, J. F.; Moore R. M. and Mokhtarian, P.L. (2000d) FUEEM Input Data Treatment: A Technology Forecast Process for a Life Cycle Inventory of Fuel Cell Vehicle Operations. Thesis proposal, November. Submitted for publication.
- Contadini, Jose Fernando (2001). Life-cycle Emissions and Energy Requirement of Fuel Cell Vehicles Use in 2010: Dealing with Uncertainties. Ph. D. thesis. Department of Civil and Environmental Engineering. University of California at Davis. To be published.

- DeLucchi, Mark A. (1997). A Revised Model of Emissions of Greenhouse Gases from the Use of Transportation Fuels and Electricity. Institute of Transportation Studies, University of California at Davis. UCD-ITS-RR-97-22.
- DTI – Directed Technologies, Inc. (1997). Hydrogen Infrastructure Report. By Thomas, C. E., Ira F. Kuhn, Jr., Brian D. James, Franklin D. Lomax, Jr. and George N. Baum. Prepared for the U. S. DOE by Ford Motor Company and Direct Technologies, Inc., Report no. DOE/CE/50389-504, July.
- DTI – Directed Technologies, Inc. (1998a). Fuel Options for the Fuel Cell Vehicles: Hydrogen, Methanol or Gasoline? By C. E. Thomas, B. D. James, F. D. Lomax and I. F. Kuhn. Presented at the Fuel Cell Reformer Conference, SCAQMD, Diamond Bar, CA.
- DTI – Directed Technologies, Inc. (1998b). Integrated Analysis of Hydrogen Passenger Vehicle Transportation Pathways. By Thomas, C. E., Ira F. Kuhn, Jr., Brian D. James and Franklin D. Lomax, Jr. Prepared for the National Renewable Energy Laboratory. Sub-contract No. AXE-6-16685-01. U. S. DOE. Golden, Colorado.
- Ogden, J.M., Larson, E.D. and DeLucchi, M.A. (1994). A Technical and Economic Assessment of Renewable Transportation Fuels and Technologies (UCD-ITS-RR-94-31).
- Ogden, J. M.; Dennis, E.; Steinbugler, M. and Strohbehn, J. W. (1995). Hydrogen Energy Systems Studies. USDOE report, contract No. XR-11265-2.
- Ogden, J. M.; Kreutz, T. G. and Steinbugler M. (1998). Fuels for Fuel Cell Vehicles: Vehicle Design and Infrastructure Issues. SAE Technical Paper Series. 982500.
- Ogden, J.M. (1999). Developing an Infrastructure for Hydrogen Vehicles: a Southern California Case Study, Int. Journal of Hydrogen Energy, 24, 709-730.
- International Standard ISO 14040 (1997). Environmental Management – Life cycle assessment – Principles and framework. First edition, International Organization for Standardization. Reference number: ISO 14040:1997(E).


**Fuel Cell System References:**

***General System***


- Barbir, F., “Air, Water and Heat Management in Automotive Fuel Cell Systems,” Presented at the Commercializing Fuel Cell Vehicles 2000 conference, 12-14 April, 2000, Berlin, Germany.
- Barbir, F., et al., “Trade-off Design Analysis of Operating Pressure and Temperature in PEM Fuel Cell Systems,” Proceedings of the ASME Advanced Energy Systems Division, AES-Vol. 39, ASME 1999
- Doss, E.D., et al., “Pressurized and Atmospheric Pressure Gasoline-Fueled Polymer Electrolyte Fuel Cell System Performance,” Presented at the SAE 2000 World Congress, March 6-9, 2000, SAE # 2000-01-2574, SAE International, Warrendale, PA, 2000
- Friedman, D.J., R.M.Moore, "PEM Fuel Cell System Optimization", Proceedings of the Second International Symposium on Proton Conducting Membrane Fuel Cells II, Edited by S. Gottesfeld et al., Electrochemical Society, Pennington, NJ, 1999

- Friedman, D.J., A.Eggert, P.Badrinarayanan, J.M.Cunningham, "Maximizing the Power Output of an Indirect Methanol PEM Fuel Cell System: Balancing Stack Output, Air Supply, and Water and Thermal Management Demands," Presented at the SAE 2001 World Congress, March 5-8, 2001, SAE # 2001-01-0535, SAE International, Warrendale, PA, 2001
- S. Ramaswamy, T. E. Lipman, "Modeling and Analysis of PEMFC Based Fuel Cell Vehicles: Technology, Performance and Costs", Fuel Cells 2001 Conference, Tokyo, Japan, July 10-11, 2001.


***Stack***


- Springer, T., Zawodzinski, T., and Gottesfeld, S., "Polymer Electrolyte Fuel Cell Model", Journal of the Electrochemical Society, Vol. 138, No. 8, pp. 2334-2342, 1991
- Springer, T. E., M. S. Wilson, S. Gottesfeld, "Modeling and Experimental Diagnostics in Polymer Electrolyte Fuel Cells", Journal of the Electrochemical Society, Vol. 140, pp 3513-3526, 1993.
- Springer, T. E., T.A. Zawodzinski, M. S. Wilson, S. Gottesfeld, "Characterization of Polymer Electrolyte Fuel Cells Using AC Impedance Spectroscopy", Journal of the Electrochemical Society, Vol. 143, pp 587-599, 1996.
- Lee, J.H., T.R. Lalk, A.J. Appleby, "Modeling Experimental performance in large scale proton exchange membrane fuel cell stacks", Journal of Power Sources, Vol.70, (1998), pp-258-268
- Thirumalai, D, Ralph White, "Mathematical Modeling of Proton-Exchange membrane Fuel cell Stacks", J. Electrochemical Soc., Vol.144, No.5, May 1997
- Fronk, M.H., Wetter, D.L., Masten, D.A., Bosco, A., "PEM Fuel Cell System Solutions for Transportation", Fuel Cell Power for Transportation 2000, Proc. of SAE 2000 World Congress, pp. 101-108, 2000


***Air Supply***


- Cunningham, J.M., D.J.Friedman, M.A.Hoffman, R.M.Moore, "Requirements for a Flexible and Realistic Air Supply Model for Incorporation into a Fuel Cell Vehicle (FCV) System Simulation," Presented at the SAE Future Transportation Technology Conference and Exposition, 17-19 August, 1999, SAE #1999-01-2912, SAE International, Warrendale, PA, 1999
- Cunningham, J.M., M.A.Hoffman, "The Implications of Using an Expander (Turbine) in an Air System of a PEM Fuel Cell Engine," Presented at the 17th International Electric Vehicle Symposium & Exposition, 15-18 October, 2000, Montreal Quebec.
- Fonda-Bonardi, G., "Turbocompressor for Vehicular Fuel Cell Service," The 2000 Fluids Engineering Division Summer Meeting, paper #FEDSM00-11307, Boston, Massachusetts, June 11-15, 2000.
- Ishino, M, et.al.,"Effects of Variable Inlet Guide Vanes on Small Centrifigual Compressor Performance," Presented at the International Gas Turbine & Aeroengine Congress and Exhibition (ASME), Indianapolis, Indiana, June 7, 1999.

- Milburn, S.M., "Introducing a High Efficiency Variable Positive Displacement Automotive Supercharger," SAE Paper #940845, 1994.
- Milburn, S.M., et.al., "A Variable Displacement Compressor/Expander for Vehicular Fuel Cell Air Management," SAE Paper #961713, 1996.
- Pischinger, S., et.al., "Integrated Air Supply and Humidification Concepts for Fuel Cell Systems," Presented at the SAE 2001 World Congress, March 5-8, 2000, SAE # 2001-01-0233, 2001.
- Roan, V.P., et.al., "Air System Technology Programs Review Panel," Presentation at the U.S. Department of Energy Air Management Workshop, Argonne National Laboratory, October 10, 2000.
- Wiartalla, A., et.al, "Compressor Expander Units for Fuel Cell Systems," Presented at the SAE 2000 World Congress, March 6-9, 2000, SAE # 2000-01-0380, 2000.

***WTM***

- Badrinarayanan, P., A.Eggert, K.H. Hauer, "Implications of Water and Thermal Management Parameters in the Optimization of an Indirect Methanol Fuel Cell System," Presented at the 35th Intersociety Energy Conversion Engineering Conference, 24-28, July 2000, Paper # 2000-3046.
- Eggert, A., et al., "Water and Thermal Management of an Indirect Methanol Fuel Cell system for Automotive Applications," Proceedings of the 2000 International Mechanical Engineering Congress and Exposition, Orlando, FL, November 5-10, 2000 (pending)
- Badrinarayanan, P., Eggert, A. and Moore, R.M., "Minimizing the Water and Thermal Management Parasitic Loads in Fuel Cell Vehicles", International Journal of Transport Phenomena, 2001 (Accepted).

***Fuel Processor***

- Amadeo, N.E. and Laborde, M.A., "Hydrogen Production from the Low-Temperature Water-Gas Shift Reaction: Kinetics and Simulation of the Industrial Reactor, International Journal of Hydrogen Energy, vol. 20, no. 12, pp. 949-956, 1995.
- Amphlett, J.C. et al, "Hydrogen Production by Steam Reforming of Methanol for Polymer Electrolyte Fuel Cells", Journal of Hydrogen Energy, Vol.19, No.2, 131-137, 1994.
- Chan, S.H. and Wang, H.M., "Thermodynamic analysis of natural-gas fuel processing for fuel cell applications," International Journal of Hydrogen Energy, v. 25, pp. 441-449, 2000.
- Ito, K., Choi, B.C, Fujita, O., *The Start-Up Characteristics of a Catalytic Combustor Using a Methanol Mixture,* JSME International Journal, Series II, Vol. 33, No. 4, pp. 778-784, 1990.
- Kahlich, M.J., Gasteiger, H.A., Behm, R.J., "Kinetics of the Selective CO Oxidation in H2-Rich Gas on Pt/Al2O3," Journal of Catalysis, v. 171, pp. 93-105, 1997.
- Podolski, Walter F. and Young, G. Kim, "Modeling the Water-Gas Shift Reaction," Ind. Eng. Chem., Process Des. Develop., Vol. 13, No. 4, pp. 415-421, 1974.
- Wark, Kenneth and Warner, Cecil T., Air Pollution, New York: Harper & Row, 1981, pp. 376-384.

- Ramaswamy, S., Sundaresan, M., Eggert, A., Moore, R.M., "System Dynamics and Efficiency of the Fuel Processor for an Indirect Methanol Fuel Cell Vehicle", Proc. of the 35th Intersociety Energy Conversion Engineering Conference, American Institute of Aeronautics and Astronautics, Vol. 2, pp.1372-1377, 2000.
- S. Ramaswamy, M. Sundaresan, K. Hauer, D. J. Friedman, R. M. Moore, "Efficiency, Dynamic Performance and System Interactions for a Compact Fuel Processor for Indirect Methanol Fuel Cell Vehicles", SAE 2001 World Conference, Detroit, MI, March 5-8, 2001, Paper Number 2001-01-0231.


***Hydrogen Storage***


- D. Corrigan, "Metal Hydride Technologies for Fuel Cell Vehicles", Commercializing FCVs 2000 4-12-00, Berlin Germany
- S. Amendola etal, "A safe, portable, hydrogen gas generator using aqueous borohydride solution and Ru catalyst", Int. J. Hydrogen Energy 25 (2000)
- A.C Dillon, etal, "Carbon Nanotube Materials For Hydrogen Storage", Proceedings of the 2000 DOE/NREL Hydrogen Program Review NREL/CP-570-28890 5/8/00
- www.prnewswire.com/cgibin/stories.pl?ACCT=104&STORY=/www/story/11-09-2000/0001361534&E DATE=
- Michael J. Moran et. al. Fundamentals of Engineering Thermodynamics, John Wiley & Sons 1992
- McCarty, D.R, "Hydrogen Technological Survey-Thermophysical Properties", Cryogentics Division, Institute for Basic Standards National Bureau of Standards, Boulder Colorado. Scientific and Technical Information Office, Washington, DC 1975
- David W. Oxtoby et. al. Principles of Modern Chemistry, University of Chicago, 1987
- M.J. Moran and H. Shapiro, "Fundamentals of Engineering Thermodynamics", 1995
- Engineering Dept of Crane Co. "Flow of Fluids Through Valves, Fittings, and Pipe", Technical paper No. 410, Joliet IL. 1998


[i] DOE's Homepage Web-site is http://www.ch.doe.gov/business/ACQ.htm under the heading "Current Acquisition Activities," Soliciation No. DE-SC02-99EE50525
Title of Project: Automotive Integrated Power Modules (AIPM), Appendix A- Attachment 1